

Investigation into long-term behaviour of a submerged tunnel in soft clay

A back analysis of time-dependent deformations for Tingstad tunnel using FEM

Master of Science Thesis in the Master's Programme Infrastructure and Environmental Engineering

TIM BJÖRKMAN THERESE HEDMAN

Department of Civil and Environmental Engineering
Division of GeoEngineering

Geotechnical Engineering Research Group

CHALMERS UNIVERSITY OF TECHNOLOGY

Göteborg, Sweden 2013

Master's Thesis 2013:68

MASTER'S THESIS 2013:68

Investigation into long-term behaviour of a submerged tunnel in soft clay

A back analysis of time-dependent deformations for Tingstad tunnel using FEM

*Master of Science Thesis in the Master's Programme Infrastructure and
Environmental Engineering*

TIM BJÖRKMAN

THERESE HEDMAN

Department of Civil and Environmental Engineering
Division of GeoEngineering
Geotechnical Engineering Research Group
CHALMERS UNIVERSITY OF TECHNOLOGY
Göteborg, Sweden 2013

Investigation into long-term behaviour of a submerged tunnel in soft clay
A back analysis of time-dependent deformations for Tingstad tunnel using FEM
*Master of Science Thesis in the Master's Programme Infrastructure and
Environmental Engineering*

TIM BJÖRKMAN

THERESE HEDMAN

© TIM BJÖRKMAN & THERESE HEDMAN, 2013

Examensarbete / Institutionen för bygg- och miljöteknik,
Chalmers tekniska högskola 2013:68

Department of Civil and Environmental Engineering
Division of GeoEngineering
Geotechnical Engineering Research Group
Chalmers University of Technology
SE-412 96 Göteborg
Sweden
Telephone: + 46 (0)31-772 1000

Cover:

One of the investigated cross-sections. Construction plan from Skanska (previously Skånska Cementgjuteriet) and input geometry in PLAXIS.

Chalmers Reproservice / Department of Civil and Environmental Engineering
Göteborg, Sweden 2013

Investigation into long-term behaviour of a submerged tunnel in soft clay
A back analysis of time-dependent deformations for Tingstad tunnel using FEM
Master of Science Thesis in the Master's Programme Infrastructure and Environmental Engineering

TIM BJÖRKMAN

THERESE HEDMAN

Department of Civil and Environmental Engineering

Division of GeoEngineering

Geotechnical Engineering Research Group

Chalmers University of Technology

ABSTRACT

The long-term behaviour of soft soil is of importance when constructing large infrastructure projects in deep layers of soft marine clay. Due to the complexity regarding time dependent deformation of soil and the accuracy needed, soil models using a finite element analysis could be a good tool to predict this behaviour. Since many soil models, which incorporate time dependent deformations, are based on laboratory experiments it is useful to compare these models with full-scale projects.

In this MSc-thesis a back calculation was executed, using FEM-software, comparing simulated behaviour in the soil model Soft Soil Creep, with measured deformation over a long time for the Tingstad tunnel, gaining knowledge useful for the design of the new Marieholm tunnel. A description of the behaviour of soft clay is included, together with an introduction to the used software.

An evaluation of the observed possibility for the model to capture the measured deformation, using evaluated input parameters was performed and discussed.

The result shows that the model is only capable of predicting the measured deformations to some extent. Many factors affect the result such as load estimations, geometry assumptions and the set of parameters.

A sensitivity analysis was performed to see which parameters had the most influence and should be prioritized in further studies. The result showed that the modified compression index, λ^* and the modified creep index, μ^* affected the simulations the most.

Some recommendations were made in the conclusion for a continuation of the project, which included obtaining a higher accuracy of the load contribution of the tunnel and geometric conditions. In addition, further evaluation of parameters used in the model was recommended as well as the possible implementation of more advanced soil models.

Key words: Clay, soft soil creep, PLAXIS, Tingstad tunnel, soil modeling, creep, long-term deformation

Contents

ABSTRACT	I
CONTENTS	1
NOTATIONS	6
1 INTRODUCTION	11
1.1 Aim	11
1.2 Limitations	12
1.3 Methodology	12
2 BACKGROUND	13
2.1 Description of the construction	13
2.2 Geology of area	14
2.3 Measured deformations	14
3 LITERATURE SURVEY	16
3.1 Structure and behaviour of soft clay	16
3.1.1 An overview of clay structure	16
3.1.2 The definition of stress and strain for a soil material	17
3.1.3 The deformation behaviour of clay	20
3.1.4 Soil stiffness	21
3.1.5 Consolidation and swelling theory	25
3.1.6 Creep	27
3.2 Soil modelling	30
3.2.1 Stress paths and yield criterion	30
3.2.2 Stress and strain invariants	32
3.2.3 Linear elasticity model	33
3.2.4 Non-linear elastic model	34
3.2.5 Elasto-plasticity and elasto-plastic models	35
3.2.6 Cam-Clay model	37
3.2.7 Elastic visco-plasticity	39
4 INTRODUCTION TO PLAXIS	40
4.1 Mesh generation	40
4.2 Geometry and plain strain	40
4.3 Material models	40
4.3.1 Hardening Soil	41
4.3.2 Soft Soil Creep (SSC)	42
4.4 Calculation modes and procedures	44
4.4.1 Drainage situation in PLAXIS	44
4.4.2 Initial stress generation	45
4.4.3 Calculation modes and analysis type	45

5	PARAMETER EVALUATION	47
5.1	Introduction to some field and laboratory tests	48
5.2	Investigations from Ringömotet and Tingstadsvass	49
5.3	Investigations from Gullbergsmotet	50
5.4	Investigations from Marieholm	50
5.4.1	Estimation of K_0^{NC}	51
5.4.2	Evaluation of the modified swelling and compression index	52
5.4.3	Evaluation of the modified creep index	54
5.4.4	Evaluation of swelling and compression index	55
6	VERIFICATION OF SOIL MODELS AND PARAMETERS THROUGH SOIL TEST SIMULATION	58
6.1	Evaluation and verification of soil parameters	58
6.1.1	CRS-tests with the SSC model	58
6.1.2	Triaxial-tests with the SSC model	61
6.1.3	Soil tests with the HS model	64
6.2	Further study of SSC-parameters through the β -factor	67
6.3	Remarks on validation of soil parameters and data quality	68
7	INPUT DATA, GEOMETRY AND MODELLING PROCEDURE	70
7.1	Input data	70
7.1.1	General assumptions	71
7.2	Section A	71
7.2.1	Assumptions and modeling procedure	72
7.2.2	Hypothesis of PLAXIS results	73
7.3	Section B	73
7.3.1	Assumptions and modeling procedure	74
7.3.2	Hypothesis of PLAXIS results	75
7.4	Section C	75
7.4.1	Assumptions and modeling procedure	76
7.4.2	Hypothesis of PLAXIS results	76
7.5	Section D	77
7.5.1	Assumptions and modeling procedure	78
7.5.2	Hypothesis of PLAXIS results	78
7.6	Section E	78
7.6.1	Assumptions and modeling procedure	79
7.6.2	Hypothesis of PLAXIS results	80
8	RESULTS	81
8.1	Section A	81
8.2	Section B	83
8.2.1	Modified calculation	84

8.3	Section C	85
8.3.1	Modified calculation with additional load from fill	87
8.3.2	Sensitivity analysis of important parameters	88
8.4	Section D	95
8.5	Section E	97
8.5.1	Modified Calculations	98
8.5.2	Modeling with HS	99
9	DISCUSSION	100
10	CONCLUSION	103
11	REFERENCES	104

Preface

The work with finding a model of the long-term soil behaviour connected to the Tingstad tunnel, have been carried out from January 2013 until June 2013, at the Department of Civil and Environmental Engineering, Division of GeoEngineering, Chalmers University of Technology and NCC Teknik, Göteborg, to which we are very thankful.

We would like to thank our main supervisor Mats Olsson for guiding us through the work and explaining theories, but also for supporting us and cheering us on when things seemed difficult.

Further we would like to thank our supervisor Ayaz Nerwey at NCC Teknik for his help with the thesis and for showing us the practical side of Geotechnical Engineering.

We are also grateful to Professor Claes Alén for all the interesting and educational discussions and to Tara Wood for the idea and inspiration of this Master Thesis.

Finally we would like to thank Per Thunstedt at Trafikverket for providing background material and information regarding the Tingstad tunnel.

Gothenburg, June, 2013

Tim Björkman

Therese Hedman

Notations

Roman upper case letters

$C_{\alpha s}, C_{\alpha e}$	secondary compression index
C_c	compression index
C_s	swelling index
$[D]$	stiffness matrix
E	Young's modulus
EA	axial stiffness
EI	bending stiffness
E_{50}^{ref}	secant stiffness at a reference stress level
$E_{\text{oed}}^{\text{ref}}$	oedometer modulus at a reference stress level
$E_{\text{ur}}^{\text{ref}}$	unloading/reloading stiffness at a reference stress level
F_{max}	toe bearing capacity for piles
G	shear modulus
G_0	initial shear modulus
G_{ur}	unloading/reloading shear modulus
G_s	specific gravity
K	bulk modulus
K_0	at-rest coefficient for earth-pressure
K_0^{NC}	at-rest coefficient for normal consolidated soils
M	slope of CSL in p'-q-plane
M_0	tangent stiffness for primary oedometer loading
M_0^{CRS}	tangent stiffness for primary oedometer loading from CRS-test
M_L, E_{oed}	modulus for stresses between σ'_p and σ'_L
E_{ur}	unloading/reloading compression modulus
R	time resistance
T_v	time factor
\bar{U}	average degree of consolidation
V_p	pore volume
V_s	solid volume
$T_{\text{top, max}}$	skin friction for piles, top
$T_{\text{bottom, max}}$	skin friction for piles, bottom

Roman lower case letters

c'	effective cohesion
c_u	undrained shear strength
c_v	consolidation coefficient
e	void ratio
e_{in}, e_0	initial void ratio
e_k	void ratio when $p'=1$
k	permeability
m	power of stress dependency
m_s	mass of solids
m_w	mass of pore water
p'	mean effective stress
p_p	isotropic preconsolidation pressure
p_p^{eq}	equivalent isotropic preconsolidation pressure
q	deviatoric stress
r_s	resistance number
s'	stress invariant
t	stress invariant
t'	effective creep time
u	pore pressure
u_B	pore pressure at bottom of sample
u_i	displacement
w_N	natural water content
w_L	liquid limit

Greek lower case letters

α_s	secondary compression coefficient
γ	radial deformation
γ_{ij}	shear strain
γ_s	deviatoric strain
γ_{sat}	saturated weight of soil
γ_{unsat}	unsaturated weight of soil
γ_w	weight of water

ε	strain
ε_v	volumetric strain
ε_v^c	volumetric creep strains
θ	Lode's angle
κ	slope of unloading/reloading line in e-lnp'-plane
κ^*	modified swelling index
λ	slope of CSL in e-lnp'-plane
λ^*	modified compression index
μ^*	modified creep index
ν	Poisson's ratio
ν_{ur}	Poisson's ratio for unloading/reloading
ρ	bulk density
ρ'	effective bulk density
ρ_m	saturated density
ρ_w	density of water
σ	total stress
σ'	effective stress
$\sigma_1, \sigma_2, \sigma_3$	principal stresses
σ_{ii}	normal stress
σ'_{h0}	in-situ horizontal effective stress
σ'_L	stress level at which the modulus is M'
σ'_p	preconsolidation stress
σ'_{v0}	in-situ vertical effective stress
σ'_v	vertical effective stress
τ	shear stress
τ_c	time dependency parameter
τ_{ij}	shear stress
τ_{max}	failure shear stress
φ'	internal friction angle

Abbreviations

CRS	Constant Rate of Strain
CSL	Critical State Line
DSS	Direct Simple Shear
HS	Hardening Soil
OCR	Over Consolidation Ratio
SPW	Sheet Pile Wall
SSC	Soft Soil Creep
VCL	Virgin Compression Line

1 Introduction

The construction of large infrastructure projects in deep layers of soft clay often initiates major deformations over a long period of time. To be able to accurately predict these deformations is important with regard to life-span, and the planning and execution of future maintenance measures. Due to the complexity of soil a good tool for more precise predictions of deformations is the finite element method with models capable of capturing the non-linear deformation behaviour of soft soil.

Many existing soil models, which incorporate the time dependant deformations, are based on laboratory experiments. Therefore it is useful to be able to compare these models with full-scale projects where measurements have been recorded for a long period of time. One such full-scale project is the Tingstad tunnel, built 1968 as a third road connection between the north and south part of Gothenburg (Vägverket, 2007).

An important aspect in engineering is to gain experience from previous projects and many years of measurements of the Tingstad tunnel provides a great opportunity for this. This knowledge can be used in new building projects such as the construction of the Marieholm tunnel, a new construction that will be located approximately 500 meter north of the Tingstad tunnel. The tunnel is a part of the West Sweden package and the construction is planned to begin in 2014.

Since the geology of the area and the type of construction are similar for the new tunnel, a back analysis of the deformations of Tingstad tunnel could be valuable both for the new construction of the Marieholm tunnel as well as being an opportunity to evaluate theoretical frameworks for long-term deformations.

1.1 Aim

The aim of this MSc-thesis is to find a set of parameters for capturing the long-term deformations of the Tingstad tunnel, based on comparison with measurement data of vertical deformations. The purpose of the sought model is the benefit it could have in the design of the new Marieholm tunnel.

The scope of the project is to implement the Soft Soil Creep model in PLAXIS to be able to account for the creep deformations occurring due to the loading of soft clay. The SSC model will be evaluated and to a minor extent compared to the Hardening Soil (HS) model.

Parameter evaluation will be performed through comparison with soil tests and through a sensitivity analysis on the tunnel model to be able to find the parameters that have the largest impact on the result.

This report is also an attempt to simplify a very complex geometry and construction process and to discuss the limitations, in the model, due to assumptions and simplifications.

1.2 Limitations

The literary study in this MSc-thesis focuses on the relevant theory for behaviour of soft marine clay. The main focus of the back analysis is the vertical deformations directly under the tunnel since the measurements come from gauges at the tunnel base level.

To capture the measured deformations five cross-sections, located in different parts along the tunnel stretch including the access ramps, will be simulated and compared to the measurements conducted at these cross-sections, during the time since completion of the tunnel.

The simulations will be executed with the finite element software PLAXIS 2D, where mainly one material model will be used and evaluated, as mentioned in the aim formulation.

1.3 Methodology

The work will begin with a review of existing literature and continue with collection of old existing geotechnical data for the Tingstad tunnel and the collection and compilation of new geotechnical data from the investigation for the Marieholm tunnel. Measurement data of movements connected to the Tingstad tunnel will also be studied. Numerical models of Tingstad tunnel will be performed with the FEM-based software PLAXIS and the result will be compared with actual measurements to calibrate the model. PLAXIS was chosen due to the user friendliness and because it is one of the most widely used FEM-programs, for geotechnical applications, in the industry.

2 Background

The Tingstad tunnel is a part of E6 and is an important traffic link in the city, connecting the central parts of Gothenburg to Hisingen. The map in Figure 2.1 shows the location of the tunnel including the approximate position of the new Marieholm tunnel.



Figure 2.1. Map over central Gothenburg, with the Tingstad tunnel (1) and the future Marieholm tunnel (2) (SWEGIS, 2006).

2.1 Description of the construction

The tunnel tube is 454 meter long and built with an immersed tunnelling technique in the river Göta älv (Gatubolaget, 2005). The technique is performed by dredging an underwater trench for the placement of the tunnel. Several tunnel elements are constructed in a dock close to the construction site. When an element is finished it is submerged and placed on the river bottom. When the tunnel elements are fit into place and connected to each-other the trench is refilled.

The lowest part of the tunnel is situated 14 meter beneath the mean water surface, which has a level of +10 meters, by the elevation system GH18, which is continuously used throughout this thesis. On the north and south sides connection ramps connect the tunnel with the surface level.

The tunnel is built with five different concrete elements, with section measures of 30x7.4 meter outer dimension (Gatubolaget, 2005). The tunnel elements are supported by wooden piles, 22 meter in length, placed in groups under the tunnel.

The tunnel is connected to the south and north side with 60 meter long access ramps. The connection ramps are constructed with sheet pile walls (SPW) and a concrete

structure supported by prefabricated struts and a 1.0 meter thick concrete slab. From the tunnel entrances up to 50 meter away, the bottom slab is supported by 23 meter long concrete piles while the last part of the slab is founded on the ground surface. To avoid hydraulic uplift seven meter long vertical drains was installed underneath the slab, which drains excess pore pressure up through the slab. To protect the tunnel and ramps from water ingress, the SPW used in the ramp construction was made water proof and a transverse sealing screen was installed on both sides of the river.

In conjunction with the tunnel construction the junctions Ringömotet, Gullbergsmotet and Olskroksmotet was built. The project was comprehensive and included the redirection of two rivers which had their outlet at the placement of the tunnel. This led to drainage and extensive filling of the old river trenches. To ensure stability and to reduce settlements the fill was supported by wooden bank-piles, with a length of 20-32 meters. In addition to this a permanent basin was constructed at the location of element 4 and 5 in the northern part of the tunnel.

2.2 Geology of area

Areas of bare bedrock and deep valleys in between dominate the Gothenburg region geology (Claesson, 2003). During the period after the last ice age the Baltic Ice Lake was drained off, discharging large quantities of fine-grained sediments in the deep valleys under salt-water conditions. Today the soil profiles in the area of central Gothenburg mainly consist of these, relatively homogeneous layers of glacial and postglacial marine clays.

The soil layers relevant for the Tingstad tunnel consist of clay to a depth of 100 meter, where a layer of friction soil separates the clay from the bedrock (Gatubolaget, 2005). The clay is typical for the Gothenburg region, meaning relatively soft with an increase in strength with depth. The clay is considered to be normal- to slightly over-consolidated.

The geotechnical conditions at the site of the Marieholm tunnel are similar to those of the Tingstad tunnel. The soil layers consist of a 60 – 100 meter thick clay layer, deepest on the eastern side and then continuously shallower further west along the planned tunnel stretch (Edstam, 2004).

2.3 Measured deformations

In 2005, Gatubolaget, today known as ÅF, issued a report called “*Tingstadstunneln; Utredning avseende bärighet, beständighet och deformationer*”, regarding the current status of the tunnel with regard to deformations. This includes a compilation of all settlement measurements which have been used as a basis for the comparisons in this report. The placement of the gauges is shown in Appendix A, where the investigated cross-sections in this report are marked.

The interval of the measurements is every third year for the south ramp and tunnel element 1. For the other elements measurements are conducted every sixth year. The latest year recorded for the tunnel elements was 2007.

Settlements in the range of 200 millimeters have been measured for the southern ramp, most probably due to the filling of the old river trenches. These deformations are also causing a settlement of the first tunnel elements. The northern ramp has not

settled the same amount and in tunnel element 4 and 5 a heave of the soil has been observed instead, which have been reduced over time. Figure 2.2 shows the settlement for the entire stretch of the tunnel over time.

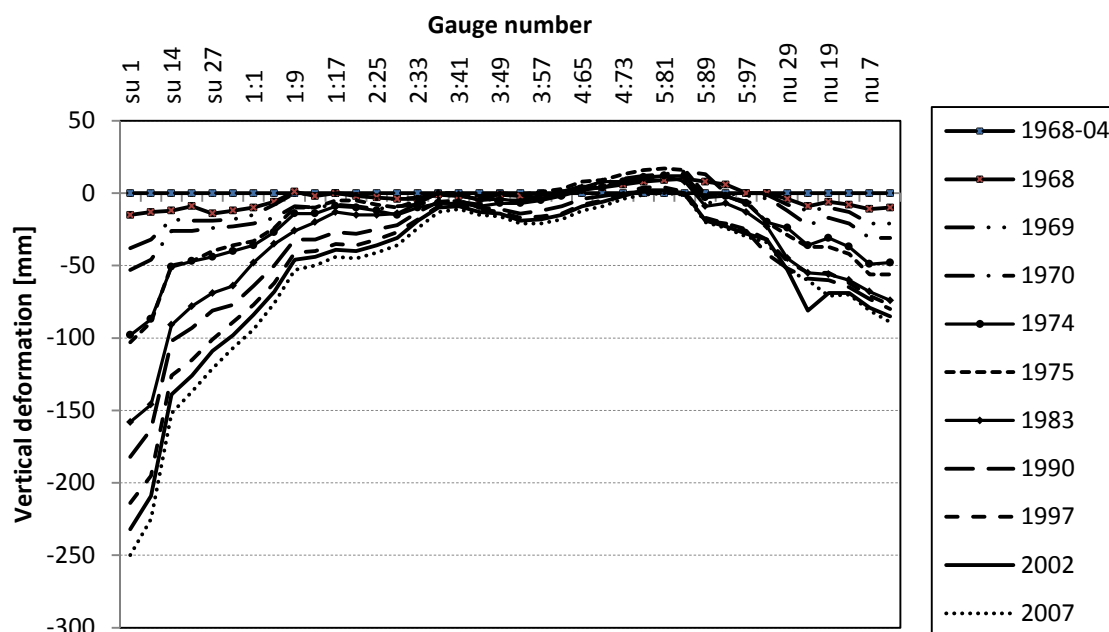


Figure 2.2. Vertical deformation along the tunnel. Data from report issued by Gatubolaget (2005).

Diagrams of the deformations for each cross-section can be seen in Appendix B. According to Gatubolagets report some measurements show insecure values due to changes to some gauges. In 1974 an adjustment was made to some of the gauges which led to errors in the data for this year. In the figures in Appendix B, the inconsistency has been adjusted to account for the trend visible in the data.

The measured deformations for the submerged part of the tunnel are small, less than 0.5 to 1 millimeter per year. For the ramps, this value is approximately 3 millimeters per year. It has also been stated that the effects of bending in the longitudinal direction, due to settlements of the ramps are small, in the range of 2-3 millimeters per 10 meters. Differential settlements in the cross-sections are also quite small with less than 1 millimeter per meter. Creep effects are, in the report, assumed to occur linearly with 1.4 millimeters per year.

Concerning longitudinal deformations, the southern ramp are shifting towards the south. There may be many explanations for this but some soil deformations due to transversal filling of the old river trench could have an effect. These deformations are not possible to take into account in PLAXIS 2D, but should be considered when evaluating the result.

3 Literature survey

To form a basis for the case study, a literary survey was conducted. This chapter aims to briefly describe some relevant soil characteristics and concepts in soil modelling.

3.1 Structure and behaviour of soft clay

This chapter aims to explain some basic theory around soil properties and behaviour relevant for this project.

3.1.1 An overview of clay structure

Soil consists of soil particles and pores. These pores can be filled with air and/or water which make soil a three-phase material. For clay, specifically, these soil particles are clay minerals that are thin with a leaf-like structure. The minerals form a microstructure of a soil skeleton by forming aggregates with bonds between them consisting of the smallest particles. These structures and bonds can be different depending on stress history and deposition environment. The most common type of clay in Sweden is illite. Specifically in Gothenburg, the clay where deposited in salt water which have formed a very open structure which also makes the soil highly compressible.

The properties and behaviour of the soil is dependent on the relationships between the three phases solids, gas and water and these relationships form a basis for deformation theory. Some basic definitions of some soil properties are presented below.

Bulk density, $\rho = \frac{m}{V}$ is defined as the mass of the soil divided with the volume. For a saturated soil the lifting force from the water is subtracted from the saturated density, ρ_m to obtain the effective bulk density according to equation (3.1).

$$\rho' = \rho_m - \rho_w \quad (3.1)$$

The water content is an important parameter where the natural water content is defined in equation (3.2).

$$w_N = \frac{m_w}{m_s} \quad (3.2)$$

m_w = mass of pore water

m_s = mass of solid particles

Another important parameter is the void ratio which describes how much of the soil volume consists of pores. The void ratio, e , is defined in equation (3.3).

$$e = \frac{V_p}{V_s} \quad (3.3)$$

V_p = pore volume

V_s = solid volume

The void ratio can also be obtained from the water content with a relationship with the specific gravity of the soil (Craig, 2004) defined in equation (3.4).

$$e = G_s w \quad (3.4)$$

The void ratio is connected to the permeability, k , which determines how fast a liquid can flow through the soil. The permeability is of great importance when calculating deformations in clay, which is a soil with relatively low permeability.

3.1.2 The definition of stress and strain for a soil material

The stresses in the soil consist, according to Terzaghi's theory, of effective stresses and pore pressures (PLAXIS, 2012) according to equation (3.5).

$$\sigma = \sigma' + u \quad (3.5)$$

The total stresses in an arbitrary point in the soil mass are defined as the sum of gravitational force acting on the soil element, which can be calculated as the weight of the materials above the point in the soil mass (Chang-Yu, 2006). The pore pressure is divided into the steady state pore pressure and the excess pore pressure (PLAXIS, 2012). The effective stresses are the stresses carried by the soil skeleton (Sällfors, 2001) and form a basis for most constitutive models since the soil strength depends on the effective stresses and not the total stresses (Chang-Yu, 2006). Since compressive stresses are governing in soils, these have a positive sign convention in most geotechnical applications. There are vertical and horizontal stresses in soil and in most cases these are not equal, hence anisotropic conditions apply. The relationship between the vertical and the horizontal stresses can be described with an at-rest coefficient, K_0 , which are defined according to equation (3.6).

$$K_0 = \frac{\sigma'_{h0}}{\sigma'_{v0}} \quad (3.6)$$

For normal consolidated soils, it was proposed by Jaky to calculate K_0^{NC} using the friction angle, φ' in the formula (3.7) (Craig, 2004).

$$K_0^{NC} = 1 - \sin \varphi' \quad (3.7)$$

An empirical relationship, presented in Larsson (2008) and used in Swedish practise, for estimating the lateral earth pressure coefficient for a normal consolidated cohesive soil is presented in equation (3.8).

$$K_0^{NC} = 0.31 + 0.71(w_L - 0.2) \quad (3.8)$$

The stresses acting on an element are geometrically described in Figure 3.1A. The stresses can be described in matrix form which, due to the fact that $\tau_{xy} = \tau_{yx}$, $\tau_{xz} = \tau_{zx}$, $\tau_{yz} = \tau_{zy}$ because of moment equilibrium reduces to a stress vector presented in (3.9).

$$\sigma = (\sigma_{xx} \ \sigma_{yy} \ \sigma_{zz} \ \tau_{xy} \ \tau_{yz} \ \tau_{zx})^T \quad (3.9)$$

For any stress state there exists a plane where the shear stresses are zero (Kullingsjö, 2007). This will produce an eigenvalue problem according to (3.10).

$$\det(\sigma' - \sigma' I) = 0 \quad (3.10)$$

The solution will give three roots, which are the principal stresses that are perpendicular to each other, and $\sigma'_1 \geq \sigma'_2 \geq \sigma'_3$ shown in Figure 3.1B (Kullingsjö, 2007). The principal stresses can be used in forming expressions of stress invariants, which are useful in soil modelling since the stress invariants are not dependant on a specific coordinate system. When the soil is normal consolidated and the ground surface is horizontal with parallel substrata, the largest principal stress are equal to the vertical stress and the smallest principal stress equals the horizontal stress (Larsson et.al., 2007).

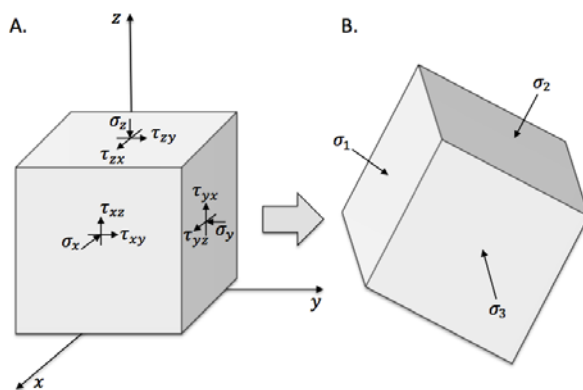


Figure 3.1. A. Stresses acting on a soil element in Cartesian coordinates B. Principal stresses

The stress history of the soil is an important factor in predicting the soil behaviour under the new loading condition and can be described with the pre-consolidation pressure, σ'_p . A simplified description of the pre-consolidation pressure is the maximum load that the soil has been exposed to previously. However, according to Kullingsjö (2007), this includes the creep and aging effects, hence a better definition is the highest stress the soil can bear until the constrained modulus decreases due to increased loading. It is essential to know the value of the pre-consolidation pressure when performing advanced laboratory tests (Larsson et.al., 2007). Estimations of this value can be retrieved from field measurements and a more accurate value from laboratory tests such as oedometer-tests and triaxial tests.

The relationship between the vertical pre-consolidation pressure and the current vertical stress state is defined by the OCR (Over Consolidation Ratio), defined in equation (3.11). If the soil is unloaded the vertical stress decreases and the soil becomes over-consolidated (Larsson, et.al., 2007).

$$OCR = \frac{\sigma'_p}{\sigma'_v} \quad (3.11)$$

A loading or unloading scenario produces changes to both the vertical and horizontal stresses that also affect the OCR. An unloading of the soil increases the OCR-value since the vertical effective stresses decrease. The change in the ratio between vertical and horizontal stresses, due to unloading, is not linear, but have been found to have a relationship with the OCR that could be expressed as equation (3.12) (Kullingsjö, 2007).

$$K_0 = K_0^{NC} * OCR^{1.2 * \sin \varphi'} \quad (3.12)$$

For $\varphi' = 30$ equals the equation reformulates to equation (3.13).

$$K_0 = K_0^{NC} * OCR^{0.5 \text{ till } 0.6} \quad (3.13)$$

There are several other proposed relationships between the OCR and the lateral earth-pressure coefficient for unloading and reloading, than presented above (Kullingsjö, 2007).

Strain, ε is a measure of deformation, which represents the displacement between particles in a body relative a reference length i.e. how much a local deformation differs from a rigid-body deformation. Since the measure is normalised, strain is dimensionless.

Calculating the mechanics for a soil body exposed to strain often needs the assumptions that the strains on the body is infinitesimal compared to the size of the body (Bo et al, 2011). Thus leaving the geometry and constitutive properties, such as stiffness and density, unchanged in each point of the space of the soil body. This assumption is called Infinitesimal strain theory or Small deformation theory. The

opposite assumption, in which the geometry and the constitutive properties are changed, is called finite strain theory.

The small deformation theory states that only the sum of complementing Cartesian shear strain results in shear stress (PLAXISa, 2012). Hence the sum of ε_{ij} and ε_{ji} could be written with the denotation γ . The strain matrix could thereby be reduced to a strain vector with normal strains and shear strains, presented in equation (3.14-3.16) with u = displacement.

$$\underline{\varepsilon} = (\varepsilon_{xx} \ \varepsilon_{yy} \ \varepsilon_{zz} \ \gamma_{xy} \ \gamma_{yz} \ \gamma_{zx})^T \quad (3.14)$$

$$\varepsilon_{ii} = \frac{\partial u_i}{\partial i} \quad (3.15)$$

$$\gamma_{ij} = \varepsilon_{ij} + \varepsilon_{ji} = \frac{\partial u_i}{\partial j} + \frac{\partial u_j}{\partial i}. \quad (3.16)$$

In clay the assumption of infinitesimal strain theory has been widely accepted, however numerical approaches gives a better possibility of implying finite strain theory, a more realistic approach to soils with large deformations.

3.1.3 The deformation behaviour of clay

Soil can, due to loading or unloading, deform by volume and/or shape (Larsson, 2008). Pure volume deformation is rare since this is possible only under isotropic conditions. Shear failure is a type of shape deformation which can occur if the difference between the largest and smallest principal stress is too large.

Deformations are divided into elastic and plastic strains, where the plastic strains are irreversible. Elastic strains occur when the effective stresses are less than the limit stress and the difference between the smallest and the largest principal stress is small. If this difference is low but the effective stresses exceed the limit stress plastic deformations occur.

Cohesive soils such as clay are a dense material which makes the dissipation of excess water very slow (Sällfors, 2001). Loading a dense soil can be seen as an undrained loading where there is no volume change of the soil mass. The load is instead transferred as an increase or decrease in pore pressure, which in turn affect the effective stresses. The undrained loading is true for clay in a short term loading scenario but for the long-term behaviour, the drained situation might become governing.

When deformations occur, a rearrangement of the soil skeleton can cause a change in volume (Larsson, 2008). An increase in volume is called dilatancy. If the opposite happens and the soil volume decreases, the soil is contractant. In undrained shearing of a soil that is contractant the pore pressure increases to compensate for the volume decrease caused by the shearing (Potts et.al., 2002). The opposite occurs for a dilatant soil in which the pore pressure decreases. Pore pressure relates to the effective stress and shear strength and hence affects the deformations which can be very large due to excess pore pressure (Larsson, 2008).

The shear strength is correlated to the effective stresses since water cannot sustain any shear stress. With larger effective stresses the intergranular friction increases and hence causes an increase in the shear strength (Larsson, et.al., 2007). Since the effective stresses increase with depth, the shear strength is also expecting to increase with depth. For an undrained loading scenario, the effective stresses decreases, also creating decreased shear strength. Hence, in this situation, it is the undrained shear strength that is governing, see Figure 3.2.

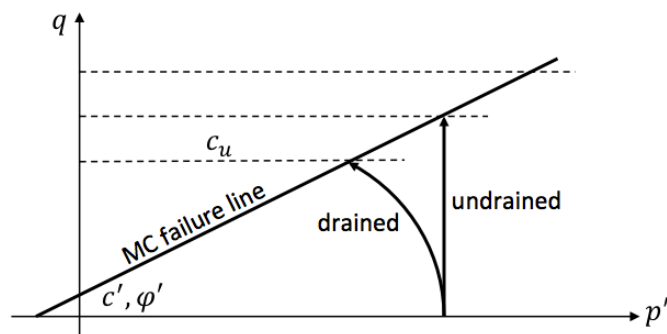


Figure 3.2. Stress path for drained and undrained loading.

For a drained situation, the effective stresses equals the total stresses and hence it is the effective friction angle, ϕ' , and the effective cohesion, c' , that determines the shear strength.

Soil is a non-linear material often with anisotropic conditions and time dependent deformation behaviour (Larsson, 2008). The anisotropy of soils shows on the undrained shear strength which is different in different loading directions (Larsson, et.al., 2007). There are three distinct cases of Active, Passive and Direct shearing which can be obtained from different forms of triaxial tests and direct shear tests. The mean value of the shear strength is often assumed to be equal to the direct shear strength.

3.1.4 Soil stiffness

In soil mechanics there are several different stiffness moduli all defining different stress-strain relationships. This chapter presents the definitions of some important moduli used for describing the behaviour of soft clay.

The bulk modulus, K , relates to the change in volumetric strain, ε_v , defined in equation (3.17) to the change in effective mean stress, p' . The definition of the tangent modulus presented in the equation shows that as the mean stress increases the material will compress or decrease in volume (Larsson, 2008). In the stress-volumetric strain response curve the bulk modulus is defined as the slope of the initial elastic part, as can be seen in Figure 3.3.

$$K = \frac{\delta p'}{\delta \varepsilon_v} \quad (3.17)$$

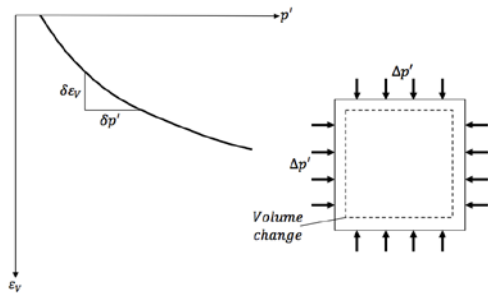


Figure 3.3. Definition of Bulk modulus.

The shear modulus G is defined by the ratio between the shear stress and the shear strain on a loading plate, according to equation (3.18).

$$G = \frac{\sigma_{xy}}{\varepsilon_{xy} + \varepsilon_{yx}} = \frac{\sigma_{xy}}{2\varepsilon_{xy}} = \frac{\sigma_{xy}}{\gamma_{xy}} = \frac{E}{2(1+\nu)} \quad (3.18)$$

In geotechnical engineering it is more commonly described as the ratio between the shear stress τ and the radial deformation, γ , in simple shear illustrated in Figure 3.4 and defined by equation (3.19) (Larsson, 2008). It can be determined either by the tangent modulus or the secant modulus.

$$G = \frac{\Delta\tau}{\Delta\gamma} = \frac{\delta\tau}{\delta\gamma} \quad (3.19)$$

The shear modulus decreases with increased deformation, which leads to an almost hyperbolic stress-deformation curve, shown in Figure 3.4 (Larsson, 2008). This curve can be estimated by the formula presented in equation (3.20), where G_0 is the initial shear modulus, the reference deformation $\gamma_r = \tau_{max}/G_0$ and τ_{max} is the shear strength (or failure stress), shown in Figure 3.4.

$$G = \frac{G_0}{1 + \frac{\gamma}{\gamma_r}} \quad (3.20)$$

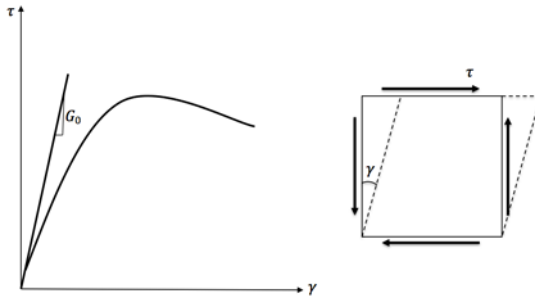


Figure 3.4. Hyperbolic stress-deformation curve and the definition of the shear modulus.

For normal consolidated clay the initial modulus G_0 can be evaluated from the undrained shear strength c_u and the liquid limit w_L according to equation (3.21) (Larsson, 2008);

$$G_{0(NC)} \approx \frac{504 \cdot c_u}{w_L} \quad (3.21)$$

For an over consolidated clay a slight correction is needed, presented in equation (3.22).

$$G_{0(OC)} \approx G_{0(NC)} * (1 - 0.4 * \log(OCR)), G_{0(OC)} \geq 0.4 * G_{0(NC)} \quad (3.22)$$

In an unloading scenario the unloading/reloading modulus, G_{ur} , can be used and can be obtained according to Figure 3.5.

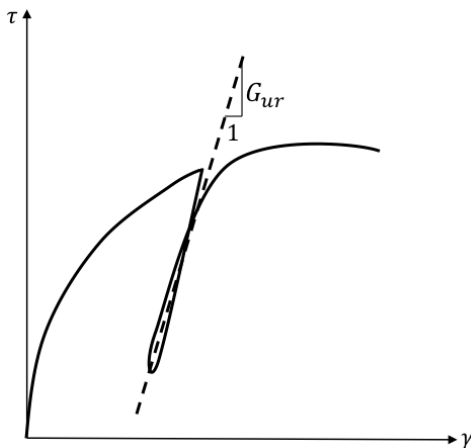


Figure 3.5. Description of the evaluation of G_{ur}

For a soil, the E -modulus is a theoretical parameter, but can often give good compliance with real soil deformation behaviour (Larsson, 2008). Together with the Poisson's ratio, ν , the elasticity modulus is derived through, K and G according to equations (3.23-3.25)

$$E = \frac{3*G}{1+G/3K} \quad (3.23)$$

$$\nu = \frac{1-2G/3K}{2+2G/3K} \quad (3.24)$$

$$E = 2 * G(1 + \nu) \quad (3.25)$$

A saturated clay could be assumed to be incompressible in an undrained state ($K = \infty$) and the equations (3.23) and (3.24) then gives $E = 3G$ and $\nu = 0.5$, provided that the comparison is made at the same level of strain (Lambe, 1969). The E-modulus can also be obtained from a drained triaxial test.

Since the clay behaviour is stress dependent several different moduli can be obtained. M_0 is the tangent stiffness for primary oedometer loading, shown in a stress-strain curve, see Figure 3.6 (Larsson, 2008). The primary modulus is most often evaluated from a Constant Rate of Strain (CRS)-test, however the M_0^{CRS} is often an underestimation of the real M_0 and hence Sällfors, cited in Persson (2004), proposed the relationship in equation (3.26).

$$M_0 = (3 \text{ to } 5) * M_0^{CRS} \quad (3.26)$$

The clay is regarded to have M_0 up to a stress level of σ'_p , see Figure 3.6. Between the stress level of σ'_p and σ'_L the modulus is M_L .

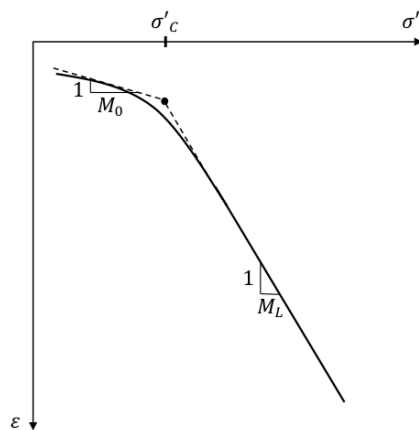


Figure 3.6. Evaluation of M_0 and M_L from an oedometer test.

3.1.5 Consolidation and swelling theory

Deformations in clay consist of both elasto-plastic deformations and time-dependant deformations. The time-dependant deformations are divided into consolidation, also called primary consolidation, and creep, or secondary consolidation as it is sometimes called (Larsson, 2008).

When loading saturated clay, there is no volume change and the stress change is initially carried by the pore water as shown as a simplification of the process in Figure 3.7 (Olsson, 2010).

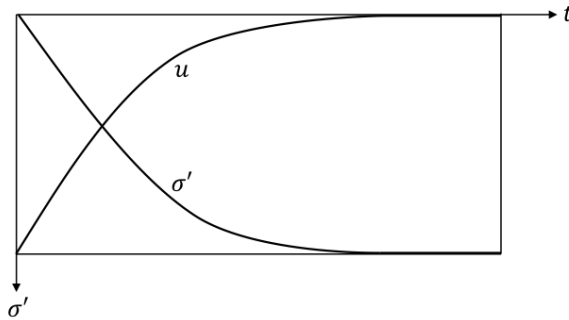


Figure 3.7. Load change in a saturated clay.

Due to the low permeability of clay this creates an excess pore water pressure which dissipates gradually while the load is transferred to the soil skeleton. This process is called consolidation and is defined as deformation by volume decrease, due to dissipation of excess pore-water pressure. To be able to predict the degree of consolidation there are several methods. Terzaghi presented what is known as the classic consolidation theory for the one-dimensional case and it is based on the differential equation (3.27), which is valid for a number of assumptions also presented (Persson, 2004).

$$\frac{\delta u}{\delta t} = \frac{M}{\gamma_w} \frac{\delta}{\delta z} k \frac{\delta u}{\delta z} = c_v \frac{\delta^2 u}{\delta z^2} \quad (3.27)$$

The last part of the equation is valid if the permeability and compression modulus is constant with depth.

- The soil is fully saturated and homogeneous
- Darcy's law is valid
- Initially $\Delta\sigma = \Delta u$
- One dimensional consolidation
- Creep is not considered
- Constant k during the consolidation process

A rough estimation of the settlement over time can be done with the time factor defined in (3.28).

$$T_v = c_v \frac{t}{h^2} \quad (3.28)$$

h = drainage path

t = time

The time factor are related to the average degree of consolidation, \bar{U} , which is the amount of excess pore pressure that have dissipated for a specific time. For simple cases the average degree of consolidation can be obtained graphically where \bar{U} is plotted for different boundary conditions. The graphs can be seen in Figure 3.8.

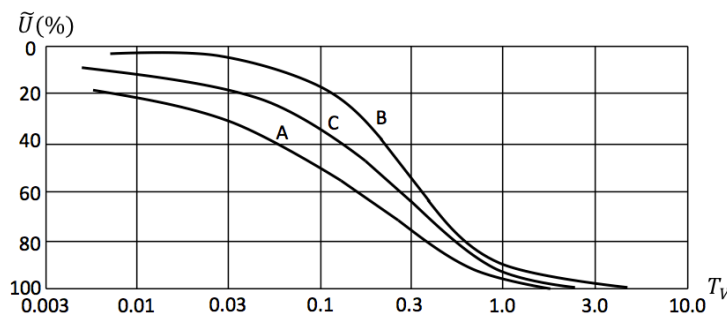


Figure 3.8. Average degree of consolidation as a function of T_v .

The assumptions made in Terzaghi's theory are not always representative of the real soil behaviour. For example, the permeability decreases with consolidation. Many of the shortcomings can be solved with numerical methods.

Another way of calculating time dependant deformations is by using the void ratio. In an oedometer test a sample is loaded incrementally and the result can be plotted in an e - $\log \sigma'$ curve. The test will produce a graph such as the one in Figure 3.9. For a normal consolidated soil the curve going from point A to C in the graph in figure 3.9 is called the Virgin Compression Line (VCL) (Potts et.al, 2002). From this graph the compression index, C_c , which is defined as the slope of the linear part of the VCL, can be evaluated (Craig, 2004). When the sample is unloaded another curve is plotted at point B, from which the swelling index, C_s , can be derived.

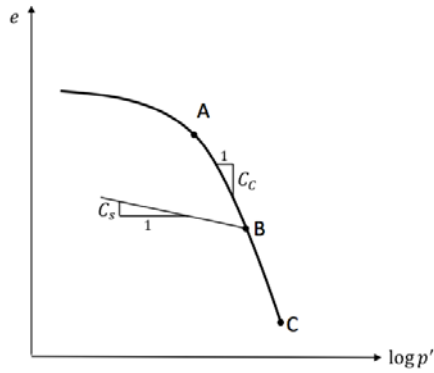


Figure 3.9. Incrementally loaded oedometer test. C_c is the slope of the VCL and C_s is the slope of the swelling line.

The compression index and swelling index can then be used to calculate the deformations due to a stress increase as the change in void ratio. If the soil is normal consolidated during the entire consolidation process equation (3.29) is used. If the soil is over consolidated equation (3.30) is used and if the soil goes from being over consolidated to normal consolidated during the consolidation period, equation (3.31) is used.

$$\Delta e = C_c \log\left(\frac{\sigma'_{v0} + \Delta\sigma'}{\sigma'_{v0}}\right) \quad (3.29)$$

$$\Delta e = C_s \log\left(\frac{\sigma'_{v0} + \Delta\sigma'}{\sigma'_{v0}}\right) \quad (3.30)$$

$$\Delta e = C_s \log\left(\frac{\sigma'_p}{\sigma'_{v0}}\right) + C_c \log\left(\frac{\sigma'_{v0} + \Delta\sigma'}{\sigma'_{v0}}\right) \quad (3.31)$$

The reverse process to consolidation is called swelling (Persson, 2004.). An excavation is an unloading of the soil which creates a decrease in pore pressure. This produces a heave of the soil as well as swelling, which are time dependant deformations. The consolidation theory presented above can also be applied on swelling with the changes that the unloading modulus is used. The assumption that $\Delta\sigma = \Delta u$ is not valid for unloading and the stress changes is instead described by equation (3.32).

$$\Delta u = \Delta\sigma_m = \frac{\Delta\sigma_v + 2\Delta\sigma_h}{3} \quad (3.32)$$

3.1.6 Creep

Creep is defined as time-dependant deformations of the soil skeleton and it can occur long after the excess pore pressure has dissipated. The phenomenon can be described as a rearrangement of the soil particles into a more stable form (Craig, 2004). The creep rate depends on soil viscosity allowing the rearrangement of the soil particles which creates new stronger aggregates which in turn causes a lower compressibility of

the soil and a decline of the creep deformations with time. For a long time it was believed that the secondary consolidation started at the end of primary consolidation but research during the recent 20-30 years have shown that creep occurs during primary consolidation as well.

The creep effects are not included in the consolidation theory presented by Terzaghi hence it is not valid for describing this phenomenon. Creep produces excess pore pressure and since creep occurs at the same time as the primary consolidation the effect will be a delayed consolidation since the excess pore pressure caused by the creep prevents the dissipation of the excess pore pressure in the primary consolidation phase. New models that take the creep into account have been and are being developed with varying range of complexity. Some of the theory is presented in this chapter.

Figure 3.10 shows the consolidation process from a stepwise oedometer test where the deformations, either as strain or void ratio, are plotted against the logarithm of time. The straight horizontal line represents the end of primary consolidation (EOC) after which the secondary consolidation is shown as an almost linear curve where the slope is the secondary compression-coefficient, α_s , also denoted $C_{\alpha e}$ (Olsson, 2007). When plotting void ratio the coefficient is called $C_{\alpha e}$. The relationships for these parameters are defined in (3.33) and (3.34).

$$\alpha_s = C_{\alpha e} = \frac{\Delta \varepsilon}{\Delta \log(t)} \quad (3.33)$$

$$C_{\alpha e} = \frac{\Delta e}{\Delta \log(t)} \quad (3.34)$$

To calculate the change in strain equation (3.35) is used.

$$\Delta \varepsilon = C_{\alpha e} \Delta \log(t) \quad (3.35)$$

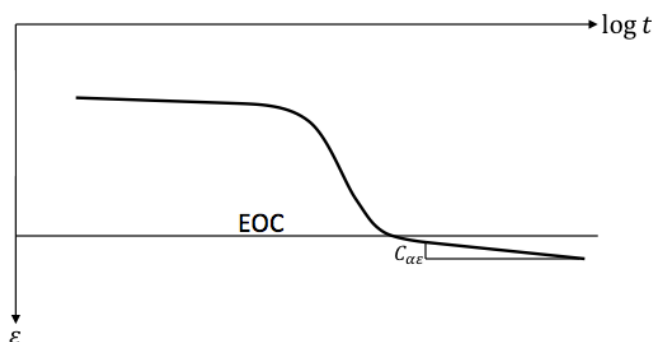


Figure 3.10. Consolidation process from oedometer test.

Creep can be described with other types of parameters, such as the time resistance concept, presented by Janbu (1969) cited in Olsson (2010).

Resistance, R is defined according to (3.36)

$$R = \frac{\text{action}}{\text{response}} \quad (3.36)$$

If plotted against time this formula turns into equation (3.37). This relationship is plotted in Figure 3.11. The slope of the straight line is the time resistance number, r_s which are related to R according to equation (3.38) which in turn gives the integral (3.39).

$$R = \frac{dt}{d\varepsilon} = \frac{1}{\dot{\varepsilon}_{creep}} \quad (3.37)$$

$$R = r_s(t - t_c) \quad (3.38)$$

$$\dot{\varepsilon}_{creep} = \frac{1}{r_s} \int_{t_0}^t \frac{1}{(t-t_c)} \quad (3.39)$$

Integrating equation (3.39) gives equation (3.40).

$$\Delta\varepsilon_{creep} = \frac{1}{r_s} \ln\left(\frac{t-t_c}{t_0-t_c}\right) \quad (3.40)$$

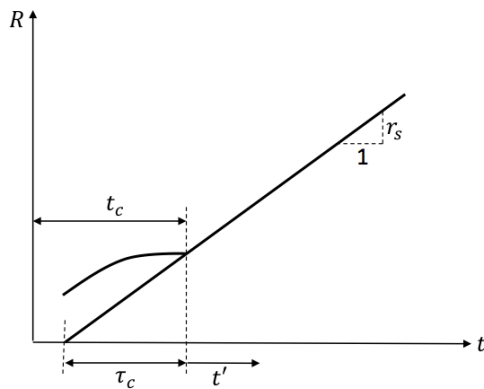


Figure 3.11. Time resistance concept.

The clay in Gothenburg is mostly normal to slightly over consolidated. This light over consolidation is probably due to creep effects. This pre consolidation effect is not related to previous loading and is called quasi-preconsolidation effect. The process is called aging or delayed consolidation and means that the soil compresses without any additional load.

Figure 3.12 shows the concept of aging, presented by Bjerrum (1967) cited in Olsson (2010) where the soil is initially normal consolidated at point A. The vertical line between A and B is the creep that occur during constant effective stress, causing a pre-consolidation of the soil. If the soil is loaded after 3000 years of creep the deformations will be elastic up to the pre-consolidation stress caused by the aging effect. After this stress level the soil will experience larger deformations.

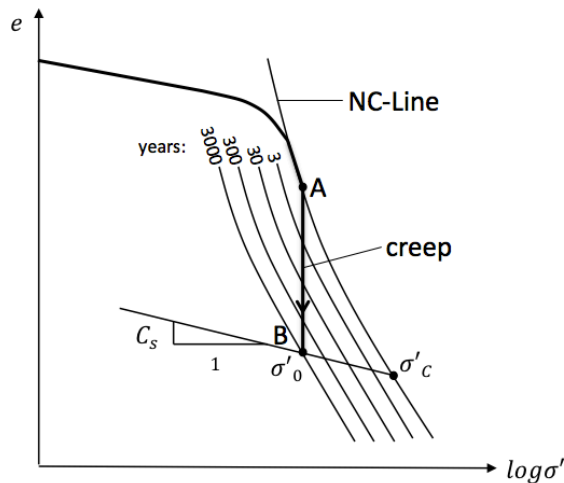


Figure 3.12. Aging effect or delayed consolidation according to Bjerrum (Olsson, 2010).

3.2 Soil modelling

There are several existing models that describe soil behaviour with different levels of complexity. Different soil characteristics, such as small strain stiffness, anisotropy and creep can be captured using different models. This chapter presents the basis for the models used in this thesis.

3.2.1 Stress paths and yield criterion

Stress paths during loading/unloading can be described by Mohr's circles. The principal stresses σ_1 and σ_3 forms the basis for Mohr's circles (Kompetenscentrum Infra, n.d.). The initial isotropic stress state are placed on the x-axis in a σ' - τ diagram according to Figure 3.13. The axis' are the stress invariants s' - t as previously described.

The largest shear stress is represented by the top point of the circle which amounts to the radius of the circle (Kompetenscentrum Infra, n.d.). In the triaxial test the stresses are changed in different ways depending on the type of test. In accordance the principal stresses change and a different circle is drawn for each stress situation, according to Figure 3.14. This is done until a circle representing a certain stress state is tangent to the failure line. Then the top point of each circle up to the failure circle forms the stress path.

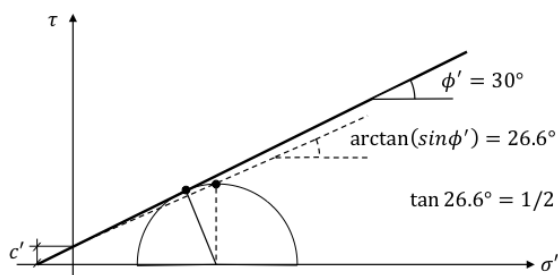


Figure 3.13. Initial isotropic stress state represented by Mohr's circle (Kompetenscentrum Infra, n.d.)

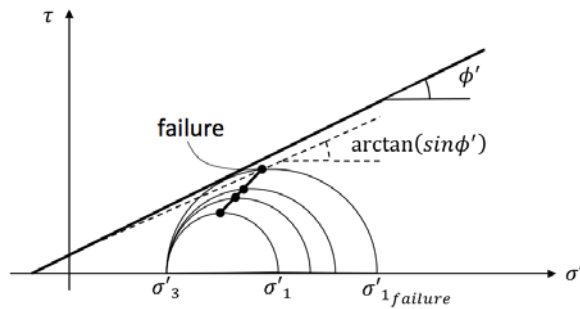


Figure 3.14. Stress path for a drained loading scenario (Kompetenscentrum Infra, 2010).

The failure line or failure envelope as it is sometimes called is a function of the effective strength properties and the normal effective stress on the failure surface with equation (3.41) (Chang-Yu, 2006).

$$c_u = c' + \sigma' * \tan\phi' \quad (3.41)$$

The determination of the undrained shear strength can be described with Mohr's circles which will show that it only depends on the effective stresses (Chang-Yu, 2006). This will produce a Mohr's failure envelope with zero inclination, see Figure 3.15, hence $\phi'=0$ and a derived value of the shear strength can be obtained.

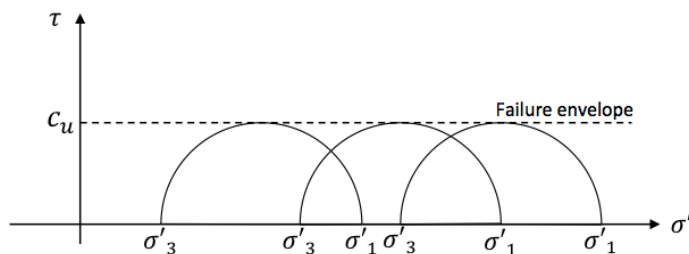


Figure 3.15. Mohr's failure envelope for undrained loading (Kompetenscentrum Infra, n.d.).

To simplify the description of soil behaviour it is considered to be an elasto-plastic material which means that for a certain stress state the material becomes plastic (Kompetenscentrum Infra, n.d.). The deformation and strength parameters of a soil are often described with a yield surface in stress space (Larsson, et.al., 2007). Stress-induced strains within this particular surface behave elastic and if they are tangent to the surface, plastic deformations occur.

If the yield surface is projected onto the σ_1 - σ_3 -plane, the Mohr-Coulombs failure lines are obtained see Figure 3.16 (Kompetenscentrum Infra, n.d.). If the current stress state is inside these lines the soil behaves elastic and if it is tangent to the failure line, failure occur. Adding the vertical and horizontal pre-consolidation pressure into this diagram a simple yield surface for a clay soil is obtained. If the stress state is above the pre-consolidation lines the material behaves plastic.

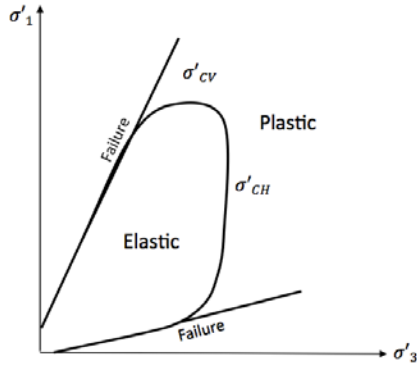


Figure 3.16. Yield surface in principal stress space.

Most common however is to represent the yield surface in a diagram with invariants s' and t on the axis by a rotation of 45° , seen in Figure 3.17 (Kompetenscentrum Infra, n.d.).

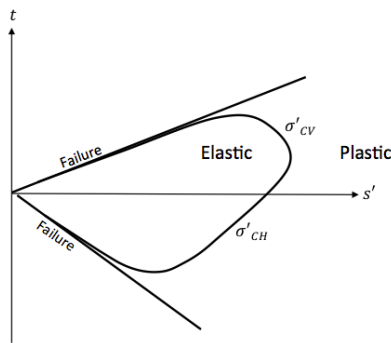


Figure 3.17. Rotated yield surface in s' - t -space.

Tresca and von Mises are yield criteria used for metals for example and they can, respectively, be correlated to the Drucker-Prager and Mohr-Coulombs theories (Kompetenscentrum Infra, n.d.). The most common is the Mohr-Coulomb yield criterion. Further description of these yield criteria are presented in chapter 3.2.5.

3.2.2 Stress and strain invariants

Three common invariants are the mean effective stress p' , the deviatoric stress q , which means the deviation from p' , and Lode's angle θ . They are defined as according to equations (3.42) and (3.43) (Potts and Zdravkovic, 1999).

$$p' = (\sigma'_1 + \sigma'_2 + \sigma'_3)/3 \quad (3.42)$$

$$q = \sqrt{1/2 ((\sigma'_1 - \sigma'_3)^2 + (\sigma'_1 - \sigma'_2)^2 + (\sigma'_2 - \sigma'_3)^2)} \quad (3.43)$$

The mean effective stress describes the distance of the stress state along a hydrostatic axis in principal stress space (Kullingsjö, 2007). The deviatoric stress describes the distance of the stress state from the hydrostatic axis along the so-called π -plane (the deviatoric shear plane), which is defined by the hydrostatic axis. Lodes angle gives the position of the stress state in the π -plane.

Other useful invariants, most common in plots from triaxial tests, are s' and t , defined according to (3.44) and (3.45). s' and t can also be expressed in horizontal and vertical stresses (Kullingsjö, 2007).

$$s' = \frac{(\sigma'_1 + \sigma'_2)}{2} \quad (3.44)$$

$$t = \frac{(\sigma'_1 - \sigma'_2)}{2} \quad (3.45)$$

Similar to stress, different invariants of strain could also be useful (PLAXISa, 2012). The volumetric strain, ε_v , defined in equation (3.46), is often used, which is the sum of all normal strain components and is defined in most geotechnical applications as positive for compression and negative for extension.

$$\varepsilon_v = \varepsilon_{xx} + \varepsilon_{yy} + \varepsilon_{zz} = \varepsilon_1 + \varepsilon_2 + \varepsilon_3 \quad (3.46)$$

A second invariant is the deviatoric strain, γ_s , defined in equation (3.47).

$$\gamma_s = \sqrt{\frac{2}{3} \left(\left(\varepsilon_{xx} - \frac{\varepsilon_v}{3} \right)^2 + \left(\varepsilon_{yy} - \frac{\varepsilon_v}{3} \right)^2 + \left(\varepsilon_{zz} - \frac{\varepsilon_v}{3} \right)^2 + \frac{1}{2} (\gamma_{xy}^2 + \gamma_{yz}^2 + \gamma_{zx}^2) \right)} \quad (3.47)$$

3.2.3 Linear elasticity model

The linear elasticity model is based on Hooke's law and requires only two parameters, Young's modulus and Poisson's ratio. It is a simple model that can be used for the modelling of structural components or very stiff materials but fails in capturing the real soil behaviour since soil is a non-linear material (Potts et.al., 2002).

The stress-strain relationship is described with a constitutive law (Kullingsjö, 2007). For an isotropic material this constitutive law is Hooke's law described in equation (3.48).

$$[\sigma] = [D][\varepsilon] \quad (3.48)$$

$[\sigma]$ = stress matrix

$[D]$ = Stiffness matrix (that defines the stress-strain relationship)

$[\varepsilon]$ = strain matrix

The stiffness matrix depends on Young's modulus, E , and Poisson's ratio, ν , according to the relationship presented in (3.49) (Potts and Zdravkovic, 1999).

$$[D] = \frac{E}{(1+\nu)(1-2\nu)} \begin{bmatrix} (1-\nu) & \nu & \nu & 0 & 0 & 0 \\ \nu & (1-\nu) & \nu & 0 & 0 & 0 \\ \nu & \nu & (1-\nu) & 0 & 0 & 0 \\ 0 & 0 & 0 & (1/2-\nu) & 0 & 0 \\ 0 & 0 & 0 & 0 & (1/2-\nu) & 0 \\ 0 & 0 & 0 & 0 & 0 & (1/2-\nu) \end{bmatrix} \quad (3.49)$$

3.2.4 Non-linear elastic model

In the non-linear elastic model the material matrix depends on stress/strain-levels (Potts and Zdravkovic, 1999). The material properties are most commonly chosen as the bulk modulus K , and the shear modulus, G . An increase in the mean effective stress will in most cases increase the bulk modulus while an increase in the deviatoric stress makes the shear modulus decrease. There are several different models to describe the non-linear elastic behaviour which is described below:

The bi-linear model, seen in Figure 3.18, applies a constant bulk and shear modulus until a failure condition is reached (Potts and Zdravkovic, 1999). The tangential shear modulus is then set to a very small value close to zero. Different failure surfaces can be applied in the model, for example Mohr-Coulomb.

Another example of a non-linear elastic model is the hyperbolic model, also displayed in Figure 3.18, where, similar to the bilinear model, the shear modulus, G , decreases to a value of 0 when the soil is at failure (Potts, et.al., 2002).

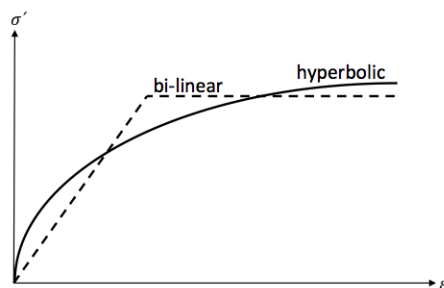


Figure 3.18. The bi-linear and the hyperbolic model.

A further development of non-linear elastic models has been to incorporate the effect on stiffness with small strains (Potts and Zdravkovic, 1999). The variation of shear moduli can be shown in Figure 3.17.

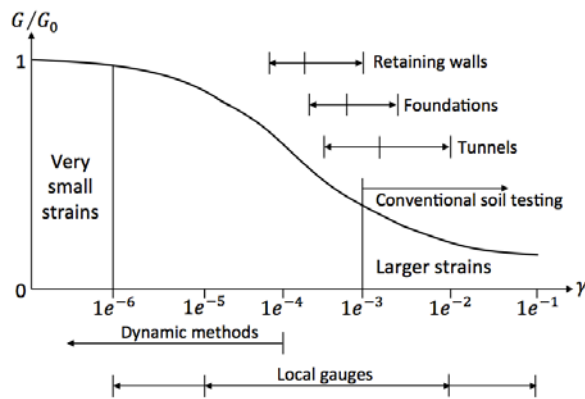


Figure 3.17. Shear moduli plotted against strain (PLAXIS manual).

This model describes the shear behaviour and is often combined with a linear elastic model to simulate compression (Potts et.al., 2002).

3.2.5 Elasto-plasticity and elasto-plastic models

If the stress after the yielding point only produces plastic strains the model is called a linear elastic perfectly plastic model, where the yielding function coincides with the failure criterion (Potts et.al., 2002). The Mohr-Coulomb model is an example of this kind of model and it means that when the stresses reach the failure surface, which coincides with the failure criterion, no plastic straining occur before failure of the soil (Kullingsjö, 2007).

Another way of describing soil behaviour is with a linear elastic elasto-plastic model which means that a linear model is used to describe the elastic soil behaviour until a point on a defined yielding surface is reached (Chang-Yu, 2006). If the stress path passes this yield surface plastic strains occur and the behaviour is described with a plastic model. When passing the yielding point the yield stress increases due to this plastic straining (Potts and Zdravkovic, 1999). This behaviour is referred to as strain hardening and this goes on until the limit stress/strain on the failure surface is reached. The hardening parameter can be described by a yielding cone within the failure cone (Potts et.al., 2002). A similar behaviour, but for softening of the soil, can occur where the yield stress decreases with increased straining (Potts and Zdravkovic, 1999). The expansion or reduction of the yield surface causes a development of plastic strains which can be described with a flow rule (Kullingsjö, 2007). The flow rule describes the directions of strains at corresponding stress states and is defined with a scalar multiplier, Λ , depending on hardening/softening and a potential function, Q , that depends on stress and some state variables (Potts and Zdravkovic, 1999). Dilatancy effects are governed by the flow rule and are an important aspect with regard to volume change and soil strength. The plasticity theory states that when the plastic strain rates are described by vectors perpendicular to the yield surface, this is called associated plasticity (PLAXISa, 2012).

The yielding surface can be described with a function F , depending on stress and/or some hardening or softening parameter and it can be plotted in principal stress space (Potts and Zdravkovic, 1999). The function F is commonly described with a failure criterion such as Mohr-Coulomb, Drucker-Prager, von Mises or Tresca, where the

Mohr-Coulomb is the most common. If the yield function equals the potential function, the flow rule is said to be associated, and otherwise non-associated. The non-associated flow rule better describes soil behaviour but requires more computer memory.

If Mohr's circles, plotted for a test with two different cell pressures, are equal in size they will give the undrained shear strength at failure (Potts and Zdravkovic, 1999). This forms the failure criterion in equation (3.50).

$$\sigma_1 - \sigma_3 = 2c_u \quad (3.50)$$

This is in the Tresca model used as the yield surface function and rewritten as equation (3.51).

$$\sigma_1 - \sigma_3 - 2c_u = 0 \quad (3.51)$$

This function plots as a hexagonal cylinder in principal stress space, see Figure 3.16. It models a perfectly plastic state in undrained conditions with an associated flow rule.

The corners of the hexagonal cone have posed a numerical problem, hence the von Mises model has been used to simplify the yield surface to a circular cylinder, see Figure 3.19 (Potts and Zdravkovic, 1999).

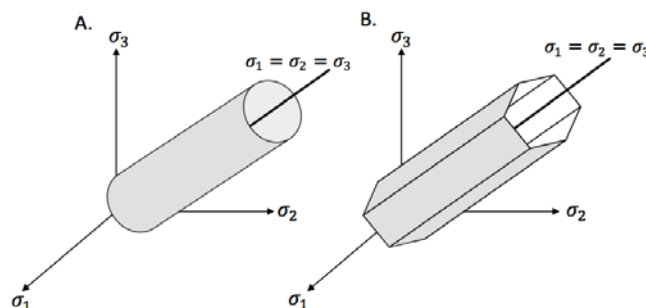


Figure 3.19. Von Mises yield criterion and Tresca yield criterion.

The Mohr-Coulomb model can be described with the failure criterion from Mohr's circles for effective stresses (Potts and Zdravkovic, 1999). The Mohr failure line can be rewritten as the yield function (3.52).

$$F = \sigma_1 - \sigma_3 - 2c' * \cos\phi' - (\sigma_1 + \sigma_3) * \sin\phi' \quad (3.52)$$

The yield function is represented by a hexagonal cone in principal stress space, see Figure 3.20 (Potts and Zdravkovic, 1999). If an associated flow rule is adopted, dilatant plastic volumetric strain may occur that is too large and never reach a limiting value, which is the case in reality. To solve this, a non-associated flow can be used instead, with the plastic potential depending on the dilatancy angle. The same

numerical problem as with the Tresca model can arise in the use of the Mohr-Coulomb model, hence the same simplification have been proposed for this case, forming the Drucker-Prager model, which plots as a circular cone, see Figure 3.20. The Drucker-Prager yield function can be described as in (3.53) (Potts and Zdravkovic, 1999).

$$F = q - (c' / \tan\phi' + p') * M_{JP} \quad (3.53)$$

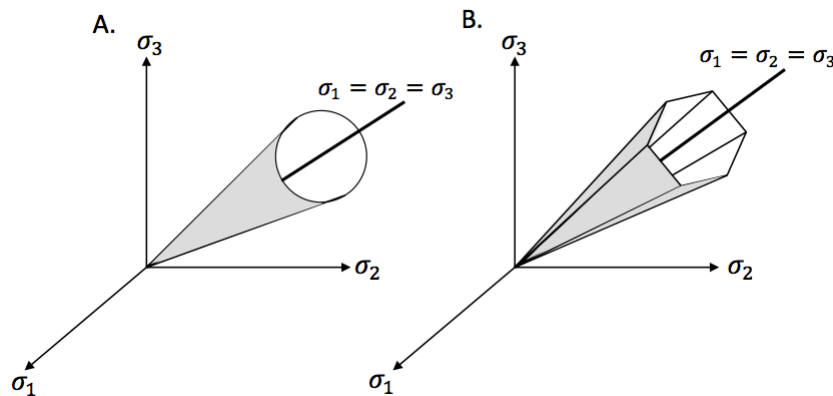


Figure 3.20. Drucker-Prager yield criterion and Mohr-Coulomb yield criterion.

Of the above mentioned models the most commonly used are the Mohr-Coulomb and Tresca models, based on effective and total stresses respectively, since these are the basis for conventional soil mechanics (Potts and Zdravkovic, 1999).

Drawbacks of the perfect plasticity models with linear elasticity are that it does not take deformation history into account which can produce unrealistic results (Potts et.al., 2002). Another disadvantage is that only contractancy can occur in the elastic zone and that the compression inside the yield cone is unlimited.

To deal with the problem of infinite compression a cap can be added to the yield cone which represents volumetric strain hardening (Potts et.al., 2002). For stresses on the yield cap this makes it possible to separate primary loading and reloading and capturing both irreversible volumetric and deviatoric strains.

3.2.6 Cam-Clay model

The Cam-clay model is an elasto-plastic model that is capable of simulating the non-linearity of a material as well as its plasticity. It can also simulate consolidation processes (Potts et.al., 2002). The shortcomings are that it cannot simulate anisotropy or over-consolidation behaviours (Chang-Yu, 2006). The difference between the original Cam-clay model and the modified model is the shape of the yield surface, which in the modified Cam-clay has the shape of an ellipse, as in Figure 3.21, which is more convenient in modelling aspects.

The basis for the Cam-clay model and thus the Modified Cam-Clay model is the critical state soil mechanics (Wood, 1990). The critical state is the point at which no volumetric strain occurs with the increase of shear strain. Equations (3.54) and (3.55)

describe the critical state. The yield surface of the Modified Cam-clay is also shown in Figure 3.21.

$$q = Mp' \quad (3.54)$$

$$e = e_{cs} - \lambda * \ln p' \quad (3.55)$$

e_{cs} = void ratio when $p'=1$ on the Critical State Line (CSL)

M = slope of CSL in p' - q -plane

λ = slope of CSL in e - $\ln p'$ -plane

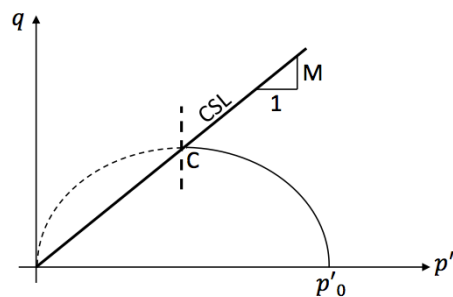


Figure 3.21. Yield surface of Modified Cam-clay.

The top point of the ellipse represents the critical state and is a point on a straight line from the origin for different yield surfaces (Potts and Zdravkovic, 1999). The slope of this line is the material parameter M_r . If yielding occurs to the left of the critical state point the soil contracts and hardening takes place while the opposite occurs to the left of the critical state.

As explained in chapter 3.1.5 a change in volume along the VCL is mainly plastic while the unloading/reloading line in the e - $\ln p'$ -plane means that the soil is in an over-consolidated state and no plastic strains occur (Chang-Yu, 2006). The equation for unloading/reloading can be expressed as in (3.56). The evaluation of λ and κ is shown in Figure 3.22.

$$e = e_K - \kappa * \ln p' \quad (3.56)$$

e_k = void ratio when $p'=1$

κ = slope of unloading/reloading line

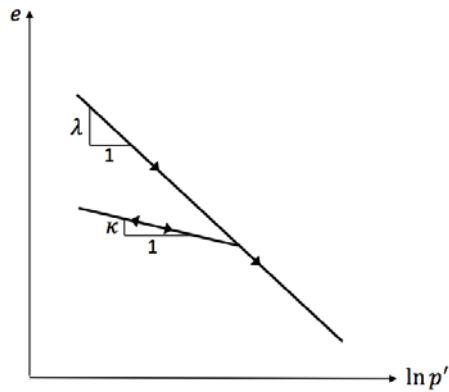


Figure 3.22. The VCL and unloading/reloading line from an incrementally loaded oedometer tests. Parameters used in the formulation of Modified Cam-clay model can be evaluated according to the graph.

The VCL, CSL and the unloading/reloading line can create a boundary surface in the e - q - p' -plane which can be projected onto the plane where $e=0$, hence onto the q - p' -plane, creating a yield surface.

The equations (3.57) and (3.58) are describing the yield surface for Cam-clay and modified Cam-clay (Potts and Zdravkovic, 1999):

$$F = q/p' * M_J + \ln(p'/p'_0) = 0 \quad (3.57)$$

$$F = (q/p' * M_J)^2 - (p'/p'_0 - 1) = 0 \quad (3.58)$$

p_0 is the value of the mean effective stress at the intersection between the swelling line and the VCL. This value controls the hardening/softening behaviour.

3.2.7 Elastic visco-plasticity

A model based on the theory of elastic visco-plasticity describes the elastic behaviour up to a yield stress after which it describes a rate dependent inelastic behaviour, i.e. the deformation of the material after the yield surface depends not only on the size of the applied load but also on the rate at which it is applied. The yield surface could either be predefined or have a strain rate dependency.

An important feature with the rate-dependent visco-plastic behaviour is that is, contrary to a rate-independent plastic behaviour, not only describes the permanent deformation after the submission of load, but also continue to undergo a creep flow as a function of time under the influence of the already applied load, which could be used to model creep for soft soils (Runesson, 2006).

4 Introduction to PLAXIS

The PLAXIS 2D is a finite element analysis program for deformation and stability calculations in geotechnical engineering and include a range of constitutive models for simulations of non-linear and time dependent behaviour of soil (PLAXISa, 2012).

PLAXIS automatically builds a finite element model i.e. generates a mesh. It divides the geometry into basic elements and structural elements and finds optimized triangles in an unstructured mesh (PLAXISb, 2012).

To be able to find a solution to a problem the program requires the stresses in the soil mass to be in equilibrium and that no holes, discontinuities or overlapping of elements occur, i.e. that the compatibility is fulfilled. Further it requires the constitutive behaviour of the material i.e. the stress-strain behaviour of the soil and finally the boundary conditions must be specified. (Potts et.al., 2002)

In PLAXIS the sign convention for stresses are the same as in mechanical theory, which means that compressive stresses are negative (PLAXISc, 2012).

4.1 Mesh generation

The elements in a finite element mesh should be as regular as possible to avoid numerical instability. The resolution of the mesh should be finer in areas with large stress and strain concentrations. Although the automatically generated mesh often is reliable, it sometimes may not be accurate enough to perform an acceptable numerical analysis. In such a case optional refinements could be done.

When a mesh has been generated for a finite element analysis of an engineering structure, it is often assumed that the deformation of the structure doesn't affect the mesh. This assumption will however not be valid for large deformations, which often is the case in a soil body.

4.2 Geometry and plain strain

Plane strain modelling means that if one dimension of the problem is very large compared to the others and the force is applied perpendicular to this dimension the analysis can be performed in one cross-section representing the whole geometry (Potts et.al., 2002). This means that no deformations are assumed to occur in this direction. Many geotechnical problems can be modelled with plane strain but in some cases, such as tunnelling problems, three-dimensional analysis is preferable. To model a tunnel in PLAXIS 2D will be a simplification of the problem.

For modelling an excavation the dimension of the geometry should be about 3-4 times the width of the excavation. This is because no deformations should be allowed at the boundaries.

4.3 Material models

There are several options when choosing a model in PLAXIS. This chapter presents the two models used in this project.

4.3.1 Hardening Soil

The HS model is a linear elastic elasto-plastic model. The yielding surface expands with plastic straining (Potts et.al., 2002) and the model can simulate both shear hardening and compression hardening behaviour (PLAXIS, Materials Model, 2012). It is based on the hyperbolic model, which describes the vertical strain and the deviatoric stress with a hyperbola that approaches a limit of the deviatoric stress. The model has some extra features compared to the hyperbolic model, such as the use of a yield cap explained in the previous chapter.

In this model the stiffness is dependent on stress levels and this behaviour is described with a power law according to the relationship presented in equation (4.1).

$$E_{oed} = E_{oed}^{ref} * \left(\frac{\sigma}{p^{ref}}\right)^m \quad (4.1)$$

where E_{oed} is the evaluated stiffness moduli at the stress, σ and E_{oed}^{ref} is the stiffness moduli at the reference stress p^{ref} . In PLAXIS p^{ref} is set to 100 kPa as a default value. The parameter, m is a power law parameter and could be set equal to 1, when modelling soft soils.

There are also relationships for E_{50} and E_{ur} including the power m and the reference pressure p^{ref} , the friction angle φ , and the cohesion c . The evaluated stiffnesses could be transformed, with regard to the reference pressure, using equations (4.2) and (4.3).

$$E_{50} = E_{50}^{ref} \left(\frac{c*\cos\varphi - \sigma'_3*\sin\varphi}{c*\cos\varphi + p^{ref}*\sin\varphi}\right)^m \quad (4.2)$$

$$E_{ur} = E_{ur}^{ref} \left(\frac{c*\cos\varphi - \sigma'_3*\sin\varphi}{c*\cos\varphi + p^{ref}*\sin\varphi}\right)^m \quad (4.3)$$

One drawback of the simpler models in PLAXIS is that compressive stresses can be infinite. In the HS model this can be dealt with by applying a yield cap, which is controlled by the input of an OCR or a pre-overburden pressure, POP. In the HS model, the cap yield surface is described by the function (4.4).

$$F^C = \frac{q^2}{\alpha^2} + p'^2 - p_p^2 = 0 \quad (4.4)$$

The parameter α is connected to K_0^{NC} , q is a measure of the deviatoric stresses and p_p is the isotropic pre-consolidation stress. The shape of the cap is an ellipse in the p' - q -plane which expands as a function of the pre-consolidation stress, see Figure 4.1.

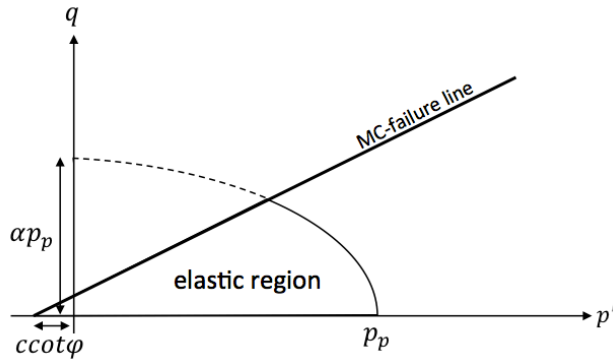


Figure 4.1. Yield surface in the HS model.

4.3.2 Soft Soil Creep (SSC)

Many problems in soft soil can be modelled with the HS model however, this model does not account for creep (PLAXISa, 2012). Soft soils differ in several aspects from hard soils where the compressibility is much higher and the stress dependency of soil stiffness is a linear relationship. The Soft Soil Creep (SSC) model uses the Mohr-Coulomb failure criterion and the Modified Cam-clay yield surface as a cap (Olsson, 2010).

The formulation of total strains can be divided into an elastic part and a time-dependent part. In the formulation used in the SSC-model this strain is defined as creep strains according to equation (4.5).

$$\varepsilon = \varepsilon^e + \varepsilon_{dc}^c + \varepsilon_{ac}^c \quad (4.5)$$

dc=during consolidation

ac=after consolidation

In the SSC model the equation (4.6) describes the total strains.

$$\varepsilon = A \ln \left(\frac{\sigma'}{\sigma_0} \right) + B \ln \left(\frac{\sigma_{pc}}{\sigma_{po}} \right) + C \ln \left(1 + \frac{t'}{\tau_c} \right) \quad (4.6)$$

The first term represents the elastic strain due to a change in effective stress. The second term of the equation describes the creep strains during consolidation depending on a change in pre-consolidation pressure. The last part is pure creep and is described with the time dependency parameters $\tau_c = \tau \left(\frac{\sigma_{pc}}{\sigma_p} \right)^{B/C}$, where τ is usually set to 1 day and the effective creep time $t' = t - t_c$, also described in chapter 3.1.7.

The parameters A, B and C are constants depending on the compression index, C_c , and the swelling index, C_s . They can also be related to the modified swelling index κ^* , the modified compression index λ^* and the modified creep index μ^* that are usually used as input parameters. The relationships and evaluation methods will be explained in chapters 5.4.2 and 5.4.3.

The extension to 3D can be described with the Modified Cam-clay ellipses in the p' - q -plane, see Figure 4.2, where the size of the ellipse is determined by the equivalent isotropic pre-consolidation pressure defined in equation (4.7). The pre-consolidation pressure is continuously updated so the position of the yield cap is time-dependant.

$$p_p^{eq} = p' - \frac{q^2}{M^2 * p'} \quad (4.7)$$

The parameter M is the slope of the CSL and is related to K_0^{NC} and the modified swelling- and compression indices.

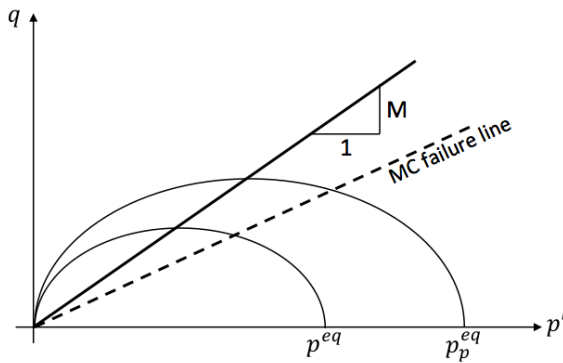


Figure 4.2. Yield surface in the SSC model.

Defining a generalised pre-consolidation pressure in 3D and replacing the one-dimensional creep strain in the differential creep equation with the volumetric creep strain, equation (4.8) is found for the volumetric creep strains, using the modified indices.

$$\varepsilon_V^c = \frac{\mu^*}{\tau} * \left(\frac{p^{eq}}{p_p} \right)^{\frac{\lambda^* - \kappa^*}{\mu^*}} \quad (4.8)$$

The factor $\frac{\lambda^* - \kappa^*}{\mu^*}$ is denoted the β -factor and is investigated in more detail in chapter 6.4.

The equation formulated above only accounts for volumetric creep strain, hence an expression for general creep strain must be formulated as well, including deviatoric creep strains. By adopting Hooke's law and p^{eq} as the potential function, the formulation ends up according to (4.9), where $\alpha = \frac{\partial p^{eq}}{\partial \sigma'}$

$$\varepsilon = [D]^{-1} * \underline{\sigma'} + \left(\frac{\varepsilon_V^c}{\alpha} \right) * \left(\frac{\partial p^{eq}}{\partial \underline{\sigma'}} \right) \quad (4.9)$$

The formulation of elastic strains in 3D will be addressed in chapter 5.4.2.

4.4 Calculation modes and procedures

This chapter describes some of the features used in PLAXIS. Focus lies on the procedures relevant for this project.

4.4.1 Drainage situation in PLAXIS

The finite element analysis can be executed in three different ways; a drained analysis, undrained analysis and partially drained analysis. The drained analysis is mainly used for friction material or for the long-term behaviour of clay. The undrained analysis is used for clay in the short-term perspective and for consolidation analysis. However, in most cases the soil is partially drained where all excess pore-pressure have not dissipated. This kind of analysis is performed with a coupled analysis, which couples the consolidation behaviour with the constitutive, equilibrium and continuity relationships.

The soil permeability often varies with depth and under isotropic conditions it can be set to vary linearly (Potts and Zdravkovic, 1999). If anisotropic conditions apply, specifications of the permeability for different directions can be used. The permeability can also be related and vary as a function of the void ratio, however, since there often is a lack of laboratory data to determine this relationship, the permeability is often set to vary with effective stresses instead.

There are three methods to evaluate undrained behaviour in PLAXIS, Method A, B and C. Only Method A will be relevant for this project and it refers to an effective stress analysis where effective strength parameters are used as input data (PLAXISa, 2012). One advantage of using effective strength parameters is that the increase of shear strength with increasing effective stresses is considered. However, in some models, the undrained shear strength is an output data that must be checked with real values, since it is often overestimated in this type of analysis. The reason for this is that the model follow an effective stress path while in real soil behaviour, p' reduces from the vertical effective stress path due to excess pore pressures caused by shear, according to Figure 4.3. Advanced models using a cap type yield surface will not produce this problem since one of the purposes of the cap is to adjust for this inaccuracy.

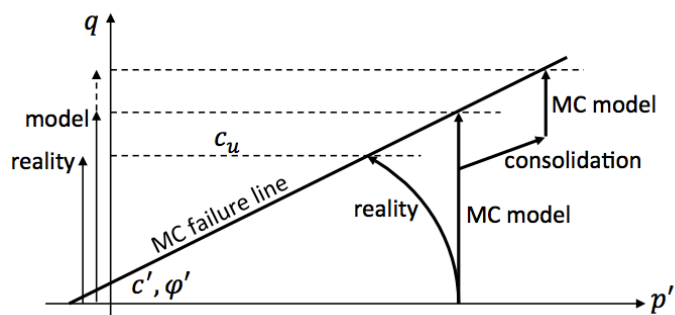


Figure 4.3. Stress path in the MC model compared to real soil behaviour.

4.4.2 Initial stress generation

The initial stresses are one of the most important parameters in soil modelling with finite element analysis. Two methods exist to be able to calculate these stresses, the direct input method and the gravity loading. The direct method is in PLAXIS called the K_0 -procedure and means that the vertical and horizontal stresses are calculated at points in the ground according to the definition of σ_v and σ_h stated in previous chapters. This method requires that the ground surface is horizontal and the soil layers parallel to the ground surface (PLAXISb, 2012). For normal consolidated soils the equations used in PLAXIS is (4.10) and (4.11) in this procedure.

$$K_0 = 1 - \sin\varphi' \quad (4.10)$$

$$K_0 = \frac{\sigma_h}{\sigma_v} \quad (4.11)$$

The coefficient for lateral earth pressure increases with the degree of over-consolidation (PLAXISb, 2012). In PLAXIS this is considered when using the K_0 -procedure for generating initial stresses in advanced models such as SSC and HS. Calculation of the current earth-pressure coefficient is done according to equation (4.12).

$$K_{0,x} = K_0^{NC} * OCR - \left(\frac{v_{ur}}{(1-v_{ur})} \right) * (OCR - 1) \quad (4.12)$$

Very high or very low values of K_0^{NC} should be avoided in order not to make the soil fail when generating the initial stresses (PLAXISb, 2012).

While the K_0 procedure gives a good ratio of the horizontal stresses over the vertical as long as the geometric conditions is horizontal, models with slopes, inclining phreatic level or soil layers etc., the Gravity loading option should be used (PLAXISb, 2012). The gravity loading method means that body forces acts through the whole area to solve for the initial stresses for each element.

When K_0 is differs from 1 the initial stress states calculated in the initial phase could reach the failure criterion, causing plastic points in the soil. This could be solved by adding a plastic nil-step, where no additional load is applied, so that the stress field can reach equilibrium. The deformations caused by the plastic nil-step should be reset to zero in the following calculation phase.

4.4.3 Calculation modes and analysis type

In PLAXIS the calculations for the finite element analysis could be done in three different calculation modes; classical mode, advanced mode or flow mode, which will be explained below (PLAXISb, 2012).

The default is the Classical Mode in which Terzaghi's definition of stress is used, defined in equation (3.5). Furthermore pore pressures are divided into steady state,

which is generated by the input of phreatic levels (or groundwater flow), and excess pore pressure, which is generated during plastic calculations or consolidation analysis in undrained material. The phreatic level also adjusts the saturated weight of the soil. In this mode it is conceivable to perform plastic calculations, calculations of consolidation based on excess pore pressure and safety calculations.

Since a geotechnical problem is divided into phases in PLAXIS, different types of analysis could be executed for each phase (PLAXISb, 2012).

In the initial phase an initial stress is generated according to chapter 4.4.2. For the other phases there are different choices of calculation such as Plastic, Consolidation, Safety and Dynamic. In this report it is only relevant to use the plastic and consolidation options.

To carry out an elastic-plastic deformation analysis a plastic calculation is used. It does not account for the decay of excess pore pressure with time and could be used for drained analysis as well as an undrained analysis for a short-term scenario (PLAXISb, 2012). A drained analysis could be done to assess the settlements after a long time with reasonable accuracy. This will however not give the intermediate loading history.

The consolidation calculation does a full analysis of the decay of excess pore pressure as a function of time (PLAXISb, 2012). The load should generally be applied in a plastic phase before the consolidation phase is performed.

5 Parameter evaluation

This chapter presents the available data for this project and the different methods used for evaluation of essential parameters.

The data from the area around Tingstad came from different sources. The investigations were executed in the years 1960-1963 by SGI, AB Skånska Cementgjuteriet (Skanska) and Göteborg Stads Gatukontor. Some investigations for the construction of Gullbergs junction and Ringö junction was available and consisted of pyramid penetration tests, vane tests, weight probing and some sampling with a standard piston sampler. The laboratory tests consisted of standard lab tests, fall cone tests and a few oedometer tests, though difficult to evaluate.

Data from a project in 2008 around Tingstadsvass was also available which included pyramid penetration tests, vane tests and sampling with a helical auger.

No data from boreholes located in the river could be found from the investigations regarding the tunnel.

Since the data from Tingstad is insufficient and difficult to evaluate in full, more recent data from the Marieholm investigations have been evaluated. For orientation see Figure 5.1 below. The available data was the RGeo established by WSP in 2004 with some of the enclosed geotechnical investigations. The investigations consisted of several pyramid penetration tests, percussion sounding, CPT, soil/rock-probing and pore pressure measurements. The pore pressure was last recorded in July 2004. Several vane tests as well as sampling with helical auger and standard piston sampler were included. The laboratory works, performed by SGI, included standard lab tests, CRS-tests, direct shear tests in 8 different boreholes and 6 triaxial tests from 5 different boreholes on different levels.

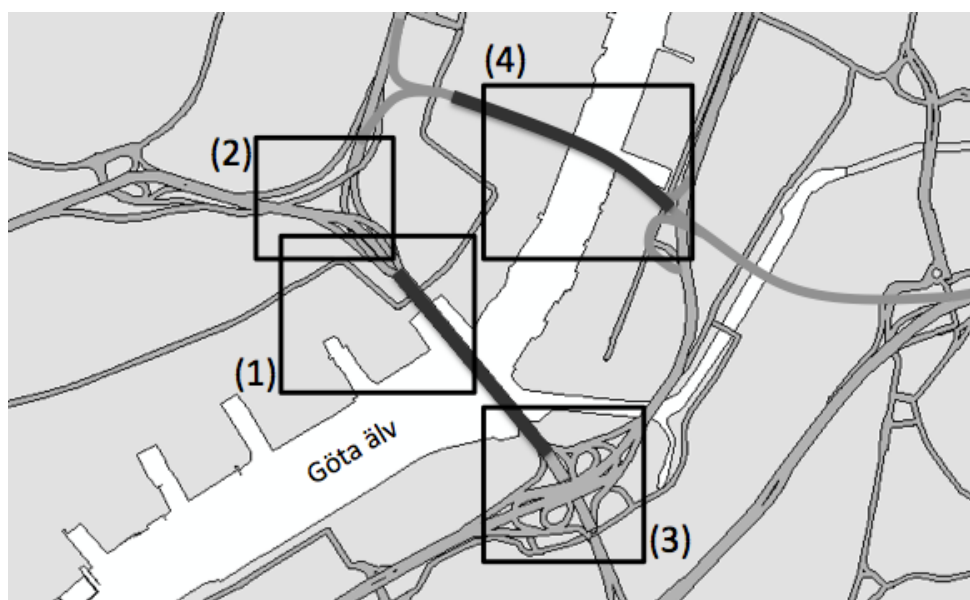


Figure 5.1. Map over central Gothenburg and areas of interest marked with squares; (1) Tingstadsvass, (2) Ringö junction, (3) Gullbergs junction and (4) Marieholm (SWEGIS, 2006).

5.1 Introduction to some field and laboratory tests

This chapter presents an overview of some methods for geotechnical investigations that have been evaluated in this project.

There are several in-situ methods for determining the shear strength, such as the vane test and the cone penetration test (Sällfors, 2001). In many cases the field test tend to underestimate the shear strength and the use of more advanced laboratory methods might in many cases be necessary (Kullingsjö, 2007).

Vane tests are performed with a probe of two intersecting panels that are pressed into the soil (Sällfors, 2001). At approximately every meter the probe is rotated until failure occurs. The obtained value needs to be reduced with the liquid limit.

The CPT test is performed with a probe, with an advanced mechanical or electrical cone at the end that is pressed into the soil. The different parameters are then measured and from this the undrained shear strength can be obtained as well as an estimation of the pre-consolidation pressure and the OCR (Larsson, 2007). Soil layers, pore pressure and other important information can also be obtained from this kind of test.

The direct simple shear test (DSS) is performed by putting a soil specimen in a shear box and apply a shear stress on the top of the specimen creating a pure shear stress situation. The drainage situation can be controlled in this testing procedure.

A triaxial test gives the most information of all laboratory shear tests. It is performed by vertically loading a cylindrical sample and register changes in pore pressure, stresses and deformations (Kompetenscentrum Infra, n.d.). There are three different boundary conditions of importance when performing a triaxial test; stresses, strains and pore pressure. A test can be executed under drained or undrained conditions. In the drained test, no excess pore pressures are allowed to form and the water can dissipate. In the undrained test there is no change in volume and this test can be performed in a shorter amount of time. The most common triaxial tests are the active, the passive and the K_0 , where the passive test means a decrease in vertical pressure, e.g. an extension test. The active test is done in the opposite way and is hence a compression test. The K_0 -test means that both the axial stress and the radial stress are increased so that the diameter of the sample is constant which also means that this type of test only can be performed under drained conditions. Before the start of the test the sample is consolidated to stresses, like the in-situ stresses, to be able to simulate reality in the best way possible.

The different tests results in different stress paths, for undrained and drained conditions, in p' - q - space as shown in Figure 5.2 and 5.3 (Kompetenscentrum Infra, n.d.).

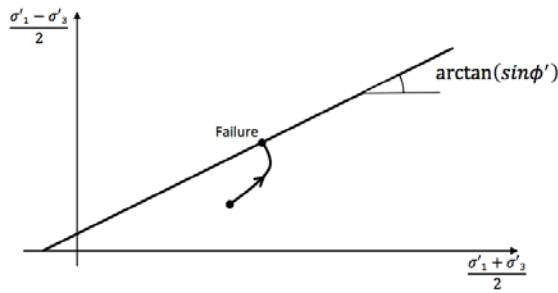


Figure 5.2. Stress path for undrained compression (Kompetenscentrum Infra, n.d.).

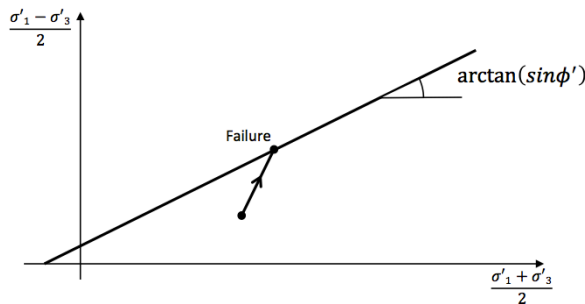


Figure 5.3. Stress path for drained compression (Kompetenscentrum Infra, n.d.).

From the stress paths, parameters such as the active and passive shear strength, the pre-consolidation pressure, E-modulus and the effective cohesion can be determined (Kompetenscentrum Infra, n.d.). If only one sample of the soil mass is tested the effective friction angle can be assumed to be 30° , otherwise all tests can be plotted in the same graph and the friction angle can be determined.

Compression characteristics and creep parameters for a soil can be obtained from an oedometer test. The test is performed by placing a sample in a confining ring and a vertical load is applied. The load can either be applied stepwise or with a constant rate. The latter is called a CRS and is the most common method in Sweden (Sällfors, 2001).

Through measuring of excess pore pressures a curve is obtained with either vertical stress against void ratio or vertical stress against strain. The CRS test is normal performed with a strain rate of 0.7 %/h and the evaluation is performed in a plot with a fixed ratio, usually 10/1 for stress/strain (Olsson, 2010). This is important to consider when evaluating raw data in Excel. The pre-consolidation stress evaluated from the CRS test is reduced due to strain rate, hence when doing back calculations, the pre-consolidation pressure might be higher than the evaluated value. In the beginning of testing there is no volume change since the pore pressure carries the load initially (Olsson, 2010). Hence the axial strain is equal to the volumetric strain.

5.2 Investigations from Ringömotet and Tingstadsvass

Boreholes along a longitudinal section along the center axis of the tunnel were investigated with emphasis on BH 1148 for evaluation of the soil profile.

The shear strengths for the different boreholes were plotted in graphs which can be seen in Appendix C. The shear-strength was evaluated according to equation (5.1).

$$c_u=7+1.5d \quad (5.1)$$

d starts from the mean water level +10.

The weight of the soil and the water content was also plotted for comparison with the data from Marieholm.

The shear strength from the more recent boreholes in Tingstadsvass was also plotted, see Appendix C. The evaluated shear strength was plotted in the same graph to see the correlation which corresponded well with the measurement.

5.3 Investigations from Gullbergsmotet

Old geotechnical investigations from Gullbergsmotet have been studied in order to get an overview of the soil profile and soil properties in the tunnel area. The old data are difficult to evaluate but some soil properties have been obtained from the geotechnical report issued by SGI. The soil layers consist of clay to large depths with an overburden of sand and/or fill with a depth of 2-3 meters, as well as a layer of muddy clay in the Gullbergsån and Sävån river trenches.

According to the SGI report, a slight pore-overpressure was measured in 1960, both in the Göta älv and the location of the southern ramp. This was probably due to ongoing settlements from previous construction. Since it is an urban area this situation could be assumed to still be the case. The extent of the overpressure has not been found from the old geotechnical data. .

The shear strength, water content and weight of the soil was plotted according to Appendix C. The evaluated shear strength corresponded well with the measurements.

5.4 Investigations from Marieholm

To evaluate the clay properties from the Marieholm test data, several boreholes were compiled, separating data from the river, the eastern side and the western side of the river. However since no significant deviation where found, the presented parameters below are average data of all evaluated boreholes at Marieholm. Graphs of the evaluated parameters are presented in Appendix C.

The data showed relatively homogenous clay typical for Gothenburg and could be assumed to be relevant for the site of the Tingstad tunnel. The soil layers in the shore areas consist of a 2 – 4 meter thick layer of fill above a 60 – 100 meter thick clay layer. Beneath the clay is a layer of friction material of undefined thickness. The soil profile in the river consists of clay overburden by sediments.

Except from the extent of the fill layer, no consistent difference where seen along the tunnel stretch. The variation of local data was larger than the differences between the riversides.

Density

The density of the clay is in the upper soil layers close to 1.6 t/m^3 , with a tendency to be slightly lower (1.55 t/m^3) on a depth of 15 to 25 m beneath the ground surface, where after it increases gradually to about 1.65 t/m^3 .

Shear strength

The evaluation of the general undrained shear strength of the clay at Marieholm gave the relationship in (5.2).

$$c_{uk} = 15 + 1.5z \quad (5.2)$$

with z starting from level +5 which seems reasonable compared to earlier studies of the clay in Gothenburg and also corresponds well with the evaluated shear strength from the Tingstad investigations.

Water content and liquid limit

For the evaluated boreholes at Marieholm, the clay has a natural water content, w_N of 70 – 90 percent near the ground surface and 55 – 60 percent at 60 meters depth, while the liquid limit, w_L range between 65 – 85 percent the first 60 meters and 60 – 80 percent below that.

Pore pressure

The pore pressure is evaluated to be hydrostatic for simplification of calculations even though a small excess pore pressure of 3 kPa is apparent at 50 meters depth, with a groundwater surface at +10.

OCR

The OCR, at the examined stretch was evaluated to 1.25 – 1.35, which can be seen in Appendix C.

5.4.1 Estimation of K_0^{NC}

According to Jaky's formula, stated in equation (3.7) the K_0^{NC} -value is depending on the effective friction angle. Assuming $\varphi' = 30^\circ$ gives $K_0^{NC} = 0.5$. As a reference, an evaluation of the empirical formula stated in equation (3.8) was also made which correlated the liquid limit to K_0^{NC} . An average value was calculated to $K_0^{NC} = 0.69$.

In PLAXIS, the $K_{0,x}$ -value is calculated according to equation (4.12). Table 5.1 presents the $K_{0,x}$ -value for the corresponding K_0^{NC} -value for an OCR of 1.3 and $v_{ur} = 0.15$.

Table 5.1. Correlation between K_0^{NC} and $K_{0,x}$ in PLAXIS.

K_0^{NC}	$K_{0,x}$
0.5	0.60
0.69	0.85

The former value seem more realistic in combination with an issue in PLAXIS where very large values of $K_{0,x}$ should be avoided since it could lead to soil failure.

5.4.2 Evaluation of the modified swelling and compression index

An idealized oedometer curve for a one-dimensional compression test was used for evaluation of the modified swelling and compression indices that are used in the SSC model. The curve is divided into incremental steps of elastic strains and creep strains according to Figure 5.4.

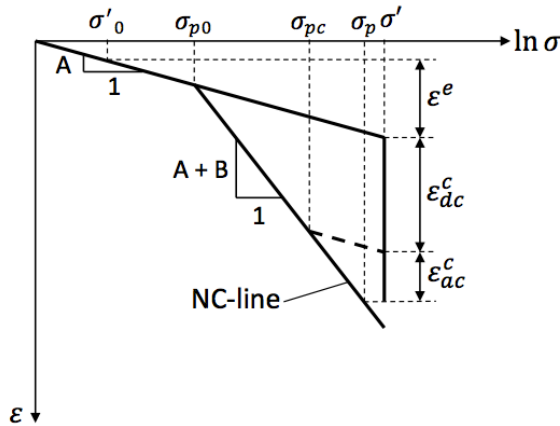


Figure 5.4. Idealized oedometer curve for one-dimensional compression test.

The constants A and B are used in the formulation of the differential law for 1D-creep strains explained in chapter 4.3.2. The slope of the unloading/reloading line, which corresponds to the elastic part of the curve at the beginning of loading, equals A, see Figure 5.4. When extending the formulation in 3D the elastic strains are depending on the mean stress, p' , and not the principal stress, σ' , as in 1D. A conversion for one-dimensional compression can be described by equation (5.3) and (5.4) which in turn will give equation (5.5).

$$3p' = (1 + 2K_0^{NC})\sigma' \quad (5.3)$$

$$3p'_0 = (1 + 2K_0^{NC})\sigma'_0 \quad (5.4)$$

$$\frac{p'}{p'_0} = \frac{\sigma'}{\sigma'_0} \quad (5.5)$$

For the 3D-formulation equation (5.6) is valid and for 1D, equation (5.7) is valid. From these equations it shows that the modified swelling index, κ^* could be set equal to A.

$$-\varepsilon_v = \kappa^* \ln\left(\frac{\sigma'}{\sigma'_0}\right) \quad (5.6)$$

$$-\varepsilon_v = A \ln\left(\frac{\sigma'}{\sigma'_0}\right) \quad (5.7)$$

Equations (5.6) and (5.7) are valid for normal consolidated soils. For over-consolidated soils the derivation in equation (5.8) is assumed in the model, which for a $v_{ur}=0.2$ will give $\kappa^*=2A$.

$$\kappa^* \approx \frac{3(1-v_{ur})}{(1+v_{ur})}A \quad (5.8)$$

The slope of the primary loading line in Figure 5.4 is denoted A+B. The constant B is related to the modified swelling and compression index according to equation (5.9).

$$B = \lambda^* + \kappa^* \quad (5.9)$$

For the project investigated in this report, the available data came from CRS-tests from Marieholm. Four different boreholes from Marieholm were evaluated where the raw data was extracted from an image of the CRS-curve and plotted in Excel.

By plotting the natural logarithm of the vertical stress, σ'_v , against the volumetric strain, which in a oedometer-test is equal to the vertical strain, λ^* and κ^* could be calculated according to the relationships presented above.

The calculations was done for several levels for each borehole and the data was then compiled in a diagram with κ^* and λ^* respectively plotted against level which can be seen in Appendix C. An average value was calculated as well as a standard deviation to obtain a range of values to be tested in the soil test facility. The values can be seen in Table 5.2.

Table 5.2. Evaluated range of λ^* and κ^* .

Parameter	Average	Standard dev.	Min	Max
λ^*	0.20	0.03	0.17	0.23
κ^*	0.2	0.005	0.015	0.025

For comparison, the value of λ^* can be compared to M_L evaluated from CRS-tests according to the relationship in equation (5.10).

$$\lambda^* = \frac{1.1\sigma'_{v0}}{M_L} \quad (5.10)$$

A rough calculation is made in Table 5.3 for different stress levels. Since M_L from CRS tests range from approximately 500 to 1000 according to Appendix C, the evaluated λ^* are reasonable.

Table 5.3. Comparison between λ^* and M_L for a stress level of 100 kPa.

λ^*	σ'_{v0}	M_L
0.17	100	647
0.20	100	550
0.23	100	478

5.4.3 Evaluation of the modified creep index

The modified creep index can be obtained by plotting the volumetric strain against the logarithm of time from a stepwise oedometer test (PLAXIS Material Model).

There is a couple of empirical ways of calculating the SSC creep index parameter, μ^* empirically. Mesri and Castro (1987) cited in Olsson (2010) showed a relationship between C_C and $C_{\alpha e}$ according to equation (5.11).

$$\frac{C_{\alpha}}{C_C} = 0.04 \pm 0.01 \quad (5.11)$$

By using the equations for calculations of C_C and C_{α} the creep parameter, μ^* could be evaluated by a combination of the formulas (5.12) and (5.13) to obtain equation (5.14). In further validation of parameters this method will be referred to as Method 1.

$$C_C = \lambda^* * 2.3 * (1 + e_0) \quad (5.12)$$

$$C_{\alpha e} = \mu^* * (1 + e_0)/0.435 \quad (5.13)$$

$$\mu^* = \lambda^* * 2.3 * 0.435 * (0.04 \pm 0.01) \quad (5.14)$$

Another empirical method is the correlation with the natural water content w_N established by Christensen (1995) cited in Olsson (2010) for Swedish and Norwegian clays, according to equations (5.15) and (5.16). This method will further be referred to as Method 2.

$$r_s = \frac{75}{(w_N)^{1.5}} \quad (5.15)$$

$$\mu^* = \frac{1}{r_s} \quad (5.16)$$

A third method to evaluate μ^* , referred to as Method 3, is by using the secondary compression coefficient, α_s . It depends on the compression, where it is very low until a critical compression is reached after which it increases fast up to a limit compression, where it starts to reduce. The critical compression is said to be $0.8\sigma'_c$. α_s can be related to the liquid limit and guideline values have been established in Larsson, Bengtsson and Eriksson (1997).

For the evaluation in this project, α_s was taken from the guideline table in Larsson, Bengtsson and Eriksson (1997) and the modified creep index, μ^* , could be calculated according to equation (5.17).

$$\mu^* = \frac{\alpha_s}{2.3} \quad (5.17)$$

The modified creep index was calculated from the same boreholes as κ^* and λ^* . A comparison was made between the different methods.

A comparison with Method 3 showed an average value of 0.005 which indicates that the values evaluated with the other methods are in the upper range. Hence a choice was made about the range of parameters used in the model based on the three different methods of evaluation. The chosen parameters are shown in Table 5.4 and the range for each individual method is shown in Appendix C.

Table 5.4. Chosen range of the modified creep index μ^ based on evaluations seen in Appendix C.*

	Min	Average	Max
μ^*	0.004	0.005	0.007

5.4.4 Evaluation of swelling and compression index

Alternative parameters that can be used as input parameters for both HS and SSC are the swelling index, compression index and creep index which is defined in chapter 3.1.5.

There exist a relationship, presented in equations (5.18) and (5.19), between the swelling and compression indices and the modified swelling and compression indices (Olsson, 2010).

$$C_r = C_s = \frac{\kappa^* \cdot 2.3 \cdot (1 + e_0)}{2} \quad (5.18)$$

$$C_c = \lambda^* \cdot 2.3 \cdot (1 + e_0) \quad (5.19)$$

The void ratio in the equations can either be the initial void ratio or the average void ratio during an oedometer test. If the parameters are used in the SSC model, PLAXIS will convert them into the modified indices according to the relationships above.

The parameters can be back-calculated from a CRS test where a plot can be constructed of void ratio and $\log(\sigma')$. The void ratio at the end of the test can be calculated according to equation (5.20) (Craig, 2004). If the water content after the test is available it can be used to calculate the in-situ void ratio.

$$e_1 = w_1 * G_s \quad (5.20)$$

w_1 = water content at the end of testing

G_s = Specific gravity, set at 2.73

Knowing the thickness of the sample and the change of thickness during the test (or the strain at the end of the test) the initial void ratio can be calculated by first equating the change in void ratio according to (5.21). The initial void ratio will be defined according to equation (5.22).

$$\frac{\Delta e}{\Delta H} = \frac{1+e_1+\Delta e}{H_0} \quad (5.21)$$

$$e_0 = e_1 + \Delta e \quad (5.22)$$

From these calculations a relationship between the change in sample height and void ratio can be obtained. A plot can then be made with the logarithm of the vertical stress on the x-axis and the void ratio on the y-axis.

The compression index and swelling index can then be evaluated as the inclination of the plastic part of the curve and the elastic part respectively.

A forward calculation was also performed for comparison since data of the water content before and after testing was not found. Initial water content from lab-tests for BH 14008 was used when calculating e_0 which was used in further calculation of the change in void ratio.

The result was then used as input values in PLAXIS to see which corresponding modified indices were generated. The result can be seen in Table 5.6.

Table 5.5. Evaluated alternative parameters with corresponding basic parameters obtained from PLAXIS.

Alternative parameters		Basic parameters	
C_c	1.5	λ^*	0.20
C_s	0.07	κ^*	0.019
C_α	0.06	μ^*	0.008

The corresponding modified indices are within the evaluated range of the basic parameters, see Appendix C, and will hence be included in the verification of parameters. This means that the alternative parameters does not need verification and will not be used in the modeling.

6 Verification of soil models and parameters through soil test simulation

Simulation of soil tests can be performed in PLAXIS soil test facility. It provides a comparison of the behaviour defined by the soil model and the parameters of a soil data set with the results of a real laboratory test. It is possible to do the simulation for any PLAXIS model and for five different tests; Triaxial, Oedometer, CRS, Direct Shear Strength and General.

The feature could be used to optimise model parameters and hence finding the optimal fit between the model results and the result of a real laboratory test. If a model is capable of capturing the behaviour of a laboratory test it indicates that the model can capture the behaviour of the soil in modelling a full-scale project (Olsson, 2010).

For this project the soil test facility is used to back-calculate laboratory tests to verify the model behaviour and to calibrate input parameters.

6.1 Evaluation and verification of soil parameters

Soil tests using the HS and SSC models were performed with test data from Marieholm for both triaxial tests and CRS tests. The boreholes chosen for investigation were based on the amount of raw data available and the location of the boreholes. No raw data files from the CRS-tests were available, hence the data were retrieved from an image of the CRS-test using Datathief.

6.1.1 CRS-tests with the SSC model

In the CRS simulation an evaluation of the parameters κ^* , λ^* and μ^* was made. Simulations for one sample were first performed and the most correlating set of parameters were then tested on another sample at a different level for comparison.

In the SSC model the stiffness's are stress dependent. The top of the soil layer experience zero vertical stress which will produce very small stiffness's. Hence large deformation will occur at the beginning of loading unless an initial stress is applied in the soil test facility. This is possible in the general mode which was used for the CRS-simulations. An initial stress of 5 kPa was added.

From the CRS-curves approximate vertical pre-consolidation stresses were obtained and used as input data. The friction angle was initially set to 30° and c' was calculated from the empirical relationship presented in equation (6.1).

$$c' = 0.1 * c_u \quad (6.1)$$

The simulated CRS-test cannot represent a real CRS test. The effective stresses in the real sample are calculated according to equation (6.2).

$$\sigma' = \sigma + 2/3u_B \quad (6.2)$$

u_B is the pore pressure at the bottom of the sample. The reason for taking 2/3 of the bottom pore pressure is to obtain an approximate average value over the sample since the sample cannot be divided into infinite layers to be able to plot the CRS-curve. To see the differences between a real soil test and the soil facility, a scale model of the sample was modeled in PLAXIS where the pore pressure at 2/3 of the sample was used to calculate the effective stresses and then compared to the simulated test in the soil test facility.

Three simulation set-ups were performed for each stiffness parameter, where one of the stiffness parameters were varied between the lower, mean and upper value evaluated from the borehole data, see Table 6.1. The simulations were then compared with measurement data for several boreholes to be able to see the correlation with different boreholes.

Table 6.1. Range of parameters investigated in the soil test facility.

Parameter	Min	Average	Max
λ^*	0.17	0.20	0.23
κ^*	0.015	0.2	0.025
μ^*	0.005	0.004	0.007

It was shown that the maximum value for λ^* had the best correlation when testing on two different boreholes at two different depths. The lower value of κ^* showed the best correlation with the measurement data. The parameters for μ^* was chosen with regard to the sample level and was given a range with regard to the different methods of evaluation. The simulations showed a small scattering and the curves almost coincided.

A test was done with the maximum value of μ^* , the maximum value of λ^* and the minimum value of κ^* and a fairly good match was found, which can be seen in Figure 6.1 and 6.2. The scale model was done for borehole 110 at a depth of 12 meters, corresponding to level +0.1 m and with the same parameter setup. The result is shown in Figure 6.1. The input parameters for both simulations in SSC can be seen in Table 6.2.

Table 6.2. Input parameters for borehole 110 at level +0.1.

	λ^*	κ^*	μ^*	σ'_c	K_0^{NC}	c'	φ'	k	ν_{ur}
SSC	0.23	0.015	0.007	110	0.66	3	30	1E-5	0.2

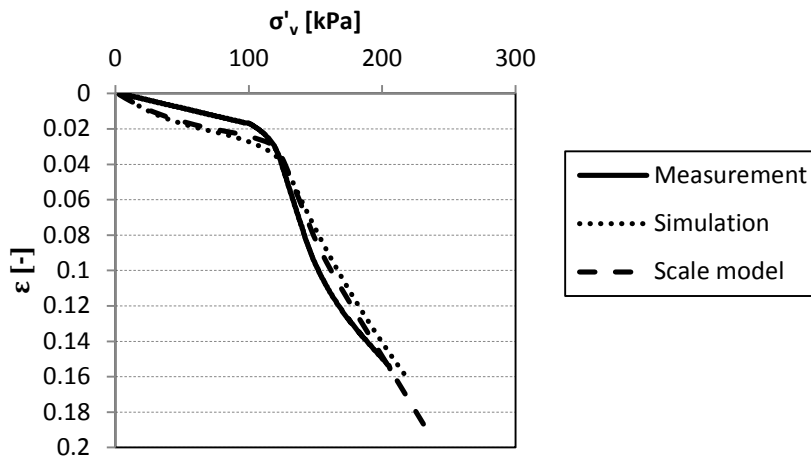


Figure 6.1. CRS simulation with soil test facility and full scale model compared to measurements for borehole 110 at level +0.1.

The parameters used in the simulation done for borehole 12001 at a depth of 48 meters, corresponding to a level of -37.9 meters, can be seen in Table 6.3. It is the same values except for the pre-consolidation pressure.

Table 6.3. Input parameters for borehole 12001 at level -37.9 m.

	λ^*	κ^*	μ^*	σ'_c	K_0^{NC}	c'	φ'	k	ν_{ur}
SSC	0.23	0.015	0.007	330	0.66	3	30	1E-5	0.2

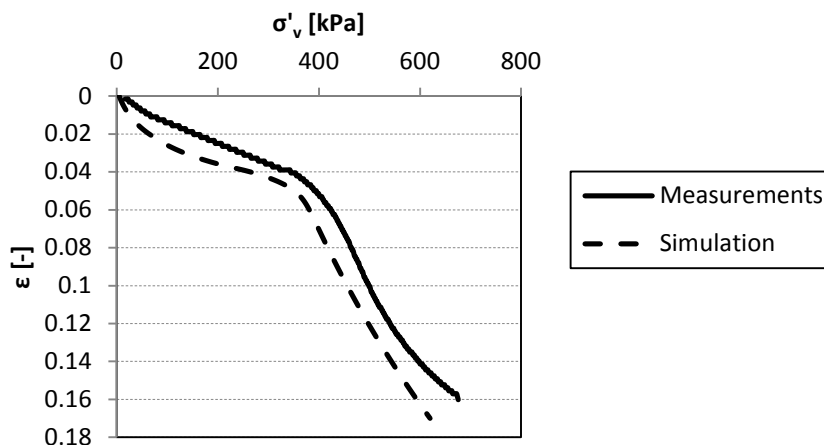


Figure 6.2. CRS simulation with soil test facility compared to measurements for borehole 12001 at level -37.9.

6.1.2 Triaxial-tests with the SSC model

Four triaxial tests were performed in the soil test facility at different depths.

The steepness of the elliptical cap yield surface is dependent on the M-value, which is the slope of the CSL. This value in turn depends on the stiffness parameters and the K_0^{NC} -value. The size along the p' -axis is determined from the isotropic pre-consolidation pressure, which is calculated from the vertical pre-consolidation pressure. The failure surface depends on c' and φ' . This gives six parameters that can be varied in the soil test to form different stress paths.

The first borehole was 11004 at 10 meters depth. At first a simulation of the effects of changes in stiffness was made. Changing λ^* to the minimum value lowered the cap which corresponded well with the measurements. The simulation and the measurement are however not a perfect fit. Keeping the λ^* value as the minimum value, κ^* was changed to the maximum value. The effect of this change was small, hence κ^* was kept constant in the further modeling. A test of the effect of μ^* was also done which also showed a quite small effect on the stress path.

The K_0^{NC} -value was changed and a good fit was obtained with a quite high value of $K_0^{NC}=0.66$. A combination with the maximum value of λ^* and a $K_0^{NC}=0.64$, also showed a good fit.

Concerning the strength parameters the empirical formula for obtaining c' was used and φ' was initially set to 30° . For borehole 11004 a $c'=3$ and $\varphi'=30^\circ$ corresponded well with the measurements. The result shows in Figure 6.3 and the input data in Table 6.4 and 6.5.

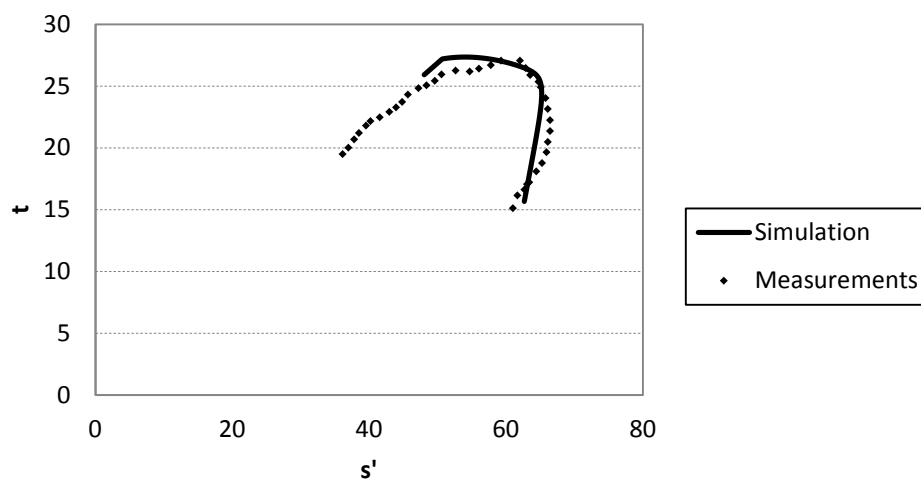


Figure 6.3. Triaxial simulation with soil test facility compared to measurements for borehole 11004 at level +1.9.

The second modeled borehole was 13114 at 12 meters depth corresponding to level +0.3. The consolidation phase was special for this sample with a preloading of 138 and 83 kPa followed by an unloading to 78 and 67 kPa. This was considered by adding a K_0 for the consolidation of 0.86.

Table 6.4. Input data for triaxial test simulation.

Indata	11004_10m	13114_12m	21015_60m	21015_66m
λ^*	0.23	0.23	0.23	0.23
κ^*	0.015	0.015	0.015	0.015
μ^*	0.007	0.007	0.007	0.007
c' ref	3	4	5	7
ϕ'	30	30	30	28
K_0^{NC}	0.64	0.6	0.66	0.63

Table 6.5. Input parameters, kept constant.

v_{ur}	γ	OCR
0.2	16	1.3

The same test configuration as borehole 11004 did not show a good correlation. A change in λ^* showed no large effect, hence the K_0^{NC} value was changed to 0.6 which, together with a slight change in K_0 for the consolidation to 0.82, showed a relatively good correlation. The strength parameters seemed to match well with the measurements as shown in Figure 6.4.

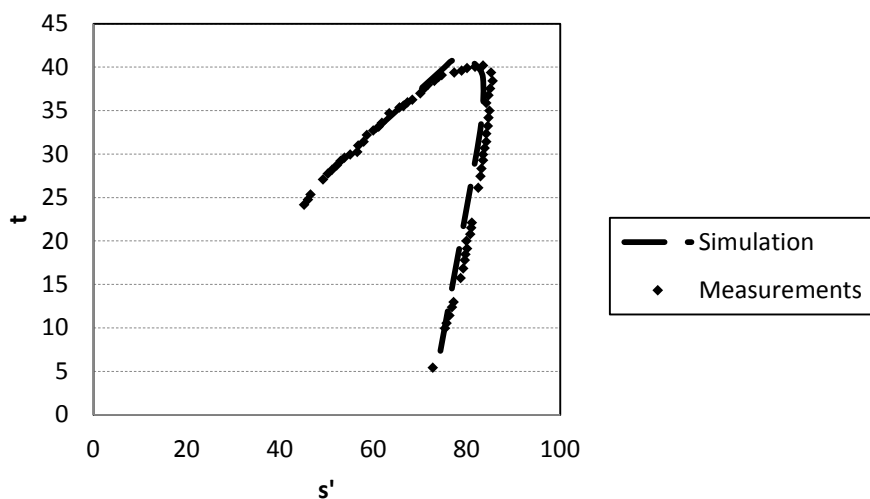


Figure 6.4. Triaxial simulation with soil test facility compared to measurements for borehole 13114 at level +0.3.

The test configuration from BH 13114 was then tested on BH 21015 for level -47.5. The result did not show a good correlation so changes was made in the λ^* -value

which gave a negligible effect. The K_0^{NC} -value was raised to 0.66 which showed a relatively good correlation with regard to the cap yield surface. The strength parameters, however, was not correlating. A lowering of c' showed a better correlation which can be seen in Figure 6.5 with the final input data shown in Table 6.4.

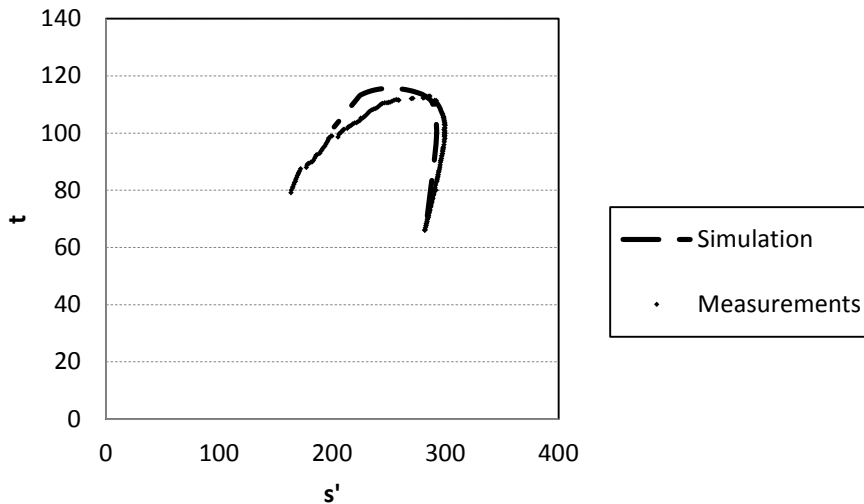


Figure 6.5. Triaxial simulation with soil test facility compared to measurements for borehole 21015 at level -47.5.

BH 21015 for level -53.5 was tested for the same configuration as for -47.5. The cap seemed to correlate well with the measurements but the strength parameters did not. A test was done with a lowered c' which showed a slightly better correlation but a worse correlation with the cap yield surface. A small change in both c' and K_0^{NC} was done which showed a better correlation which can be seen in Figure 6.6 with the final input data shown in Table 6.4.

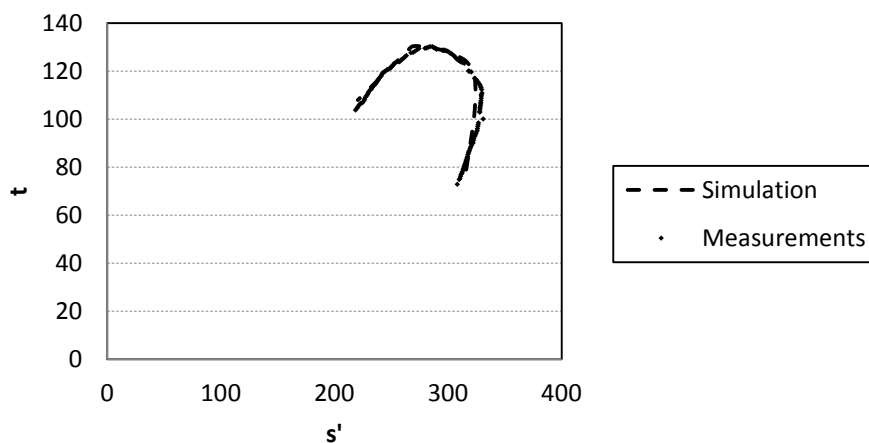


Figure 6.6. Triaxial simulation with soil test facility compared to measurements for borehole 21015 at level -53.5.

6.1.3 Soil tests with the HS model

The evaluated parameters from actual soil tests, performed on soil from three boreholes, were compared to simulated soil tests with the HS model in PLAXIS. The borehole where chosen with regard to site condition, matching the soil conditions near the Tingstad tunnel, further the amount of data available for respective borehole motivated the choice, since triaxial test were needed to enable a good analysis. Figure 6.7, 6.8 and 6.9 below only accounts for one of these three boreholes since the focus of this report is on the SSC-model.

To be able to assess the modulus required as input data for the HS-model, different empirical relationships and evaluation methods were assessed. Assuming that $m = 1$ in equation (6.3) gives the relationships in equations (6.4-6.6), which were used to calculate the required input data.

$$E_{oed} = E_{oed}^{ref} \left(\frac{\sigma}{p^{ref}} \right)^m \quad (6.3)$$

$$E_{oed}^{ref} = \frac{p^{ref}}{\lambda^*} \quad (6.4)$$

$$E_{ur}^{ref} = \frac{2p^{ref}}{\kappa^*} \quad (6.5)$$

$$E_{50}^{ref} = 2E_{oed}^{ref} \quad (6.6)$$

Where p^{ref} was set to 100 kPa and a range of κ^* and λ^* was evaluated from CRS curves according to chapter 6.1.1. Based on κ^* and λ^* four different alternatives were evaluated; HSA, HSB, HSC and HSD. Regarding c' and φ' lower values was first set compared to the SSC soil testing, since this showed a better correlation with the initial tests; see Table 6.6 for constant parameters and Table 6.7 for the parameters in the different alternatives.

Table 6.6. Input parameters, kept constant.

c'	φ'	m	v_{ur}	γ	OCR	K_0^{NC}
2	26	1	0.2	16	1.3	0.6

Table 6.7. Alternatives HSA, HSB, HSC and HSD for different combinations of κ^* and λ^* resulting in different modulus, provided m equal to 1.

	κ^*	λ^*	p^{ref}	E_{oed}^{ref}	E_{ur}^{ref}	E_{50}^{ref}
HSA	0.015	0.23	100	435	13333	870
HSB	0.015	0.14	100	714	13333	1429
HSC	0.025	0.23	100	435	8000	870
HSD	0.025	0.14	100	714	8000	1429

Plotted towards a CRS curve, seen in Figure 6.7, curve it becomes clear that E_{ur}^{ref} determines the inclination of the stress-strain relationship for stresses $< \sigma'_p$, while E_{oed}^{ref} determines the inclination of the curve for stresses $> \sigma'_p$. Comparing the different alternatives shows that Alternative HSA is the best fit.

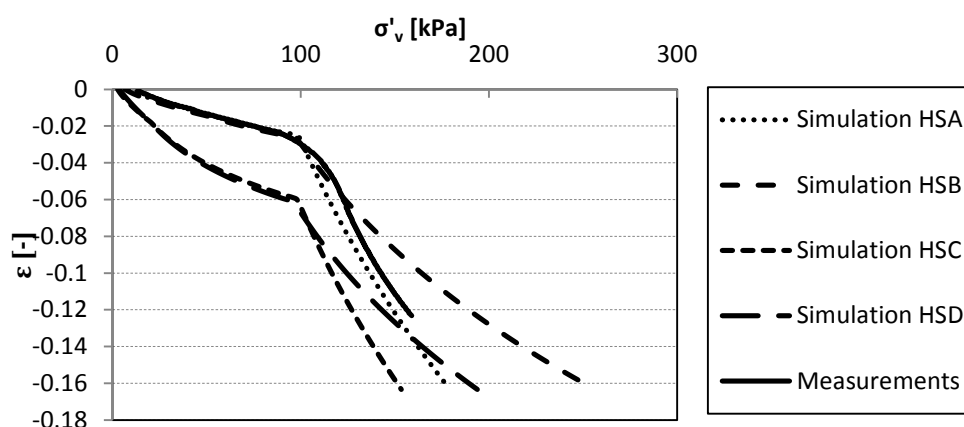


Figure 6.7. CRS simulation with soil test facility compared to measurements for borehole 11004 at level ± 0 .

To make a better evaluation, E_{50}^{ref} was compared towards a DSS curve. The soil test shows a lower deviatoric strength for small strains. The initial inclination can be changed to a certain degree with a changed m -value, however a larger E_{50}^{ref} and thereby a stiffer initial reaction could be assumed. PLAXIS does only allow for a certain relationship range between modulus parameters so this is not always possible. To increase the initial deviatoric strength it is also possible to change the friction angle, φ' of the material. This is done according to Table 6.8 below and illustrated in Figure 6.8.

Table 6.8. Strength parameters and K_0 used, HSA1 is the evaluated parameter set, while HSA2 illustrates that an increased friction angle may better capture the DSS.

	φ'	K_0^{NC}	c'
HSA1	26°	0.6	2.0
HSA2	30°	0.6	2.0

Figure 6.8 also shows that the HS-model does not have a relaxation when maximum deviatoric strength is reached. To better catch the relaxation the SSC-model should be used.

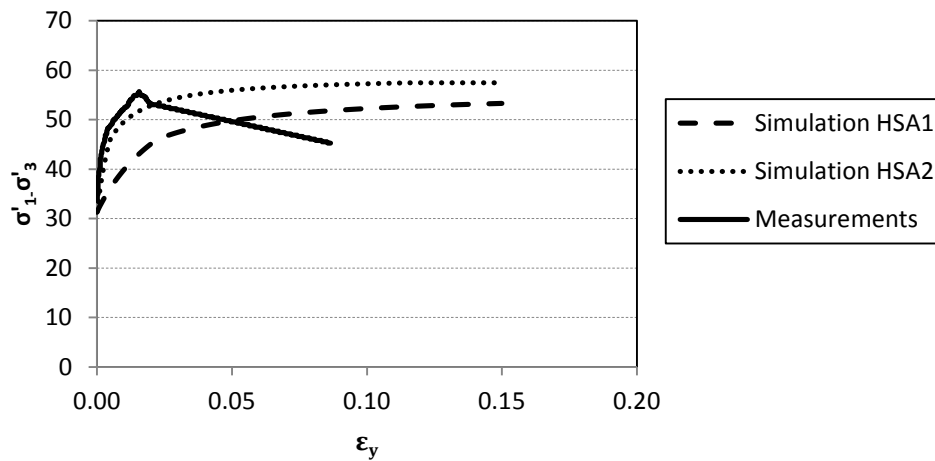


Figure 6.8. DSS simulation with soil test facility compared to measurements for borehole 11004 at level ± 0 .

A third way of comparing the simulated graphs towards the measurement data is the triaxial $s'-t$ plot. Figure 6.9 shows that an increase in φ' gives an increased value of the shear strength.

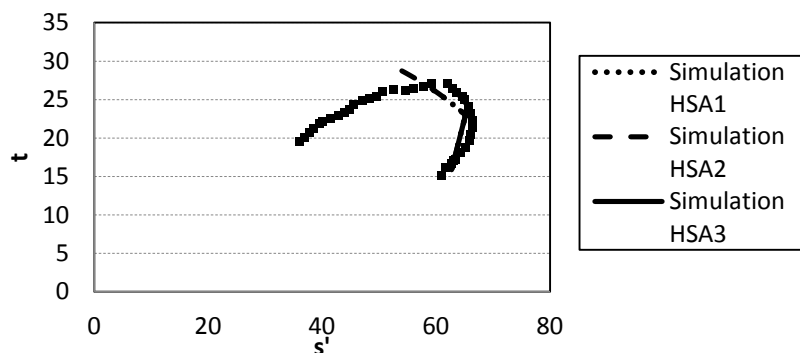


Figure 6.9. Triaxial simulation with soil test facility using values in table 6.8, compared to measurements for borehole 11004 at level ± 0 .

6.2 Further study of SSC-parameters through the β -factor

As a cross-check the β -factor was back-calculated with equation (6.7) where the β -factor is calculated according to equation (6.8) and by using an OCR=1.3, as evaluated in Appendix C.

$$OCR = e^{\left(\frac{1}{\beta} \ln(\Delta t)\right)} \quad (6.7)$$

$$\beta = \frac{\lambda^* - \kappa^*}{\mu^*} \quad (6.8)$$

The calculations gave $\beta=55$, with an age of the soil of 5 000 years. The choice of time when comparing thousands of years is insignificant since the equation includes the logarithm of time. The result is high compared to the evaluated β marked with a shaded area in Table 6.9, which was based on the range evaluated in previous chapters. The result in Table 6.9 shows that both μ^* and λ^* and has a large influence on the β -factor while κ^* has little influence.

The reverse calculation was also made where the evaluated β of 31, together with an OCR=1.3, was used to calculate the age of the clay used in the model. The result was an age of approximately 9 years, which is not realistic for the investigated clay. To be able to find a set of parameters giving a representative age of the soil a test was done with $\beta=55$ and where κ^* was held constant at a value of 0.015 and the value of μ^* was changed to obtain a value of λ^* . The result is shown in Table 6.10.

Table 6.9. The β -factor for different setups of parameters and the calculated OCR-value.

Parameter	Changed value	β -factor	OCR
λ^*	0.17	22	1.9
	0.20	26	1.7
	0.23	31	1.6
κ^*	0.015	31	1.6
	0.02	30	1.6
	0.025	29	1.6
μ^*	0.004	54	1.3
	0.005	43	1.4
	0.007	31	1.6
	0.009	24	1.8

Table 6.10. Calculation of the parameter λ^* for a β -value of 55 by varying the μ^* -value.

μ^*	λ^*
0.004	0.23
0.005	0.29
0.007	0.40

The result in Table 6.10 shows that the evaluated parameters from CRS tests might be in the lower range. The former values correlated however well with the simulation of the soil tests and were hence used in the further simulations.

6.3 Remarks on validation of soil parameters and data quality

Based on the soil tests models presented in this chapter parameters were obtained to use in the large scale PLAXIS model. The parameters of a sample are altered as soon as it is retrieved from the soil. Hence, the lab tests will not completely capture the natural behaviour. The amount of alteration from in-situ conditions determines the quality of the sample which also influences the test result.

Figure 6.10 shows a diagram for sample quality assessment (Larsson, et.al., 2007). To evaluate a CRS-test the volumetric strain for the corresponding pre-consolidation

pressure is compared to the natural water content to obtain an estimate of the quality of the sample. A rough estimation of the CRS tests from Marieholm showed that most samples are acceptable with some better samples and just a few bad ones.

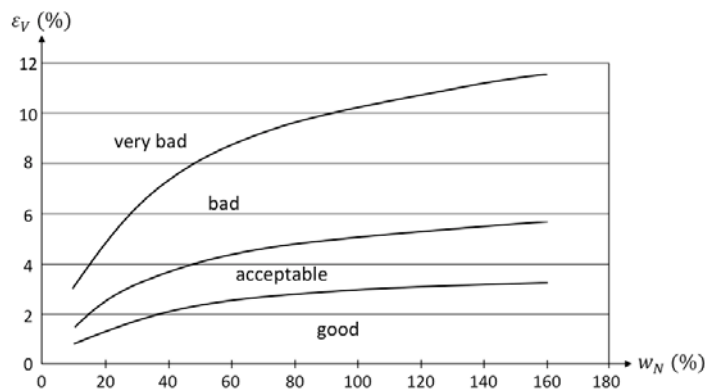


Figure 6.10. Evaluation method of sample quality according to Lunne, cited in Larsson.

Regarding the triaxial tests the volumetric strain after consolidation is compared to the natural water content. A rough estimate was made of the quality of the six triaxial tests performed for Marieholm which showed that four of the tests had an acceptable quality and two tests showed a good quality. The visual appearance of the tests showed however a bad quality where the plotted curves were rough and showed an irregular pattern.

The above presented method is only one example of how to evaluate test quality which still presents an insecurity of whether or not the soil test facility models should aim at capturing the curves exactly.

Another issue is how far off the modelled graphs should be versus the measurements. For example, the CRS-curves from Marieholm are as previously described plotted with an average pore pressure, which is not the case in the soil test facility. The full scale model showed no larger deviance from the soil test facility simulation.

Since several combinations of parameters could give a good fit of the curve a potential risk, with verifying parameters with simulations, is that if the parameters are being altered too much, the connection to reality is lost. The Gothenburg clay is however quite homogenous and comparison with previously evaluated parameters shows that evaluated parameters for this project are within a reasonable span of what could be expected.

7 Input data, geometry and modelling procedure

To be able to capture the deformation pattern along the length of the tunnel, in 2D modeling, five representative cross-sections were chosen both in the submerged tunnel part and in the access ramps. The location of the sections can be seen in Figure 7.1. Two sections were chosen for the southern ramp, one in the un-piled part and one in the piled part to capture the effect of the concrete piles and the effect of the extensive fill added on the south side. Two sections in the tunnel part were chosen, the first one is located in tunnel element 1, where a settlement has occurred, and the second is located in element 5, where an initial heave was observed. The last section is located in the northern access ramp. A more precise choice of location was based on the gauge placement, which could be seen in Appendix A, and the available cross-sections on old construction plans.

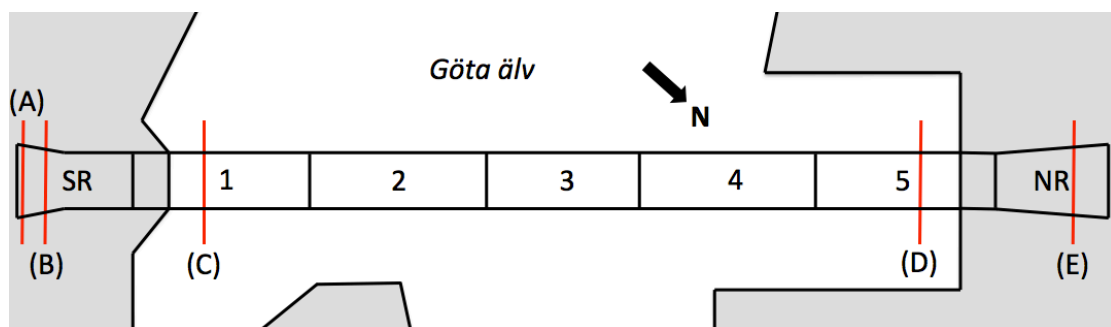


Figure 7.1. Schematic plan over the Tingstad tunnel, with Sections C and D chosen over the tunnel elements 1 and 5, and Section A, B and E over the South and North Ramp (SR, NR).

The geometry for each section and the assumptions made are described in the following chapters, together with a hypothesis and presentation of the calculation including any modified calculations, for each section.

7.1 Input data

Input data for the soil used in the models are presented in Appendix D. The data used are from the parameter validation as well as some assumed values. Plane strain conditions were assumed to apply for all sections even though, as previously stated, this is a simplified assumption.

The material parameters used for the construction parts are assumed from general values, however increased slightly since failure in the construction is excluded from the scope of this report. Further the weight of the tunnel was set to 0 and the load from the construction was instead accounted for using a distributed load in PLAXIS. The input parameters for the construction can be seen in Appendix D and the load calculation can be seen in Appendix E. The same load was assumed to be valid for both the enclosed tunnel part and the ramp construction and was calculated to 80 kPa.

The bearing capacity for the piles has been calculated according to Appendix F, where the design shear strength was obtained from old pile plans. Material parameters, seen in Appendix D, were taken as, slightly increased, standard values.

7.1.1 General assumptions

This chapter will list some of the assumptions that were valid for all the modeled sections.

- The water level was set to a constant level of +10 meters.
- The initial pore pressure was not quite hydrostatic due to ongoing settlement of previous construction, however, the deviance from hydrostatic was so small that the effect was disregarded.
- The soil layers for all sections were modeled very coarse with no variation of density or strength parameters. In the area for the southern side a layer of muddy clay which had a density of 1.5 t/m^3 and slightly smaller shear strength, was not included due to numerical difficulties.
- Closed hydraulic boundaries were added on the sides of the geometry creating a double-sided drainage situation.
- As stated previously, there are insecurities in the retrieved data, for example construction load and geometry of the refill. An assumption has been made that the simplifications done in the model are negligible for the result.

7.2 Section A

Section A is located in the southern area on the part of the ramp that has not been piled and where large deformations have been observed. The corresponding gauge number to compare with in the settlement diagram is su1. The location of the section can be seen in Appendix A. The ramp is located in the old river trenches of Gullbergsån and Sävån, hence drainage and filling have affected the deformations in this section. As explained previously the outlet of Sävån has been moved to the east of the tunnel. This dredging of a new river trench is also part of the cross-section and its effect on the deformations of the tunnel and ramp was investigated in a hypothetical case seen in Appendix G. Underneath the tunnel there are vertical drains installed to avoid hydraulic uplift.

Some soil masses have been dredged but most part of the altered geometry consists of filling. Bank-piling has been done to support the filling and reduce settlements. The cross-section cuts through transversal SPWs, approximately 60 meters away from the tunnel axis, on both sides of the ramp. The geometry can be seen in Figure 7.2 where the PLAXIS model is compared to the construction plan used as a basis.

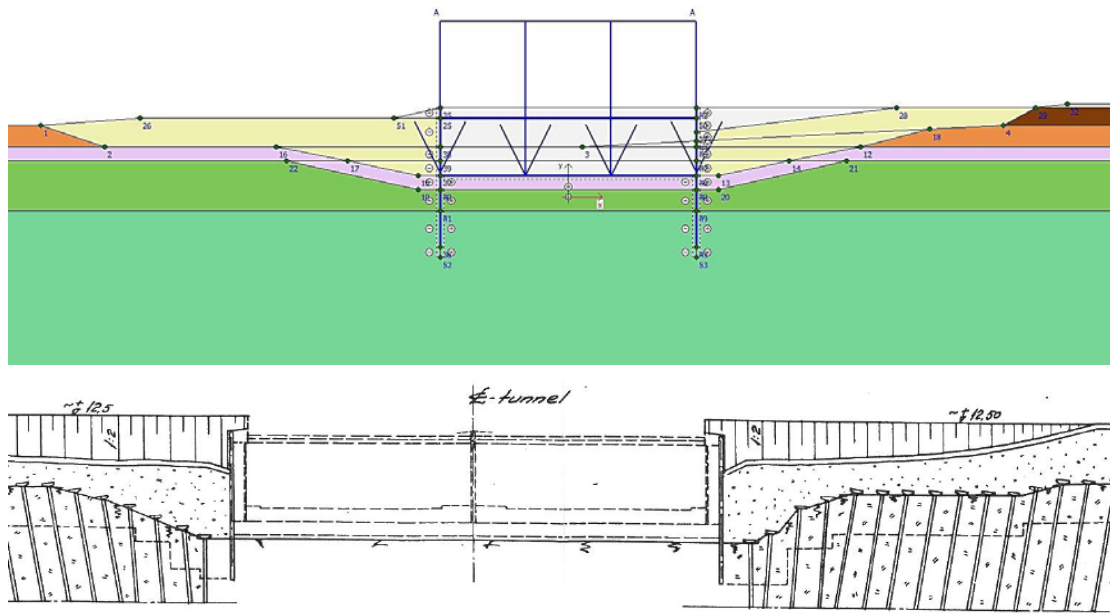


Figure 7.2. Geometry of Section A in PLAXIS and from the construction plan.

7.2.1 Assumptions and modeling procedure

The fill on both sides of the tunnel are not similar and the settlement data for the cross-sections show a small deviance of approximately 10 millimeters, hence the whole tunnel was modeled. The bank piling was disregarded in a first calculation. The geometry of the fill was simplified and the transverse SPWs were disregarded since the effect on the settlements was assumed to be small. The effect was investigated in a hypothetical case seen in Appendix G.

For simplification the vertical drains were not included in the model but the effect was investigated in a hypothetical case in Appendix G and in a modified calculation for Section A.

Due to non-horizontal ground surface the Gravity loading option was used to calculate the initial stresses. The soil material was in this phase chosen as linear elastic to avoid too many plastic points when generating the initial stresses. The initial phase was followed by a plastic step where the soil model was changed to SSC. The time step for this phase was set to 3650 days to be able to capture the “current” stresses at the time of construction as well as a more realistic OCR-value.

Having a SSC material at the top of the geometry, when draining the river outlet, can cause problems due to the generation of large excess pore pressures at the top boundary. To solve this, a one meter thick linear elastic interface layer was added at the ground surface. The time for draining the rivers was assumed to be one year before dredging hence a consolidation time of 365 days was applied. Secondly, the dredging was modeled followed by applying the construction and the refill, which was modeled as a linear elastic material. The SPWs were elongated in relation to the original geometry to avoid too large deformations.

There was a problem with the boundary between the linear elastic material and the SSC material where very large strains occurred. The reason is that the softer clay

deforms more than the LE material which is very stiff, leading to failure in the soil at the boundary. In the following sections these deformations were disregarded but in Section A, the deformations in one area were so large that the calculations could not converge. To solve this, a layer with a stiffer SSC material was added under the LE interface material where the strength properties were raised considerably. The material properties for this layer are found in Appendix D.

7.2.2 Hypothesis of PLAXIS results

There have been large filling works executed in the area for the southern ramp as well as drainage of the river mouths. Hence initial heave followed by large settlements surrounding the ramp are expected in the simulation. Since the section is located in the un-piled part of the ramp the settlements should be larger than for the other sections.

The 3D-effects on this section might affect the result in comparison with measurement data. The section is close to the piled part of the ramp which should cause less settlement in Section A. Hence the result from PLAXIS should, based on this, overestimate the deformations.

Vertical drains affect the dissipation rate of the excess pore pressure and have a large effect on the result. According to the hypothetical case the simulation with vertical drains showed a much larger settlement than without them, see Appendix G. For simplification these drains was not included in the model which should give quite a large under-estimation of the settlement since the pore pressure dissipation is much slower.

Another hypothetical case was done regarding the bank piling which showed a small effect with the increase of spacing. A slight over-prediction of the deformations can be expected since the spacing is larger in the model.

In conclusion the result from PLAXIS should show under-estimation if the vertical drains is disregarded.

7.3 Section B

As for Section A, Section B is also located on the southern ramp, where the previous outlet of Gullbergån and Sävån were located and correspond to the gauge number su14. The geometry and soil layers of the section are similar to Section A, while the refill differs slightly.

The large difference in Section B compared to Section A is that it is situated where concrete piles reinforce the ramp. As can be seen the concrete piles are absent in Figure 7.3, however the piles should be present according to piling plans. The bank-piling and SPWs are present as in Section A.

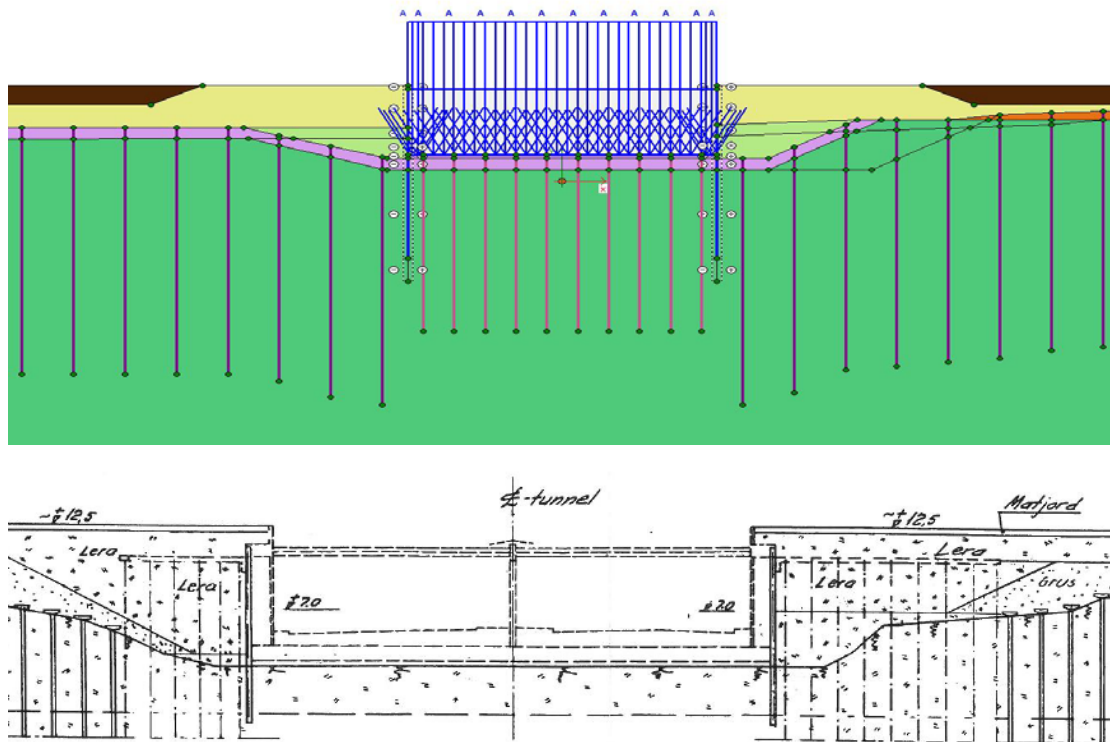


Figure 7.3. Geometry of Section B in PLAXIS and from the construction plan.

7.3.1 Assumptions and modeling procedure

Several assumptions were made to be able to do a model of the cross-section of the south ramp. First gravity loading was applied followed by simulating the clay several years in a plastic step, described in chapter 7.2.2, to obtain a realistic OCR matching what could be expected in field.

When the river outlet of Mölndalsån/Säveån was drained there was, as for Section A, a need for a thin layer of a linear elastic material. The pore pressures in this interface are interpolated from adjacent clusters.

After drainage of the river, the excavation for the tunnel was carried out, and the trench was continuously drained after which the model was consolidated for 365 days. This consolidation leads to failure in a quite steep slope next to the planned tunnel stretch, which is irrelevant in the sought model and was hence bypassed by increasing strength parameters for the soil around the slope.

When modelling the SPW after old construction plans the deformations of the wall toe were too large, creating unrealistic pore pressures. To avoid an irrelevant failure for the sought model, the length of the SPW had to be slightly increased to a ratio of 1:1 over and under the excavation bottom.

Concrete piles with a length of 22 meters were modelled under the ramp-construction. The SPW were then connected with a stiff slab, resting on the concrete piles and a strut 0.5 meter below surface level.

Bank piling with 32 meter long wooden piles was carried out before refilling with gravel, clay and coke slag, see Appendix I for geometric properties. The bank piling was simplified since the spacing was increased.

When the construction was finalised the model was consolidated for approximately 40 years.

7.3.2 Hypothesis of PLAXIS results

Since this part of the ramp, in contrary to Section A, is piled with concrete piles, the settlements are expected to be smaller than for Section A. Due to 3D-effects from the settlements of the un-piled ramp the deformations might however be under-estimated in the PLAXIS model.

Similar to Section A, vertical drains were installed underneath the slab. The drains were disregarded in the PLAXIS model which also should present an under-estimation of the deformations.

The bank-piling was, as for Section A, simplified with regard to spacing between the piles. This might result in slightly larger settlements than the measurements but are regarded as less significant. In conclusion to this, the settlements are projected to be under-estimated in the PLAXIS model.

7.4 Section C

Section C is located across tunnel element 1 and the corresponding gauge number is 1:5, see Appendix A. The level of the tunnel at this point is ± 0 . Before the excavation, the eastern part of the location for the tunnel was located above the shoreline with the shoreline running through the midpoint of the section. The tunnel is piled with 22 meter wood piles grouped in pairs of two and placed at the edges and in the middle of the tunnel. The piles are concentrated around the intersections between tunnel elements and hence are not equally spaced in the z-direction.

Since this part of the tunnel is located close to the intersection between the ramp and the tunnel the settlement of the ramp also affects this section. The geometry of the cross-section is seen in Figure 7.4.

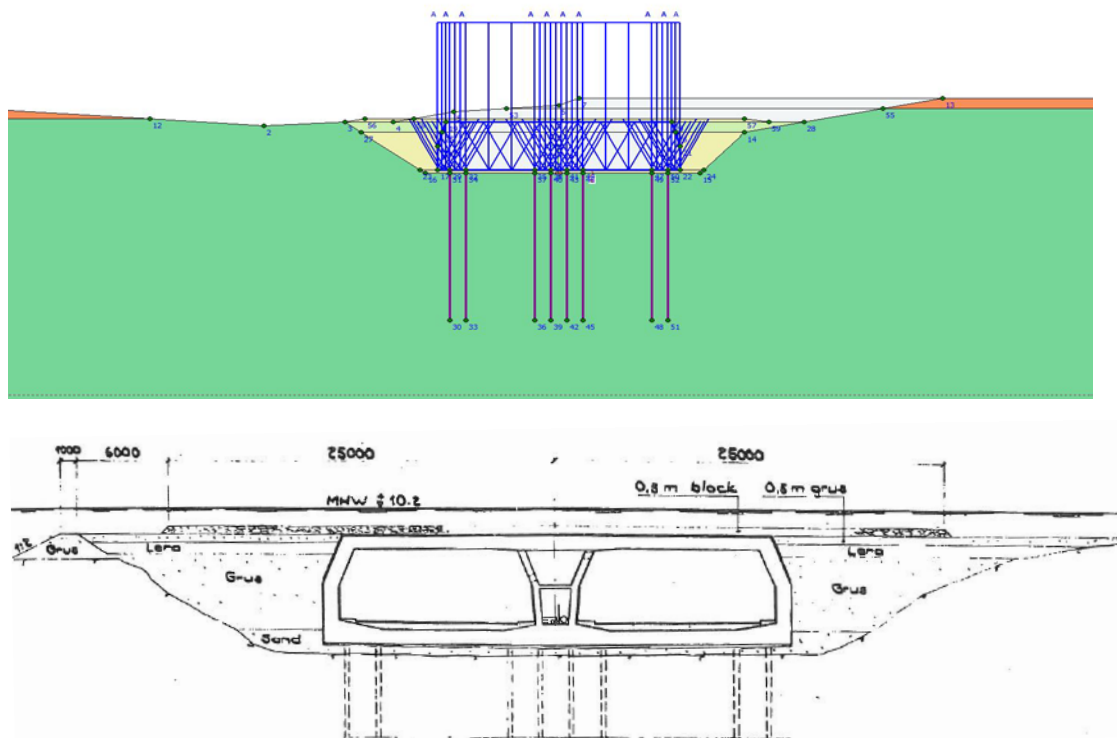


Figure 7.4. Geometry of Section C in PLAXIS and from the construction plan.

7.4.1 Assumptions and modeling procedure

There is no symmetry around the tunnel axis, hence the both sides of the tunnel had to be modelled in PLAXIS. The original surface as well as the geometry of the refill differs from the east to the west side.

The Gravity loading procedure was used to calculate the initial stresses followed by a plastic step to obtain a more realistic OCR-value. The dredging was then performed in two steps with a consolidation time of 130 days in between. The piling and construction of the tunnel was consolidated for 200 days before adding the refill material. The final phase was consolidated for approximately 40 years.

The extensive filling of the old river trenches also affects this section, hence a hypothetical case was constructed to simulate the load effect from the fill. The description and result of these calculations can be seen in Appendix G. According to the hypothetical case, the fill have little effect on the settlements and were disregarded in the original model.

7.4.2 Hypothesis of PLAXIS results

As for all sections the process is an unloading scenario but as stated previously, the extensive filling works in the southern part of the area affects the deformations of this cross-section, hence a settlement is expected.

The settlements of the south ramp are causing settlement in this tunnel section which might cause a slight under-estimation of the vertical deformations due to the lack of

3D-effects in the model. A modified calculation with an added equivalent load effect from the fill around the southern ramp should however better capture the settlement behaviour. The 3D-effect of the piles under the tunnel could also affect the result since in reality the piles are not equally spaced in the z-direction. This could produce a slight under-estimation of the settlements.

7.5 Section D

Section D is located across tunnel element 5 see Appendix A, where a heave has been observed. The corresponding gauge number in the settlement diagram is 5:85. The entire section was, before construction, located above the shoreline. A permanent harbor basin was constructed in the location. This implies that the unloading due to tunnel construction has been larger than for the other tunnel elements.

In conjunction with the construction of the harbour basin, another basin was constructed west of the tunnel element. Since the basin was probably present only during the tunnel construction it was disregarded in the model.

Due to the probability that the basin was present only during the tunnel construction, it will be disregarded in the model. The tunnel is as previously described piled with wood piles in groups of two. The geometry can be seen in Figure 7.5.

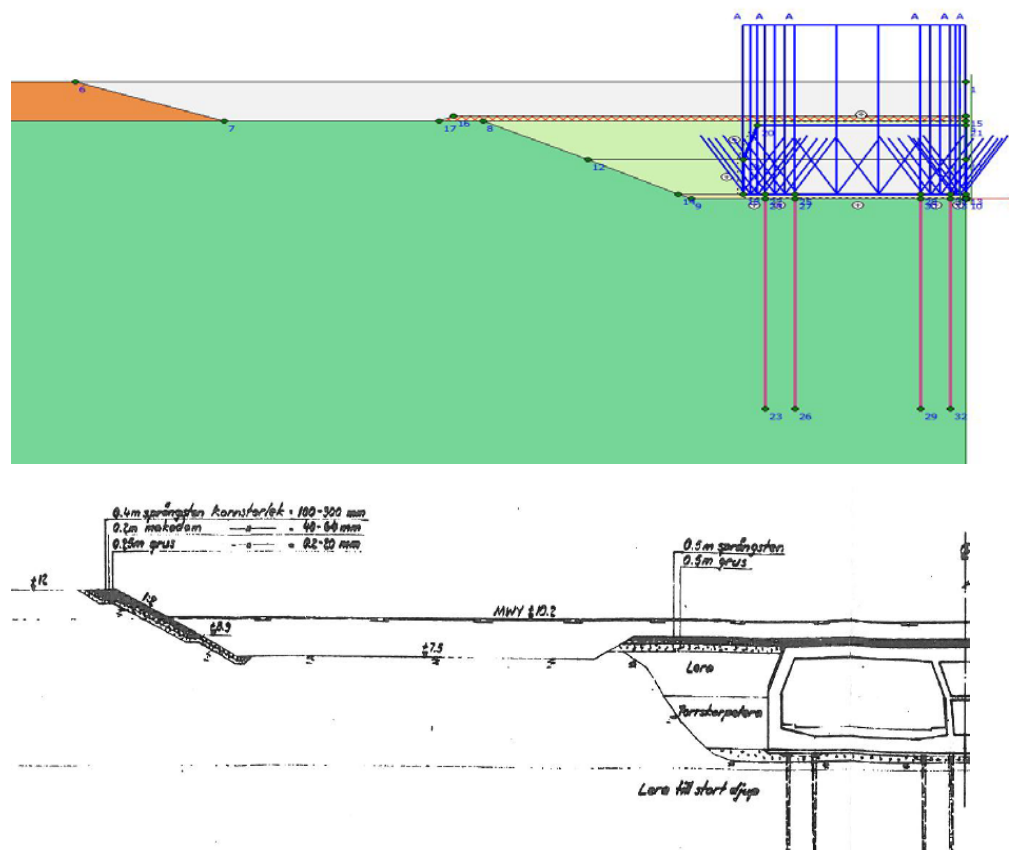


Figure 7.5. Geometry of Section D in PLAXIS and from the construction plan.

7.5.1 Assumptions and modeling procedure

Since the geometry was quite similar on both sides of the tunnel symmetry about the tunnel axis was assumed for simplification.

The initial stresses were calculated with a K_0 -procedure and followed by a plastic nil-step with a time span of 3650 days to simulate a more accurate stress situation.

The first part of modeling the tunnel section on the northern part was the dredging. The estimated time for completion was 270 days.

Secondly the tunnel element and the piles were applied followed by the refill. The refill consists of clay which was modeled as a very stiff material since the focus does not lie on the behaviour of the refill. The last phase was consolidated for approximately 40 years.

7.5.2 Hypothesis of PLAXIS results

Due to the large excavated load, a heave is expected in all stages of construction. The initially large heave will be reduced by the tunnel load, gradually turning into a very small settlement.

As for all sections, the 3D-effects are not considered in the model which might contribute to the settlement rate. The general simplifications made regarding geometry and input data also affects the result.

In conclusion, the behaviour that should be captured by the model is hence an initial heave that is reducing over time.

7.6 Section E

Section E is located across the northern ramp and the corresponding gauge number is nu14. The area was earlier above the shoreline with a surface layer on +12 m. Excavation down to +2 m has been conducted, with excavation slopes of 1:1.7. The construction is similar to the southern ramp, with 24.5 meter long concrete piles connected to the bottom slab at +2.5 m, but a not so extensive bank piling. After construction, clay and a layer of coke slag was used as refill, see Figure 7.6.

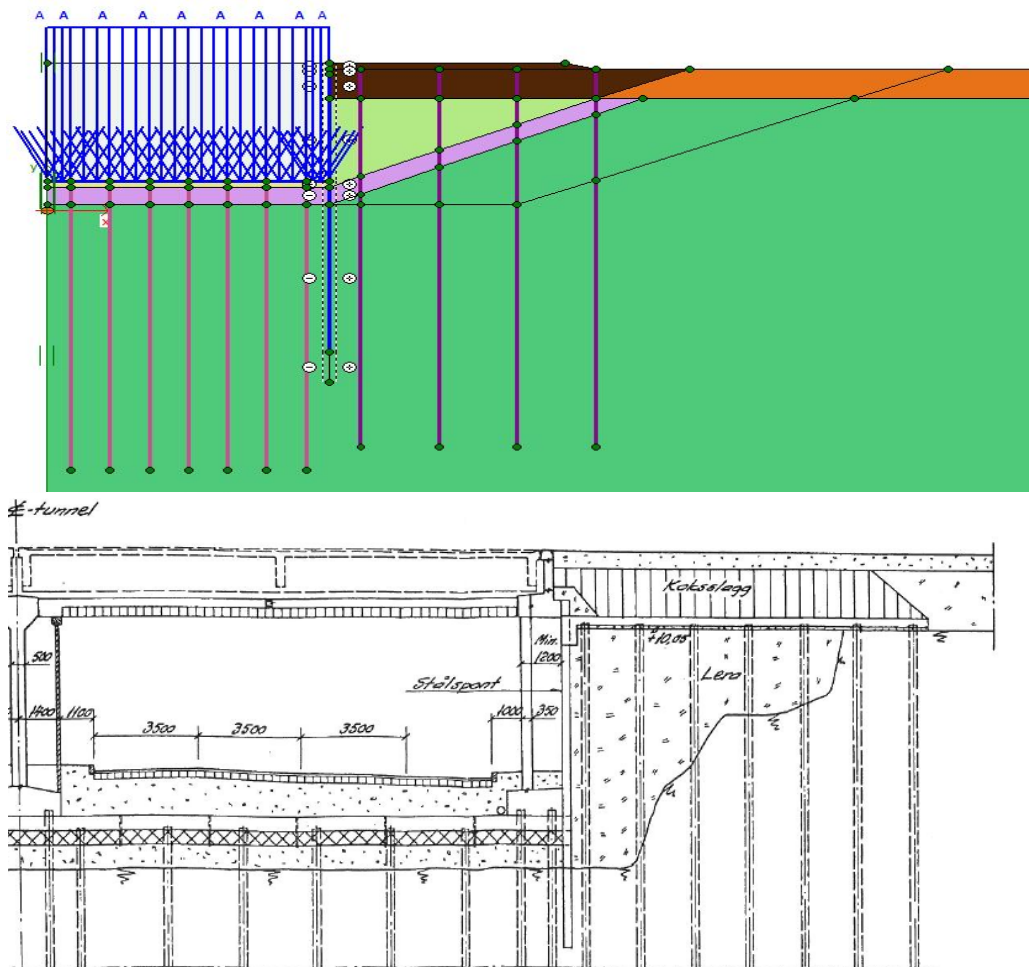


Figure 7.6. Geometry of Section E in PLAXIS and from the construction plan.

7.6.1 Assumptions and modeling procedure

Since Section E was estimated to be fairly symmetrical along the tunnel axis only one side was modelled. Horizontal surface and soil layers enable the initial stress generation to be carried out using K_0 -procedure. A plastic phase was then initiated to raise the OCR to assumed field conditions. The excavation was performed in combination with drainage of the pit and installing of bank piling. This drainage led to possible failure in the surrounding slopes so slightly higher strength parameters had to be assumed for the slope to avoid extensive excess pore pressure to be built up around the SPW. An interface for the top layer of clay was also needed as described in earlier sections.

The same assumptions as in the other Cross-Section were done for the SPWs, which had to be lengthened compared to old construction plans. After construction a refill with clay and coke slag was made, according to Appendix I. Finally the model with construction was consolidated for 40 years.

On Section E, a HS analysis also was performed, using the indata shown in Appendix C.

7.6.2 Hypothesis of PLAXIS results

Since the old ground level is nearly identical to the new, except for a thin layer of lightweight coke slag, no substantial additional load could be expected from the refill. The calculated load or stress increase from the construction is 80 kPa, while the weight of the removed clay is larger giving an unloading-reloading scenario where the final load is smaller than the earlier. This leads to the prediction that, as for section D, an initial heave will occur and decay with time, due to creep. As for the southern ramp, the vertical drains were disregarded in the modelling of the northern ramp, which would indicate that the PLAXIS model will under-estimate the final deformation.

The HS model does not account for creep, which for this simulation should produce a heave that decreases with time. Hence the settlements for this section will probably not be captured by the model.

8 Results

The results from the PLAXIS SSC modelling of the five sections, A-E, are presented in this chapter. The simulated vertical deformations over time are obtained from one point directly under the western edge of the tunnel to be compared with the measured deformations in the western gauge in the cross-sections. The relevant gauge number is presented in conjunction with the result. Settlements with depth are also presented, even though no such measurements are available.

In Figure 8.1 the measured settlements and the modelled settlements are plotted over the entire length of the tunnel, including both connecting ramps, for three different years; 1968, 2007, 2045. As can be seen the PLAXIS simulations only capture the behaviour to some extent. At the southern ramp the simulations for Section A and B predicts large settlements with time, but overestimates it compared to real measurements. The simulation for Section C and E underestimates the settlements, while the simulation for Section D over estimates the settlements.

It could also be seen that the error in simulated settlements in general increases with time. Since no data is yet available for 2047, these settlements are a projection based on an assumption, made by Gatubolaget, of an average yearly settlement of 1.4 millimeter.

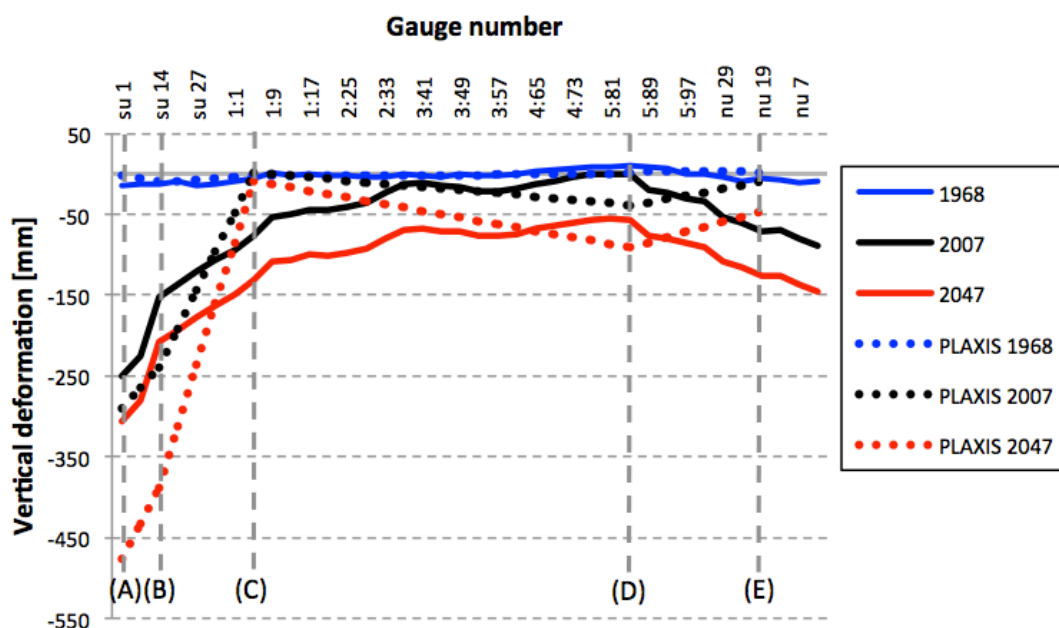


Figure 8.1. Simulated settlements from PLAXIS compared to measurements for 1968, 2007 and a projected result in 2047.

8.1 Section A

Figure 8.2 shows the vertical deformations with time for a point under the western edge of the ramp. The result show that the simulation is under-estimating the deformations for the first 20 years, where the settlement rate for the measurements seem to decline and the simulated settlements do not. One explanation could be that the parameters affecting the creep rate need to be adjusted.

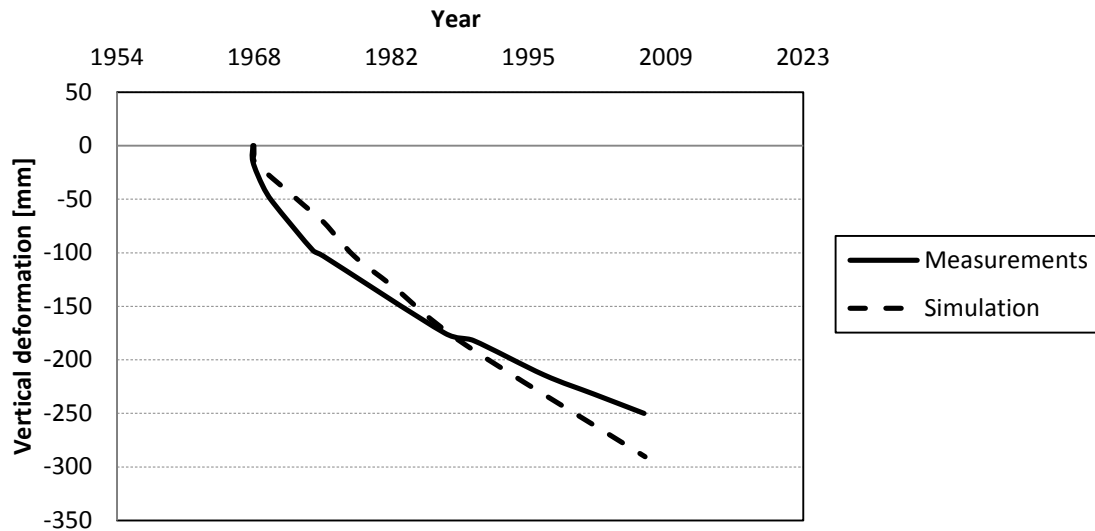


Figure 8.2. Vertical deformation over time for Section A, gauge su1. Simulation in PLAXIS compared to measurements.

The problem with large deformations at the boundary between the LE material and the SSC material has not been solved entirely but there are still large strains in the boundary between the materials. The produced settlements on both sides of the ramp amount to approximately 500 millimeters as a maximum.

The settlement with depth is shown in Figure 8.3 where it is shown that the largest settlements occur in the top layers of the soil. The effect of large strains in the boundary is also evident in the graph where the deformation declines most rapidly between level -3 and -10.

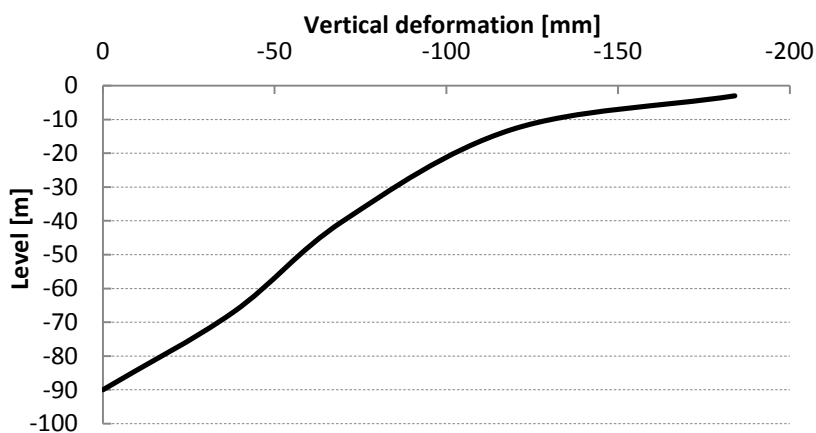


Figure 8.3. Vertical deformation with depth for Section A for a vertical section under the ramp construction.

The differential settlements are shown in Figure 8.4, where the result shows a larger deviation between the east and the west side compared to the measurements. This is most probably due to the larger extent of the heavy refill material on the west side.

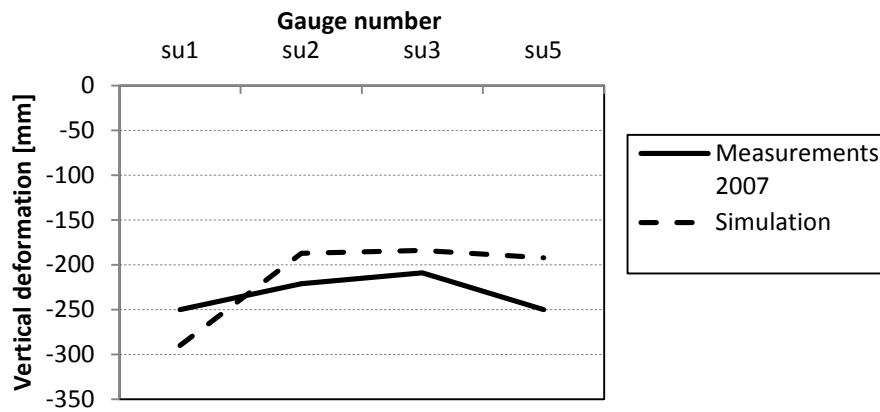


Figure 8.4. Differential deformation across Section A. PLAXIS result compared to measurements for the years 2007.

The remaining pore pressure after consolidation under the tunnel is maximum 22 kPa in the middle of the soil layer, which is too large regarding that no excess pore pressure is expected to be found at present time. Approximately 12 percent of the pore pressure in the middle of the soil layer has dissipated over the consolidation time. The consolidation process reduces excess pore pressure and creep creates it which means that these two processes compete. The result for Section A is an indication that either the consolidation rate is too low due to a low permeability or the creep rate is too large. The creep rate in the plastic step where the material is changed is approximately 1.2 millimeters/year which is a reasonable and even a quite low value. The vertical drains also affect the dissipation rate which should be lower if the vertical drains are excluded.

8.2 Section B

The result, with vertical deformation plotted against time, can be seen in Figure 8.5. The SSC-model in PLAXIS gives a settlement for the cross-section in gauge su14 of 240 millimeters accumulated year 2007, while the measured deformation at the same time is 152 millimeters.

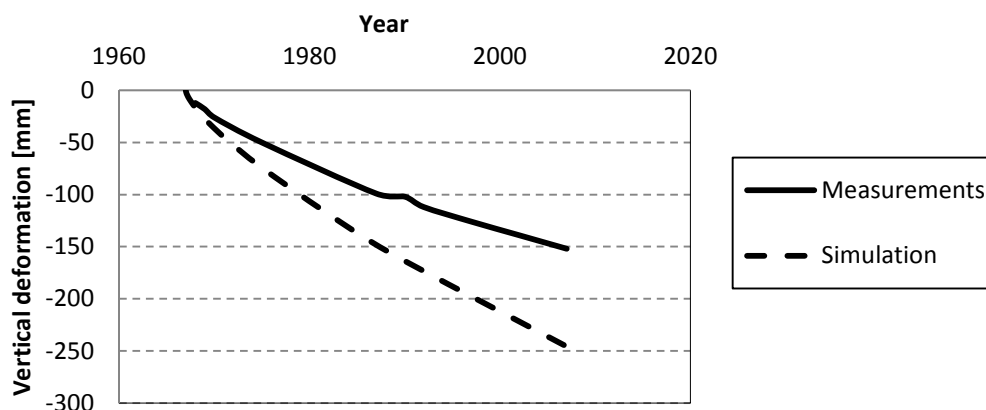


Figure 8.5. Vertical deformation over time for Section B, gauge su14. Simulation in PLAXIS compared to measurements.

An excess pore pressure of 34 kPa is still present in the middle of the clay layer, at the end of the consolidation phase. The model also shows deviatoric strains at 1.5 percent between the linear elastic layers and the soft soil creep layer, causing a settlement of the fill.

Plotting the deformation towards the depth, shows that the concrete piles beneath the ramp immerse the load effect of the ramp, causing the vertical deformation to peak ten meter beneath the bottom slab, see Figure 8.6. The fact that the load effect is brought down through the profile actually leads to that the upper ten meter of soil experience unloading.

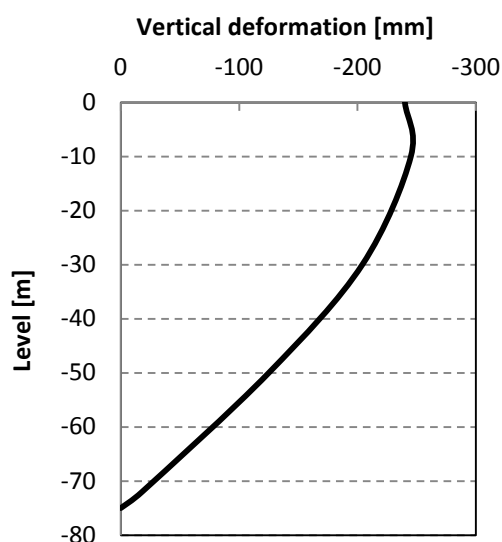


Figure 8.6. Vertical deformation with depth for Section B for a vertical section under the ramp construction.

The simulation in PLAXIS SSC-model gives an overestimation compared to the measured deformation for the section. Since the vertical drains are excluded from this simulation would invoke even bigger settlements, as stated in the hypothesis for Section B. Other reasons such as overestimation of the load effect are also possible. The effect of a slightly lowered weight of the refill is addressed below in a modified calculation.

8.2.1 Modified calculation

To address the effect of a decreased load from the refill a modified calculation was performed, where the density of the gravel-refill was decreased from the original 2.1 t/m^3 to 1.6 t/m^3 , see Table 8.1, while the weight of the clay-refill was kept to the original 1.6 t/m^3 . This resulted in deformations shown as “Modified simulation” in Figure 8.7. The simulated deformation in 2007 was 179 millimeters, compared to the measured deformation of 152 millimeters.

Table 8.1. Modification of density of the refill gravel for Section B. Other parameters according to Appendix D.

Original weight of gravel [t/m ³]	2.1
Modified weight of (refill) gravel [t/m ³]	1.6

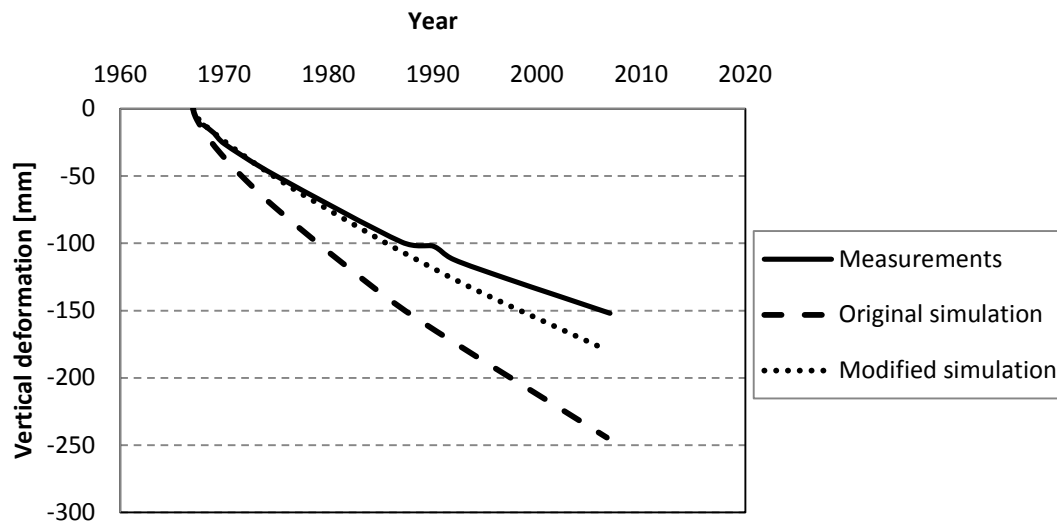


Figure 8.7. Deformation over time for Section B. The original simulation in PLAXIS is compared to a simulation with a decreased weight of the fill and compared to the measured deformations.

8.3 Section C

The result for the simulation with the original setup of parameters specified in Appendix D is presented in this chapter for Section C. A modified calculation and a sensitivity analysis were also done for this cross-section. To truly evaluate the parameters used, a sensitivity analysis of some parameters would need to be done for several sections to investigate the behaviour for different loading scenarios.

As can be seen in Figure 8.8, there seem to be an error in the measurement data where the settlement curve first drops and then show an almost horizontal deformation behaviour. This behavior is probably due to the replacement of the gauges that occurred at the time around 1975. This part will be considered as a disturbed measurement in further comparisons.

The dredging of the trench causes an initial heave of the soil. The eastern part of the tunnel experience larger deformations since the unloading was larger. The magnitude of the heave at a point directly under the tunnel, after all the dredging is completed, is 110 millimeters.

The settlements at a point A, located directly under the western edge of the tunnel, are compared to measurements in gauge 1:5. The result can be seen in Figure 8.8. The PLAXIS simulation shows a large under-estimation with a continuation of the heave caused by the unloading. This indicates that some parameters need adjustment or that the load is too small, which was investigated in a modified calculation in chapter

8.3.1. The small settlement in the beginning of the simulation is probably an instantaneous settlement that is turning into a heave when the negative pore pressure dissipates.

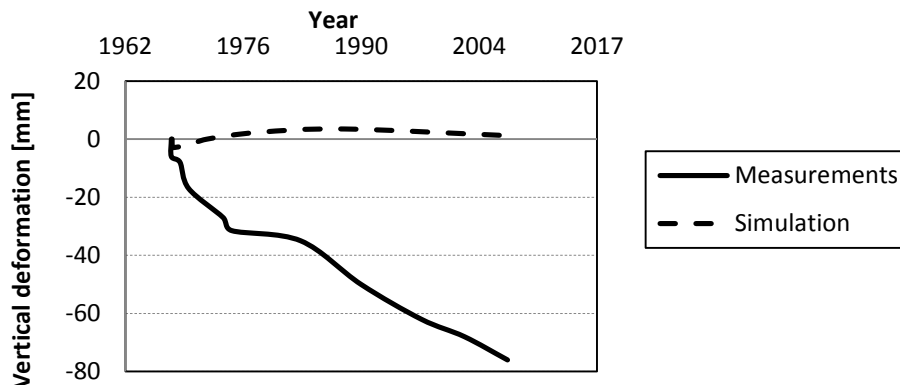


Figure 8.8. Vertical deformation over time for Section C, gauge 1:5. Simulation in PLAXIS compared to measurements.

The settlements with depth can be seen in Figure 8.9, where the data points are in the tunnel axis along the depth of the soil profile. The graph shows that there is a heave directly under the tunnel, probably due the load transfer in the piles to deeper soil layers. The heave should be suppressed by the added load indicating that some parameter needs adjustment.

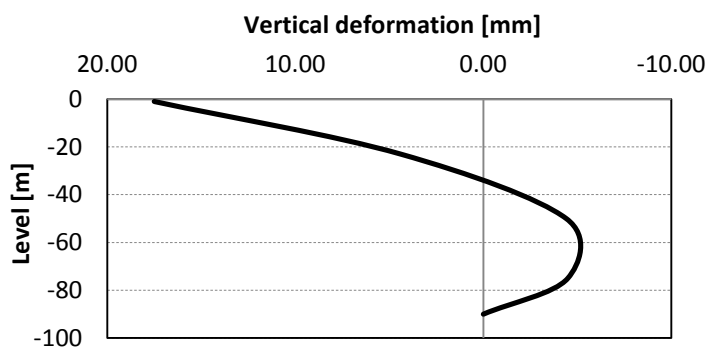


Figure 8.9. Vertical deformation with depth for Section C for a vertical section under the tunnel. Positive values on the x-axis represents a heave.

The differential settlements can be seen in Figure 8.10. The simulated deformations show a heave which is larger in the eastern side due to larger unloading in the eastern part of the tunnel. The magnitude do not correlate with the measurements but the behaviour is somewhat captured. The difference between east and west is 2 millimeters in the measurements and approximately 20 millimeters in the simulation.

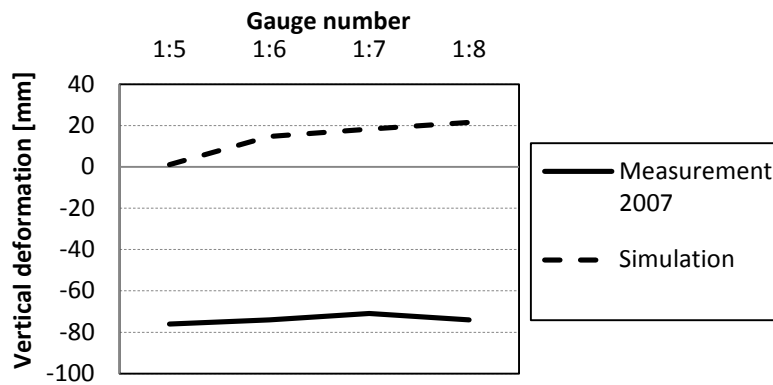


Figure 8.10. Differential deformation across Section C. PLAXIS result compared to measurements for the years 2007.

The soil at the edges of the model experience creep settlements, which amounts to approximately 50 millimeters. This corresponds to a creep rate of approximately 1.3 millimeters /year. This is a reasonable value even though it might be a bit too low for a disturbed soil. These settlements are causing excess pore pressures in the middle of the clay layer which amounts to approximately 5 kPa as a maximum. This might be reasonable considering that no excess pore pressures are expected to be found in the clay at present time.

In comparison, the creep rate occurring in the plastic nil-step is 33 millimeters per year, which is a very large value. A realistic value of the creep rate would be 5-10 millimeters /year. This indicates that the creep parameter, the OCR-value or λ^* might need to be adjusted.

At the end of consolidation there is almost no excess pore pressure remaining under the tunnel. There is a slight negative pore pressure in the upper part of the soil layer and positive underneath the piles.

When comparing to the pore pressure after 40 years of further consolidation, the remaining pore pressure is almost 2 kPa due to the build-up of excess pore pressures from creep settlements.

8.3.1 Modified calculation with additional load from fill

A simulation was made to see a possible effect from the fill for the southern ramp. The fill calculations were made in a hypothetical case in Appendix G. An equivalent load according to Table 8.2 was added at a level of -56 meters.

Table 8.2. Load input in modified calculation.

Original load (not including refill material) [kPa]	80
Added equivalent load [kPa]	17

The remaining excess pore pressure after the consolidation time is slightly increased amounting to maximum 2 kPa under the tunnel. The deformations in a point directly under the tunnel can be seen in Figure 8.11, where a larger settlement rate is observed however, is still substantially under-estimating the deformations.

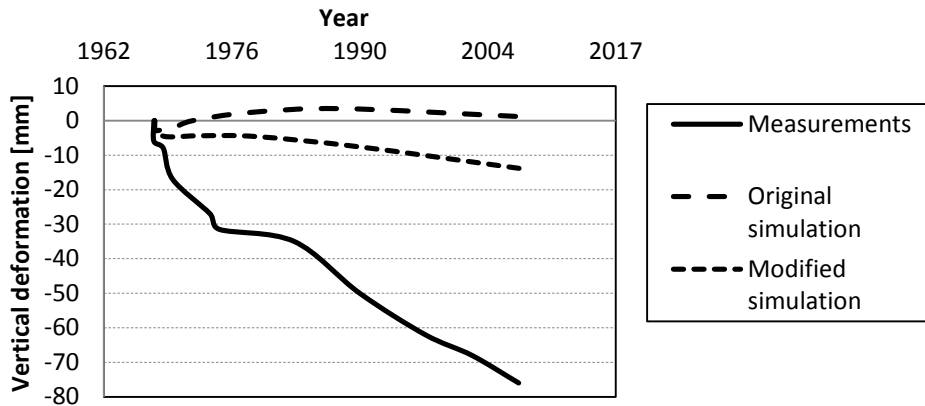


Figure 8.11. Vertical deformation over time for Section C. The original simulation in PLAXIS is compared to a modified simulation with an added load from the fill and compared to the measured deformations.

The settlement with depth is shown in Figure 8.12, where the simulation is more realistic showing a decrease in the heave of the upper soil layer. The differential settlements show similar behavior.

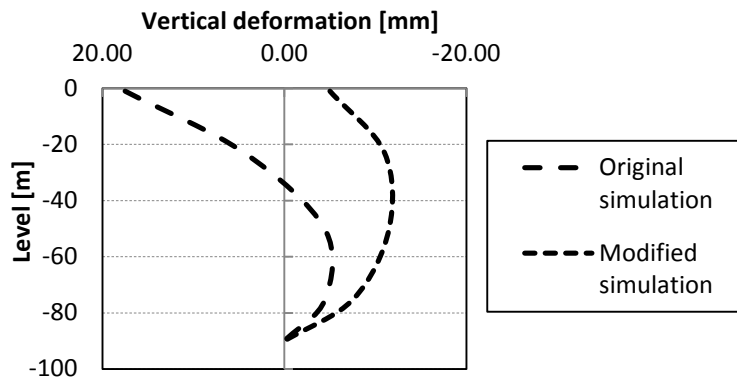


Figure 8.12. Vertical deformation with depth for Section C. The original simulation in PLAXIS is compared to a modified simulation with an added load from the fill. Positive values on the x-axis represents a heave.

8.3.2 Sensitivity analysis of important parameters

A sensitivity analysis was performed for some input parameters. Each parameter was investigated individually and the result evaluated.

Permeability, k

An increase in k gives an increase in consolidation rate according to equation (3.28). The sensitivity analysis was performed with parameters according to Table 8.3.

Table 8.3. Range of data for the permeability. In the sensitivity analysis the maximum value was investigated. The average value was used in the original simulation.

	Min	Average	Max
k [m/day]	4E-5	5E-5	7E-5

The change of the permeability to the maximum value is referred to as Modified calculation A. The result show a slight increase in the remaining positive pore pressure is observed. The negative pore pressure present in the original simulation has dissipated due to the higher permeability. The pore pressure at the edges of the model is almost unchanged.

Regarding the settlements with the maximum value of the permeability there seem to be no change, as can be seen in Figure 8.13. Since the excess pore pressures had dissipated with the average value this result was expected. The deviation in settlement across the cross-section is still apparent between the east and the west side. The settlement with depth follows the same behaviour as the original setup.

Since no measurement data of the permeability in the horizontal direction was available the assumption was that the same value was valid in both x- and y-direction. Due to a complex structure and formation history this is probably not the reality. To see the effect this would have on the deformations and development of pore pressure, a test was done where the permeability in the horizontal direction was increased according to Table 8.4. This simulation is referred to as Modified simulation B.

Table 8.4. Input data for a simulation with different permeability in different directions.

k_x [m/day]	7E-5
k_y [m/day]	5E-5

The simulation with different permeability in the x- and y-direction showed no impact on the settlements or the pore pressure. In conclusion, the deviance between the minimum and maximum value was too small to be significant in this particular model.

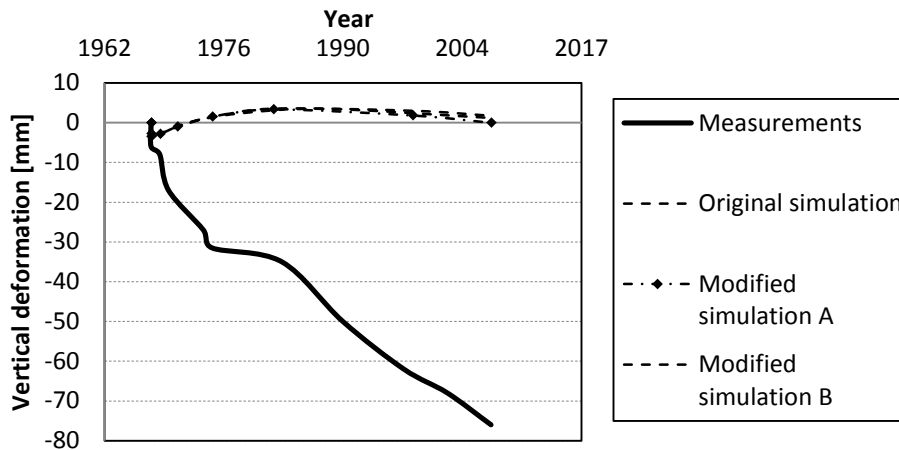


Figure 8.13. Sensitivity analysis of the permeability for Section C. Modified calculation A is a simulation with a maximum value of k and the Modified calculation B simulates different k in the x - and y -direction.

Modified compression index, λ^*

Decreasing λ^* should give a stiffer soil response since the slope of the primary loading line is less steep. However, λ^* also has a large effect on the creep strains in the model through the β -factor explained in chapter 6.3, and hence the governing effect would be the increase of the creep strains which a decrease in λ^* would cause.

There are indications that λ^* varies with depth. According to evaluated data from CRS tests there is a slight increase of the parameter with depth. The soil layer could be divided into several layers, however, this will not be done for this investigation.

Simulations were first performed with the minimum value of λ^* according to Table 8.5 and validated through the soil tests. This simulation is referred to as Modified simulation A. The result showed that the creep rate in the nil-step is approximately 50 millimeters per year which is an unrealistic value. The result shows that the creep rate increases with a decrease in λ^* due to the effect of the β -factor. This implies that λ^* is an important parameter with large effects due to small changes. It is unfortunately not possible to differentiate the elastic strains from the creep strains in PLAXIS, which means that the effect on the creep strains cannot be fully evaluated.

The deformations under the tunnel showed a much better correlation with the measurement, see Figure 8.14, showing the large effect of the parameter λ^* on the creep rate.

Table 8.5. The range of the parameter λ^* . The maximum value was used in the original simulation and the others were used in the sensitivity analysis.

	Min	Average	Max
λ^*	0.17	0.20	0.23

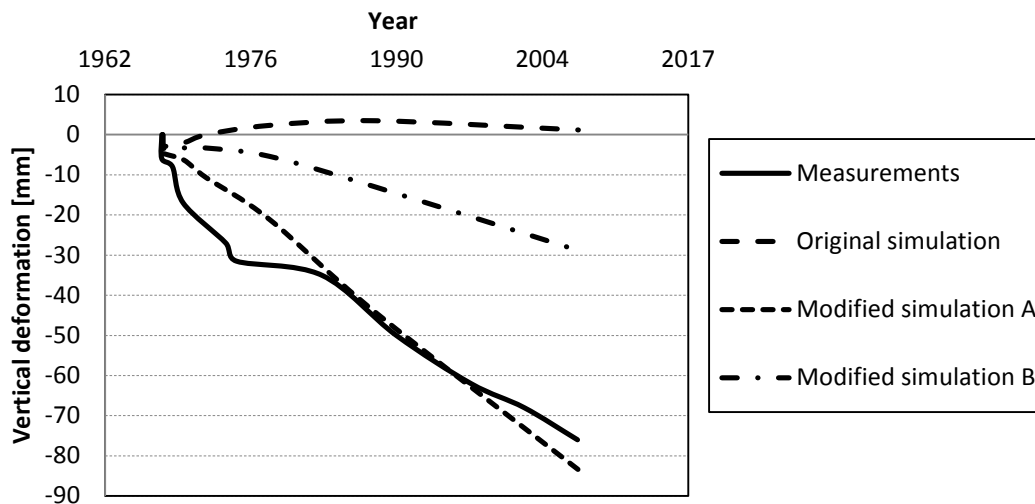


Figure 8.14. Sensitivity analysis of λ^* for Section C. Modified calculation A is a simulation with the minimum value of λ^* and the Modified calculation B simulates the average value.

The remaining pore pressure is much larger than the original simulation, with a maximum excess pore pressure of 14 kPa under the tunnel after the consolidation time. The pore pressure at the edges of the model is also larger due to the increased creep settlements. The remaining pore pressure seems to be too large since there is probably no excess pore pressure left at present time. Changing a combination of parameters could produce more realistic results but will not be covered in the scope of this investigation.

Another simulation was made with the average value of λ^* according to Table 8.5. The creep rate in the nil-step was 37 millimeters /year which is still large. The creep rate during consolidation time at the edges of the model is approximately 2.5 millimeters /year which is more reasonable and also higher than the original simulation, substantiating the effect of λ^* . When plotting deformation against time, no decrease in the settlement rate is observed which would have been expected.

The settlements after the consolidation time are shown in Figure 8.14 and show an under-estimation of the settlements. This result further displays the influence of the parameter where small changes of the value give large effects on the deformations.

Referring to chapter 6.3, where the evaluated λ^* with an OCR of 1.3 was much higher than the values used in this model, for this particular section a higher value of λ^* would create an even larger under-estimation of the deformations. Hence, no further simulation with other values than those in Table 8.5 was performed.

Modified swelling index, κ^*

A decrease of the parameter κ^* gives a stiffer response in the soil due to that the slope of the unloading/reloading line is flatter. In the original simulation the minimum value of κ^* was used. A change in this parameter is not expected to affect the settlements significantly but will mainly influence the magnitude of the initial heave.

As for λ^* , the evaluated data from Marieholm show a slight increase of the value with depth. Further division of soil layers could increase the accuracy of the model but will not be performed in the scope of this investigation.

The initial simulation was performed with the average value of κ^* , shown in Table 8.6. The creep rate in the nil-step amounts to 43 millimeters /year which is higher than the original simulation. This indicates, as previously shown in Table 6.9, that the effect of κ^* on the creep rate is smaller than for λ^* . In comparison with the creep rate in the edges of the model after the consolidation time, these amounts to 1.4 millimeters /year which is practically no difference from the original simulation indicating the smaller influence of κ^* .

Table 8.6. Range of the parameter κ^* . The minimum value was used in the original simulation and the sensitivity analysis was performed with the average value of κ^* .

	Min	Average	Max
κ^*	0.015	0.020	0.025

When comparing the initial heave it amounts to 150 millimeters with the modified simulation which is reasonable since the stiffness decreases with an increase in κ^* . The effect of this on the final settlements after the consolidation time shows in Figure 8.15. As expected the deformations are almost unchanged showing that κ^* has a small effect on the settlements.

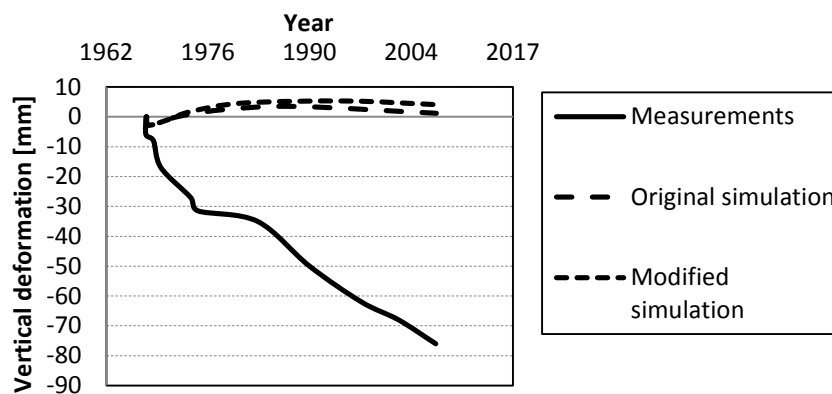


Figure 8.15. Sensitivity analysis of κ^* for Section C. The Modified calculation is a simulation with the average value of κ^* .

The remaining pore pressure under the tunnel is almost zero showing no deviation from the original simulation. The excess pore pressures at the edges of the model are also approximately the same as the original simulation.

Modified creep index, μ^*

The creep strains are largely affected by the creep index μ^* . An increase in this parameter will give larger creep strains. In this report, three methods were used for

evaluation of the creep index both with empirical basis. The chosen range for evaluation was Method 3. The maximum value according to Table 8.7 was used in the original simulation and the average value was evaluated in this sensitivity analysis, referred to as Modified simulation A.

Table 8.7. The range of the parameter μ^* . The maximum value was used in the original simulation and the sensitivity analysis was performed with the average value of μ^* .

	Min	Average	Max
μ^*	0.004	0.005	0.007

Since two of the evaluation methods suggests a relationship with the water content, this implies that μ^* decreases with depth. As for previous simulation, division of the soil layer will not be performed.

Simulations with the average value of μ^* the creep rate in the nil-step amounts to 29 millimeters /year which is large but smaller than the original simulation showing the effect of the parameter on the creep strains. Comparing the creep rate in the edge of the model after consolidation showed a creep rate of 0.2 millimeters /year which is unrealistically small. But the impact of a small change in the creep parameter is clear.

The settlements according to Figure 8.16, show that the creep rate is so low that settlements never start to occur during the investigated consolidation time.

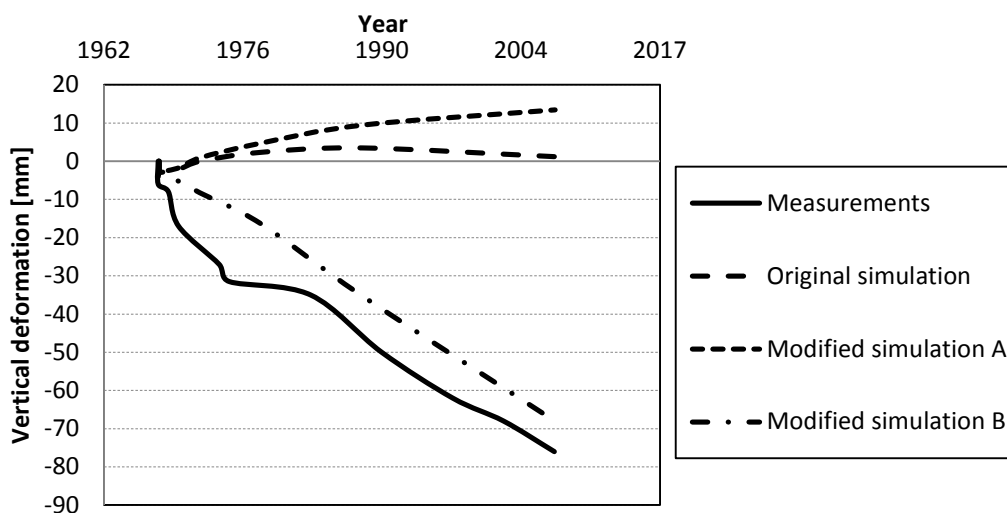


Figure 8.16. Sensitivity analysis of μ^* for Section C. Modified calculation A is a simulation with the average value of μ^* and the Modified calculation B simulates a value of $\mu^*=0.009$, which is higher than the maximum value.

There is almost no observed excess pore pressure at the edge of the model indicating that no creep settlements have occurred. A very small negative pore pressure of approximately 2 kPa is observed underneath the tunnel also indicating very small creep strains.

Since the simulations showed hardly any creep strains a simulation with a higher value than maximum was performed. The value was chosen to 0.009 since this was the maximum value for two of the three evaluated methods. This simulation is referred to as Modified calculation B.

The result showed that the creep rate in the nil-step increased to 50 millimeters /year showing the large effect a small change in μ^* gives. The creep rate at the edge of the model increased to approximately 4 millimeters /year. The settlement curve in Figure 8.16 shows the effect of the settlements under the tunnel and the result is a much better correlation to the measurement data.

The remaining pore pressure under the tunnel amounts to 12 kPa also indicating the increased creep rate.

OCR

The stress history of the soil is an important aspect in soil modeling. A higher OCR means that the soil has been exposed to larger loads in the past and is more resistant to loading up to the pre-consolidation pressure. Hence an increase in the OCR value should give a stiffer response.

The connection of the OCR to the β -factor is given in equation (6.7) which showed a very high β -factor with the OCR-value evaluated from laboratory tests. If the reverse calculation is performed with the β -factor used in the original simulation an OCR=1.6 is obtained, as shown in Table 6.9.

Raising the OCR to 1.6 resulted in an unchanged creep rate in the nil-step to 50 millimeters /year. The creep rate in the last consolidation stage is also unchanged with approximately 1.3 millimeters /year. The settlements under the tunnel is shown in Figure 8.17 and is also unchanged from the original simulation indicating that this change in OCR has little impact. The distribution of excess pore pressure is unchanged as well.

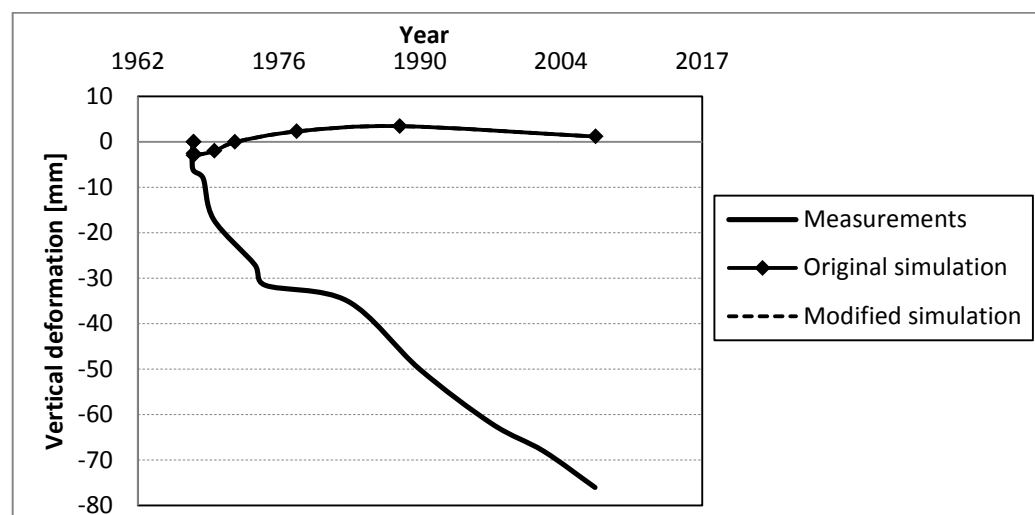


Figure 8.17. Sensitivity analysis of OCR for Section C. Modified calculation is a simulation with an increased OCR to 1.6 from 1.3.

ϕ' and K_0^{NC}

A simulation with a slightly decreased value on ϕ' to 28° , referred to as Modified simulation A, showed a small decrease in the creep rate of the soil at the edge of the model. The settlements under the tunnel are shown in Figure 8.18, which showed a lower settlement rate where the soil has not started to settle after the consolidation time has ended.

ϕ' is a strength parameter that determines the slope of the failure line. It also affects the K_0^{NC} -value through the relationship in equation (3.7). This equations states that a lower ϕ' gives a higher K_0^{NC} . K_0^{NC} in turn affects M , the slope of the CSL which for a high K_0^{NC} gives a low M which results in a less steep cap in p' - q -plane. Due to this a smaller deformation with a smaller ϕ' is reasonable. The result is however not correlating well with the measurements.

The validation of soil tests showed good correlation with triaxial tests when K_0^{NC} was set as a relatively large value. In addition, K_0^{NC} evaluated with the empirical method stated in equation (3.8) also gave a large value. Therefore, a simulation with a K_0^{NC} -value of 0.6 was performed, referred to as Modified calculation B. The settlements are shown in Figure 8.18 where it shows that decrease in the settlement rate is apparent, hence not correlating with the measurements.

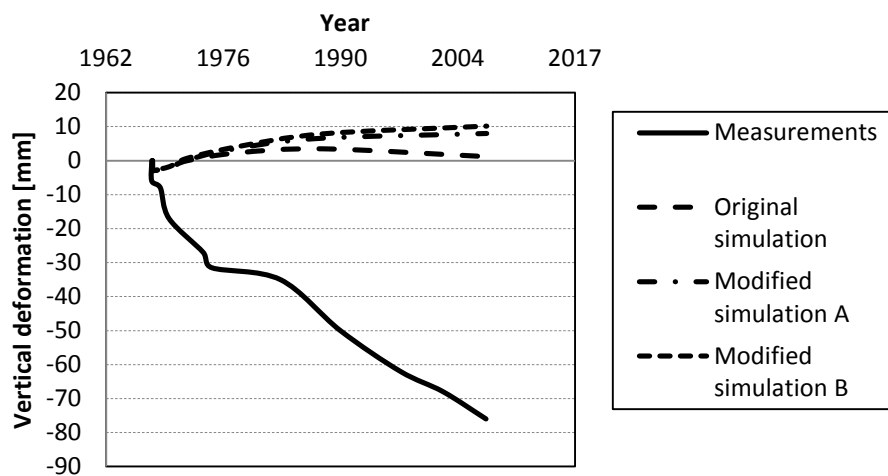


Figure 8.18. Sensitivity analysis of ϕ' K_0^{NC} and for Section C. Modified calculation A is a simulation with $\phi'=28$ and the Modified calculation B simulates a value of $K_0^{NC} = 0.6$.

8.4 Section D

The creep rate in the nil-step is very large with 55 millimeters /year. As for Section C, the edge of the model is experiencing creep settlements, causing a large remaining excess pore pressure of approximately 34 kPa in the middle of the clay layer. The corresponding creep rate is 8 millimeters /year which is reasonable though.

Underneath the tunnel there is a maximum remaining excess pore pressure of 9 kPa, which is a slight over-estimation since no excess pore pressure is expected to be found

at present time. The deformation in a point under the tunnel edge is compared to measured deformations in Figure 8.19. The settlement rate is overestimated in the simulation but captures the initial heave quite well.

The vertical deformation with depth is plotted in Figure 8.20. The piles transfer the load from the tunnel down into the soil. This probably causes the negative excess pore pressure, from previous unloading, to dissipate slower in the upper layers of the soil.

The differential settlements are approximately equal across the section.

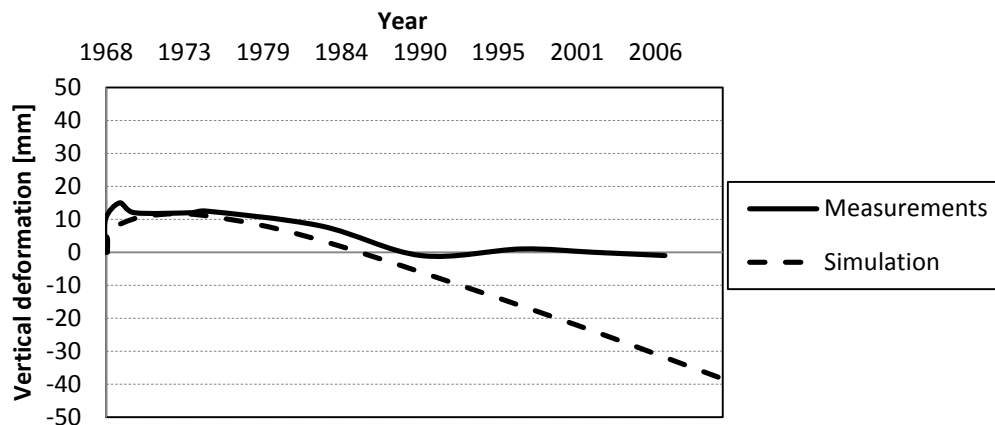


Figure 8.19. Vertical deformation over time for Section D, gauge 5:85. Simulation in PLAXIS compared to measurements.

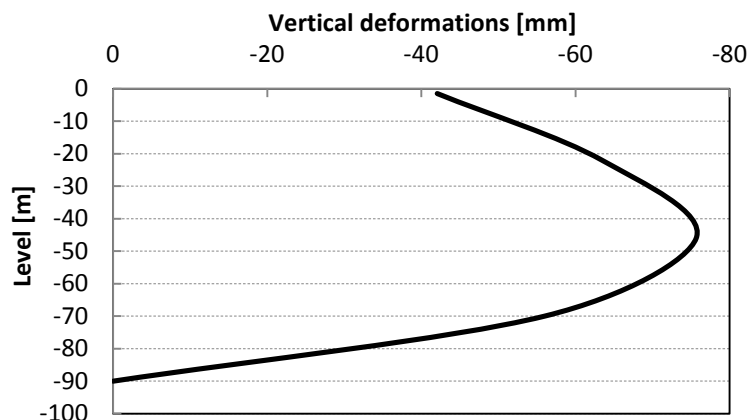


Figure 8.20. Vertical deformation with depth for Section D for a vertical section under the tunnel.

The simulation for the year 2047 show an excess pore pressure under the tunnel of maximum 9 kPa which means that the creep rate should have decreased over time. The same result is shown in the edge of the model where approximately 31 kPa remains. When plotting the deformations against time however, the settlement rate is not decreasing but instead the vertical deformations follow almost a linear relationship. This implies that adjustments is needed for the parameters affecting the creep the most, which is the creep parameter μ^* and the modified stiffness parameter λ^* .

8.5 Section E

Looking at the measured deformation for Section E, the settlement rate has subsided and in the year 2007 the accumulated settlement from the day of completion was 70 millimeters. The corresponding calculated deformation from the SSC model was 10 millimeters, see Figure 8.21. The simulation also shows swelling, which gradually are declining and turning into a settlement due to the creep.

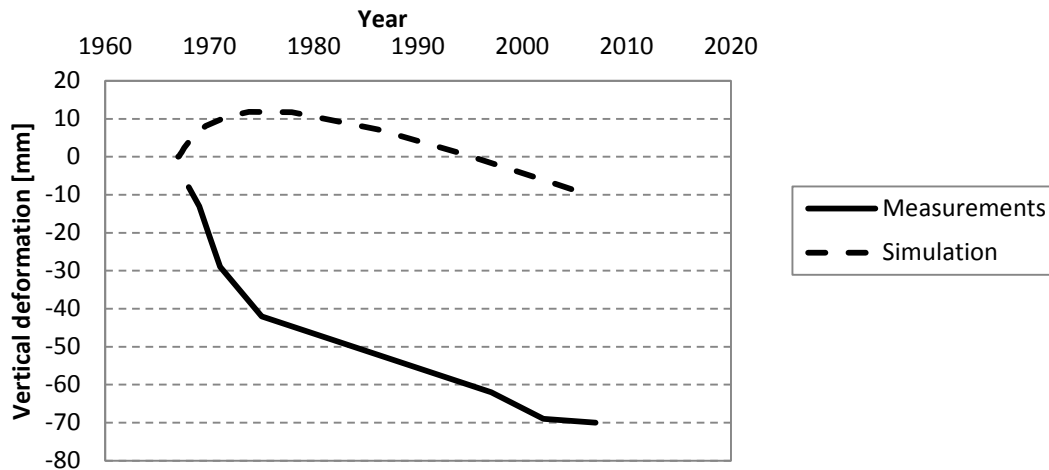


Figure 8.21. Vertical deformation over time for Section E, gauge nu18. Simulation in PLAXIS compared to measurements.

After the consolidation phase the pore pressure in the middle of the profile measures a maximum of 15 kPa, with about 5 kPa directly under the construction. Noteworthy is also that the model predicts a strain of 3 percent between the linear elastic layer and the soft soil creep layer, as for the other modeled sections. The swelling is continuing for a long time before the creep effect becomes governing. This occurs after approximately 10 years.

Plotting the deformation over the depth, in Figure 8.22, shows a similar scenario as other sections where the soil experience a heave in the upper soil layer and a settlement further down. This might be explained by the load transfer produced by the piles.

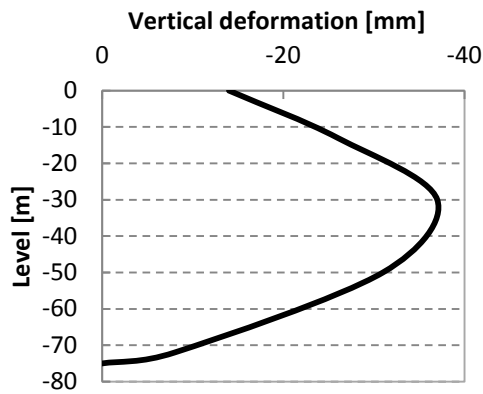


Figure 8.22. Settlement with depth for Section D for a vertical section under the tunnel construction.

8.5.1 Modified Calculations

The underestimation in the simulation compared to the measured deformation could imply that the load from the ramp or the fill is underestimated.

Since the load from the ramp is an uncertainty in this section an increased load where simulated, and the results can be seen in Figure 8.23, together with the original simulation. To emphasize the result of a change in the load it was increased significantly. The results show that an increase of the load from the original 80 kPa to the modified 120 kPa, see Table 8.8, changes the deformation from 10 millimeters to 61 millimeters, which is close to the measured 70 millimeters.

Table 8.8. Modification of load for Section E. Other parameters according to Appendix D.

Original load [kPa]	80
Modified load [kPa]	120

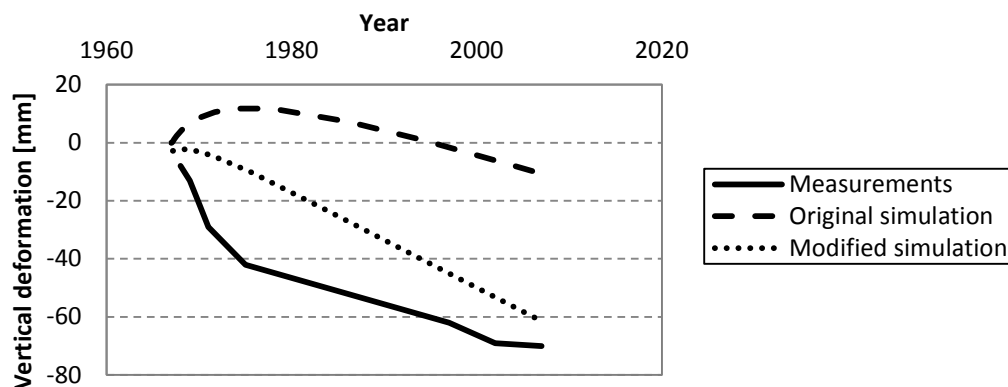


Figure 8.23. Deformation over time for Section E. The original simulation in PLAXIS is compared to a simulation with an increased load and compared to the measured deformations.

8.5.2 Modeling with HS

For this section the alternative soil model HS was evaluated, the input data can be seen in Appendix C, and the result is shown in Figure 8.24. Since the HS-model does not account for creep, the simulation only shows a heave that subsides in phase with time. Accumulated deformation by the year 2007 was simulated to 35 millimeters.

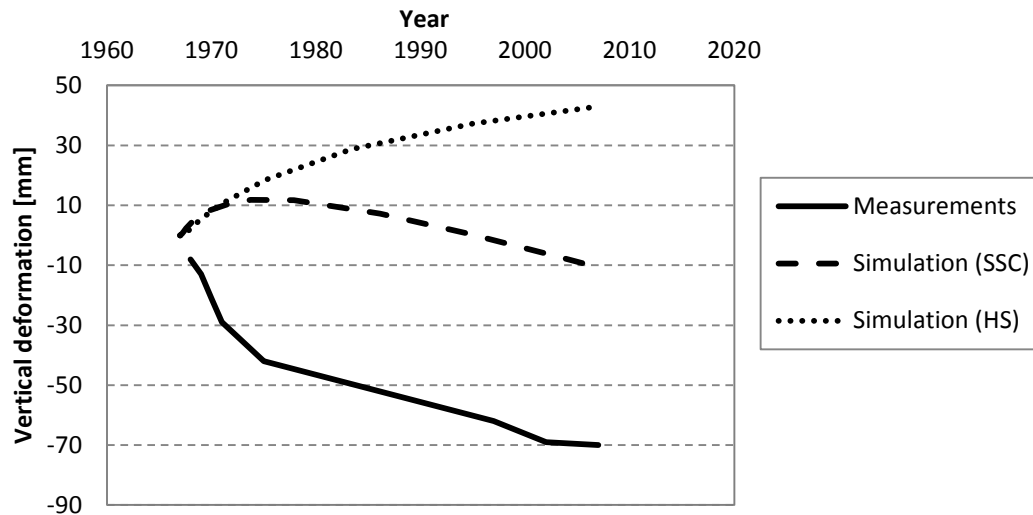


Figure 8.24. Deformation over time for Section E with the HS model. The simulation is compared to measurement data.

9 Discussion

In a new construction project, gaining experience from a similar project constructed in similar conditions is a helpful tool in projecting future behaviour of the new construction. The model can also work as a validation for the parameters used in the new design.

When studying the deformations along the tunnel stretch it is apparent that the PLAXIS simulations only capture the behaviour to some extent. Generally there is a tendency that the deformations are over-estimated. Most simulations are incapable of capturing the decreasing settlement rate observed in the measurement data.

In conclusion of the results the hypothesis was not confirmed for most sections. The prediction for Section A was that PLAXIS would give an underestimation of the settlements, while the calculations showed a slight over-prediction. The same result was obtained for Section B but with a larger over-estimation. The expectation that the deformations for Section A would be larger than Section B was however confirmed.

Section C was projected to show a slight underestimation of the settlements. The result showed a very large under-estimation of the deformations. The sensitivity analysis performed on this section showed a large effect from a change in the parameters λ^* and μ^* which both have a big impact on the irreversible strains. In a possible continuation of this project further investigation into these parameters, and the relationship between them, is suggested

The calculations for Section D were projected to present an initial heave reducing over time, which was the result from PLAXIS even though the settlement rate was too large. Lastly, Section E were projected to show a small settlement after construction but the result showed an initial heave that did not decline for a relatively long period of time.

The result summarised above indicates that further investigations are needed regarding both model parameters and geometric conditions. Some modified calculations were made for certain sections but to truly be able to see the effect of specific parameters, these analyses need to be performed for all sections.

The objective of this report was attempting a simplification process of the investigated construction project. This resulted in several insecurities and assumptions present in the models, such as structural behaviours, geometric conditions and assumptions regarding soil input data.

The available data from Tingstad is somewhat scarce and difficult to evaluate due to the age of the documents and the methods used for presenting the data. A reasonable assumption was made that the data retrieved from Marieholm could be used in the model. The evaluated parameters were validated through soil tests in PLAXIS and the results compared with the real tests. The data used, however, is current data and some parameters might not be representable for the soil conditions in the area 44 years ago. For example, ongoing settlements from surrounding urban exploitations have probably affected the properties through aging effects, described in previous chapters. Other effects, such as groundwater fluctuations and pore pressure changes might have affected the evaluated parameters.

The quality of the data can also be questioned. A rough estimation was made on the quality of the CRS tests and triaxial tests which showed an acceptable level. However, other methods of evaluating data would have been good to analyze. The insecurities in evaluated data and geometry made the modeling of the soil profile including the soil layers coarse regarding variation of the soil parameters.

The correctness of the input data is essential for a model to correspond to the measurements and to thoroughly investigate the insecurities in the model, the effects of a possible error in input data could be found. As stated previously the sensitivity analysis performed in this report might need to be extended to other sections to get a full understanding of the effect of certain parameters.

If the geometry of a model is too complex, there is a large risk that numerical difficulties occur in PLAXIS with the result that the calculations cannot converge. Therefore the geometry of the models has been made very rough which have an effect on the result. In many cases, where parts of the geometry have been removed, an attempt to investigate the effects of this action has been made through the construction of hypothetical cases. This is however a difficult task, since these hypothetical cases in turn are simplified and the true effect may be lost. In conclusion to this though, the main engineering task is to create a manageable simplification of the reality as accurately as possible and as long as there is awareness of the limitations made, the result will be useful.

PLAXIS is a user-friendly software but have some disadvantages. For example, if several changes are made in the model the program can store unwanted data and include it in the calculations even though the data is removed. There are other FEM-programs that are more flexible and transparent than PLAXIS, however, since PLAXIS is aimed specifically for geotechnical engineering purposes it suited this project well.

The models should also be checked for mesh dependency i.e. the model should predict the same results for a regenerated mesh as for previous generated mesh, ensuring that mesh influence are kept to a minimal. This is however a time-consuming procedure that was not performed in this thesis. PLAXIS also tends to store deleted structures when regenerating mesh which can cause problems in some calculations.

The pre-defined material model mainly used in this project was the SSC model. It is the only available pre-defined model that can account for creep effects, which means that the compared model HS does not account for creep. This shows in the result for Section E, where the two models were compared. The HS modeling shows a heave during the consolidation, but since the creep effect is excluded the heave during consolidation only subsides in rate, not turning into a settlement as the result for the SSC model. Section E is an example why the SSC model is superior to the HS model for prediction of long term soil behaviour. Since the project is complex with many aspects in consideration regarding loads, geometry and construction processes etc., the performance of the model is difficult to evaluate.

The SSC model has its limitations since it, for example, cannot account for anisotropy or clay structure. There is a possibility to apply user-defined models for modeling long-term behaviour. A continuation of the project presented in this report could be to apply a more advanced model and compare the result with the SSC. This would however require a higher degree of accuracy regarding many of the uncertainties

presented in the thesis, to be able to truly evaluate SSC and compare it to other models.

Another aspect to look at is the fact that the different cross-sections are interconnected with each other by the semi-continuous beam that is the tunnel structure. These 3D effects could be taken into consideration in a further continuation of the project by modeling the tunnel in PLAXIS 3D. The complexity will increase and probably several limitations as well but it could also result in a captured behaviour closer to reality.

10 Conclusion

It is possible to capture the behaviour of the soil around Tingstad and the measured long-term deformation of the Tingstad tunnel with a FE-analysis and with the Soft Soil Creep model in PLAXIS. However, due to the large amount of insecurities regarding input data and soil parameters, the model investigated in this thesis is not directly applicable as a benchmark for the Marieholm tunnel. Despite the execution of a sensitivity analysis, the parameters used could not be validated in the models for the different sections due to large effects from loads and unknown geometric conditions. In addition the complex geometry of the models makes it difficult to evaluate possible errors and the performance of the chosen material model.

Further studies would be required to increase the accuracy of the model, for example, through access to more construction documents and a larger time span for the project. Some recommendations of future research within this project are listed below:

- Load contribution from the tunnel and the ramp construction
- Load contribution from the refill material
- Geometric conditions regarding original surface level and dredging level
- Construction processes with regard to sequence and construction times
- More extensive evaluation of input parameters where focus should lie on the stiffness parameter λ^* and the creep index μ^* .
- Sensitivity analysis for other sections to be able to capture deformations along the whole tunnel stretch.

In addition, if a higher degree of accuracy could be obtained a comparison with a more advanced model could be useful to see if the effect of anisotropy and clay structure could capture the deformations in a better way. An extension of the model to 3D could also be performed to be able to more accurately capture the deformations since the assumption of plain strain is not entirely accurate

11 References

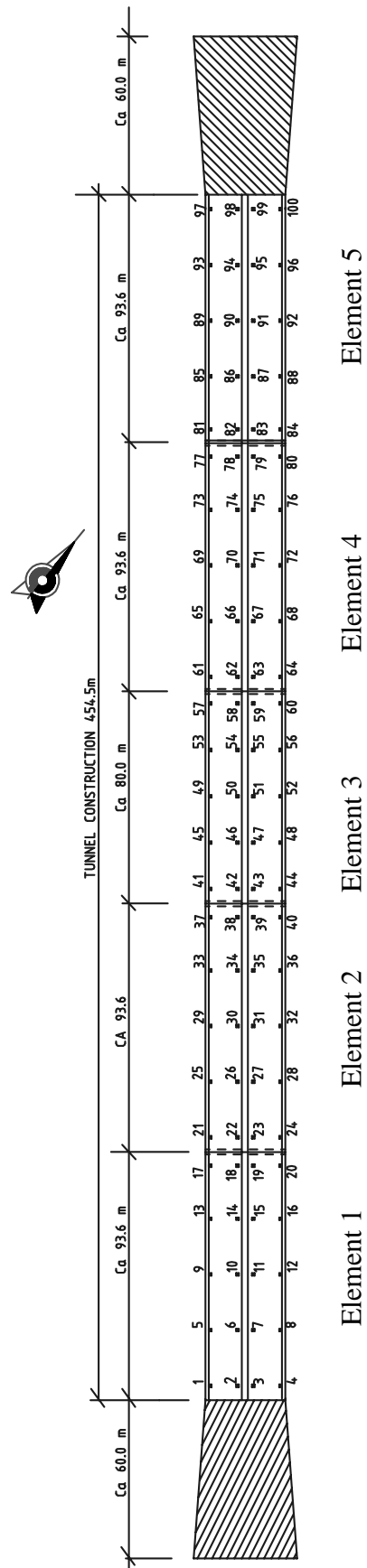
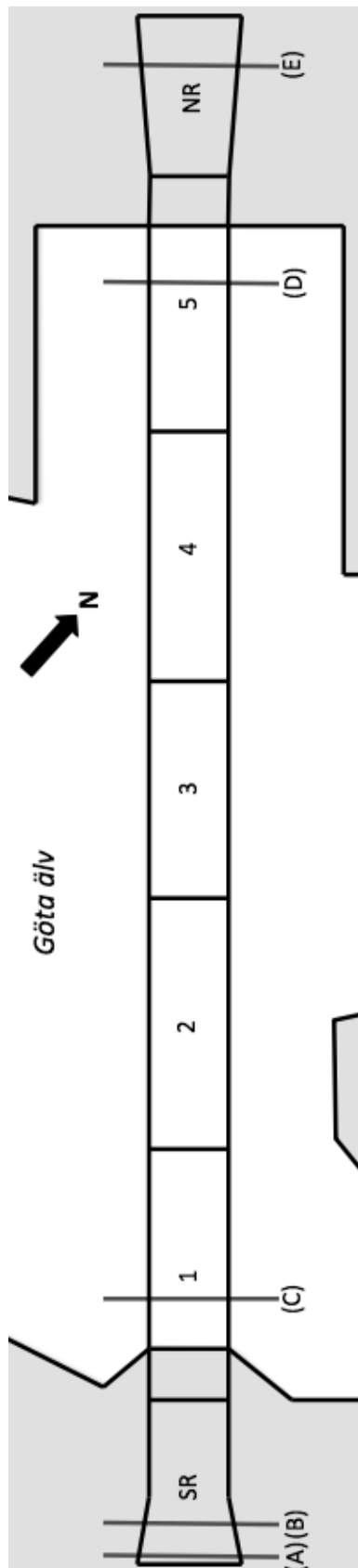
- Bo, M., et.al. (2011): *Predicting consolidation settlements using small-strain, large-strain and stress path methods*. IOS Press, Amsterdam.
- Chang-Yu, O. (2006): *Deep excavation: Theory and practice*. Taylor and Francis group, London.
- Claesson, P. (2003): *Long term settlements in clay*. Chalmers University of Technology, Gothenburg.
- Craig, R.F. (2004): *Craig's Soil mechanics*. Spon Press. London.
- Edstam, T. (2004): *E6/Väg 45/E20 Marieforsförbindelsen; Analys- och Beräknings-PM*. WSP, Gothenburg.
- Gatubolaget (2005): *Tingstadstunneln; Utredning avseende bärrighet, beständighet och deformationer*. Gothenburg.
- Karstunen, M. (2012): *Deformations and preloading methods*. (Education Material in Infrastructural Geo-engineering). Chalmers University of Technology, Gothenburg.
- Kompetenscentrum Infrastruktur (n.d.): *En kortkurs om triaxialförsök på främst normalkonsoliderade och svagt överkonsoliderade leror*.
- Kullingsjö, A. (2007): *Effects of deep excavations in soft clay on the immediate surroundings - Analysis of the possibility to predict deformations and reactions against the retaining system*. Chalmers University of Technology, Gothenburg.
- Lambe, W. (1969): *Soil Mechanics*. John Wiley and Sons, New York.
- Larsson, Bengtsson and Eriksson, (1997): *Prediction of settlements of embankments on soft, fine-grained soils. Calculation of settlements and their course with time*. Swedish Geotechnical Institute. Linköping.
- Larsson, R., et.al. (2007): *CPT-sondering*. Swedish Geotechnical Institute. Linköping.
- Larsson, R. (2008): *Jords egenskaper*. Swedish Geotechnical Institute. Linköping.
- Larsson, R. et.al.(2007): *Skjuvhållfasthet – utvärdering i kohesionsjord*. Swedish Geotechnical Institute. Linköping.
- Meyer Karel, L. (1984): *Comparison of Finite and Infinitesimal Strain Consolidation*. Delft Hydraulics Laboratory, Delft.
- Nilsson, B. (2012): *Finite elementmetoden. En kort introduktion till teorin*. Högskolan I Halmstad, Halmstad.
- Olsson, M. (2010): *Calculating long-term settlements in soft clays – with special focus on the Gothenburg region*. Thesis for the degree of licentiate of engineering. Department of civil and environmental engineering. Division of GeoEngineering. Chalmers University of Technology. Göteborg, Sweden.
- Persson, J. (2004): *The Unloading Modulus of Soft Clay: A Field and Laboratory Study*. Thesis for the degree of licentiate of engineering. Department of civil and environmental engineering. Division of GeoEngineering. Chalmers University of Technology. Göteborg, Sweden.

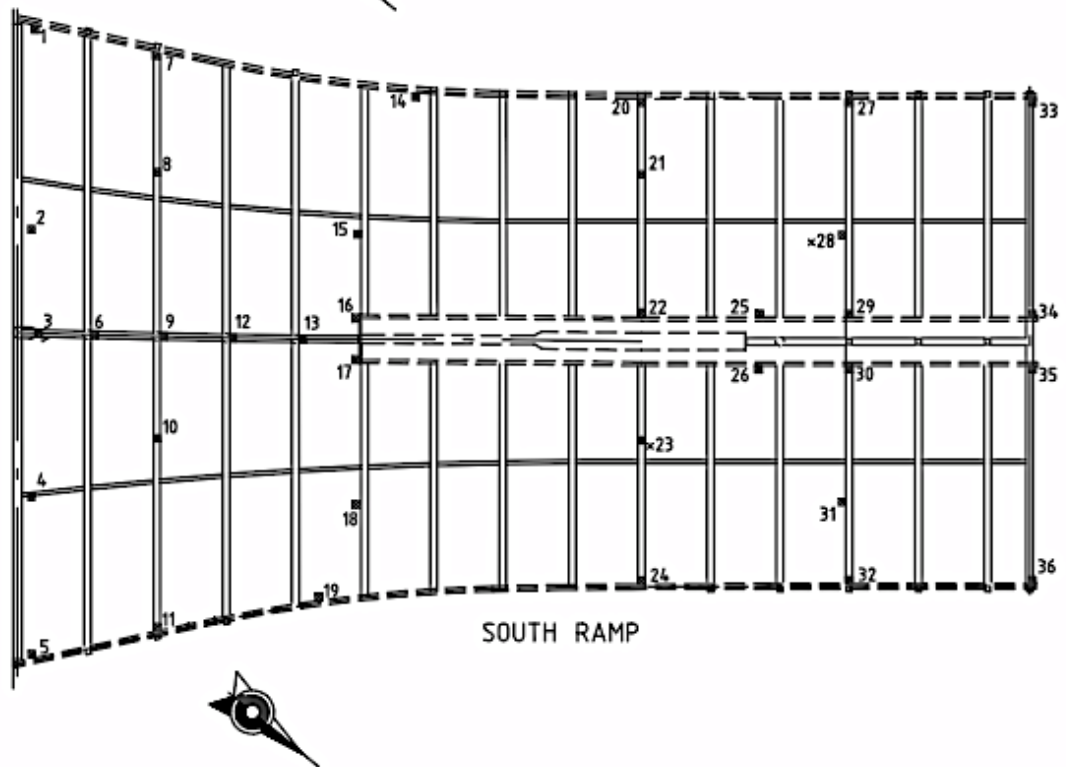
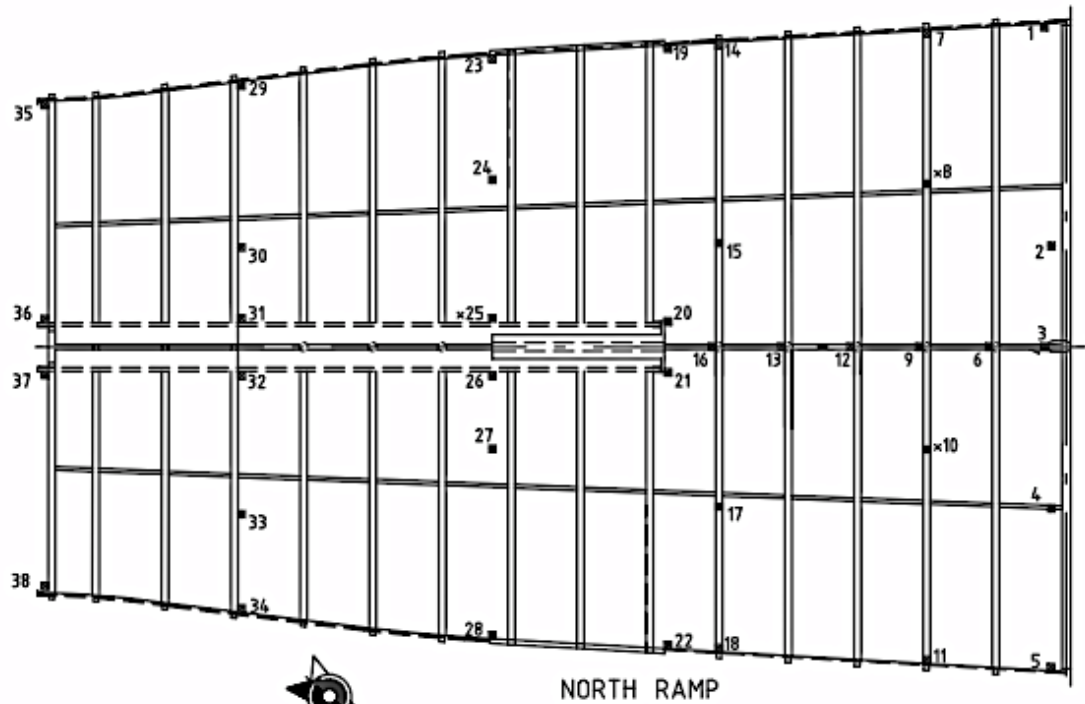
- PLAXIS, a (2012): *Material Models Manual*. [online] Available at: <<http://www.plaxis.nl/files/files/2D2012-3-Material-Models.pdf>> [Accessed 2013-01-22].
- PLAXIS, b (2012): *Reference Manual*. [online] Available at: <<http://www.plaxis.nl/files/files/2D2012-2-Reference.pdf>> [Accessed 2013-01-22].
- PLAXIS, c (2012): *Scientific Manual*. [online] Available at: <<http://www.plaxis.nl/files/files/3D2012-4-Scientific.pdf>> [Accessed 2013-02-22].
- Potts, D. et.al.(2002): *Guidelines for the use of advanced numerical analysis*. Thomas Telford Limited, London.
- Potts, D., Day, R. (1991): *The effect on wall stiffness on bending moments*. [online] Available at: <http://jdfields-cp.com/pdf/highway_transportation/wp_dfi_effects_of_wall_stiffness_on_bending_for_sheet_pile_walls.pdf> [Accessed 2013-05-28]
- Potts, D., Zdravković, L. (1999): *Finite element analysis in geotechnical engineering: theory*. Imperial College of Science, Technology and Medicine, London.
- Runesson, K. (2006): *Constitutive Modeling of Engineering Material*. Chalmers University of Technology, Gothenburg.
- SWEGIS (2006): *GeoWebShare*. [online] Available at: <maps.arch.chalmers.se> [Accessed 2013-05-28].
- Sällfors, G. (2001): *Geoteknik*. Gothenburg.
- Vägverket (2007): *Älvförbindelse i Göteborg*. [online] Available at: <http://publikationswebbutik.vv.se/upload/2924/2007_30_alvforbindelse_i_goteborg_och_sarbarhet.pdf> [Accessed 2013-02-15]
- Wood, D. (1990): *Soil behaviour and critical soil mechanics*. Cambridge University Press, Cambridge.

Appendices

- A. Section and Gauge placement
- B. Diagram of measured deformations
- C. Soil properties
- D. PLAXIS Input data
- E. Load calculations
- F. Pile calculations
- G. Hypothetical cases
- H. Cross-section geometry
- I. PLAXIS geometry

Appendix A. Section and Gauge placement





Appendix B. Measured deformations

Data obtained from the report issued by Gatubolaget (2005).

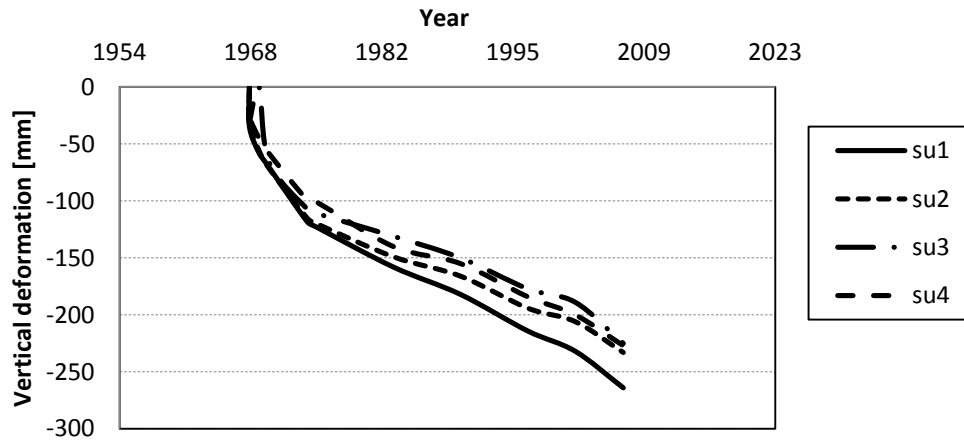


Figure B.1. Measured deformations over time for Section A.

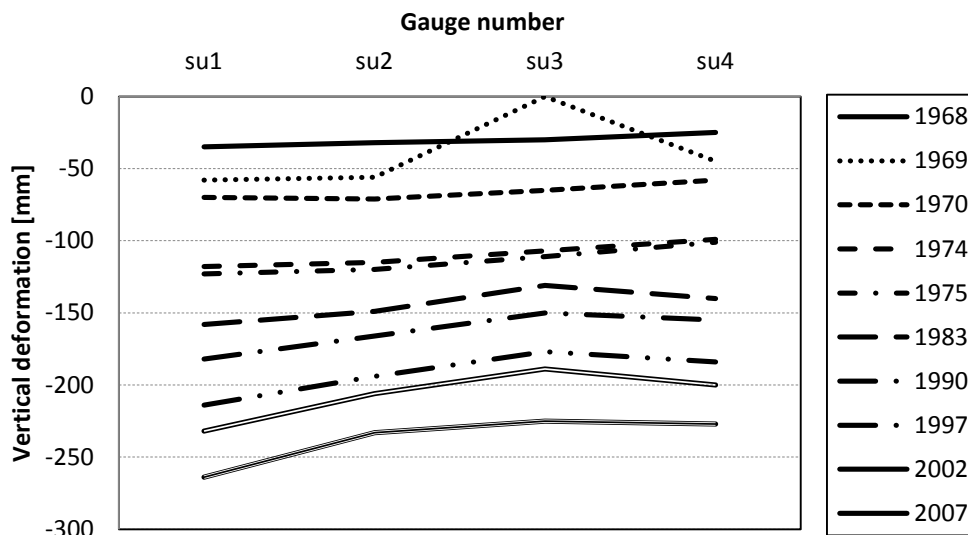


Figure B.2. Differential settlements in Section A for different years.

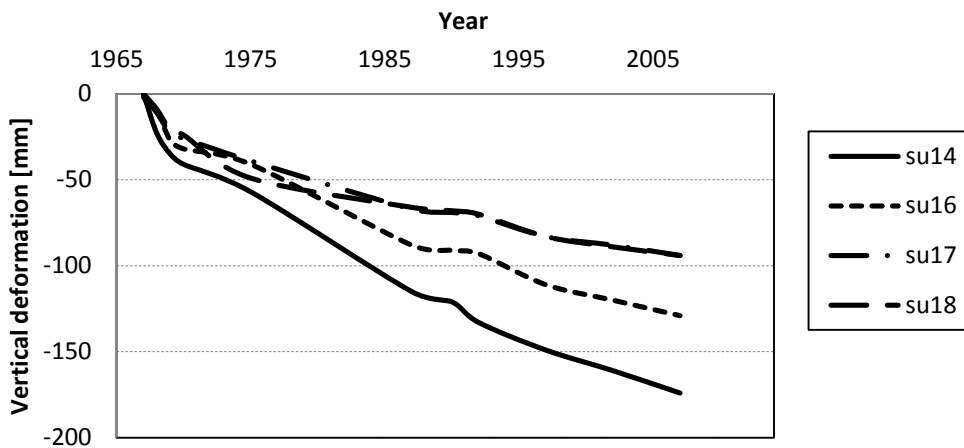


Figure B.3. Measured deformations over time for Section B.

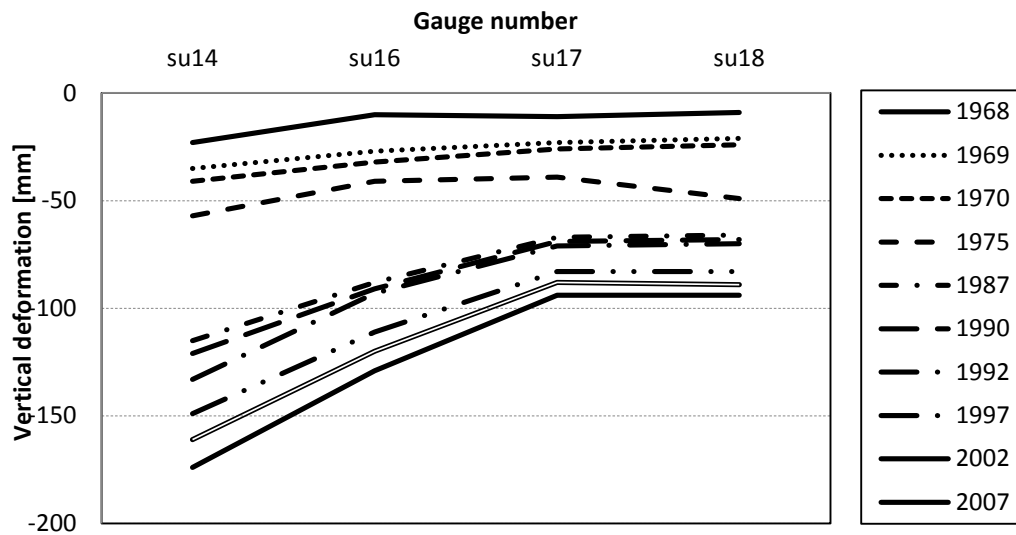


Figure B.4. Differential settlements in Section B for different years.

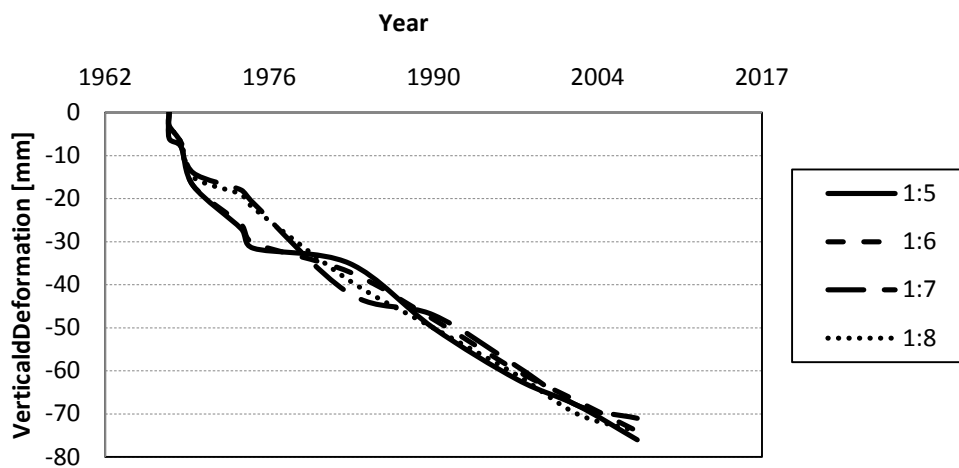


Figure B.5. Measured deformations over time for Section C.

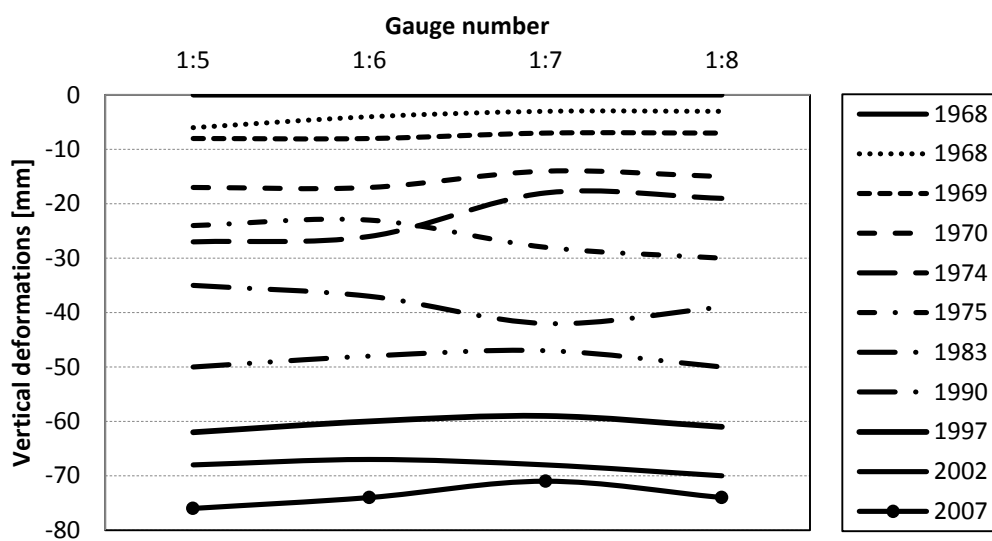


Figure B.6. Differential settlements in Section C for different years.

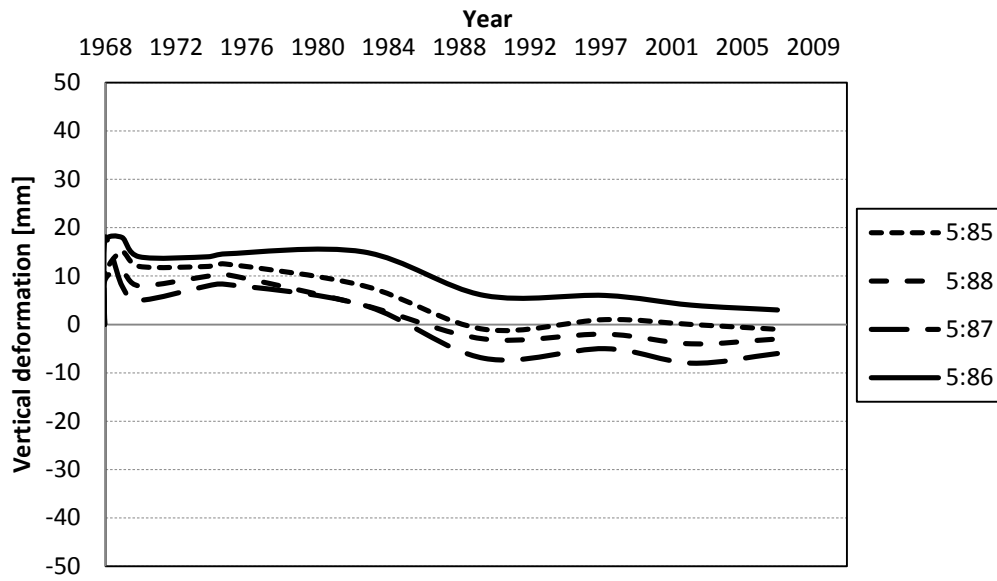


Figure B.7. Measured deformations over time for Section D.

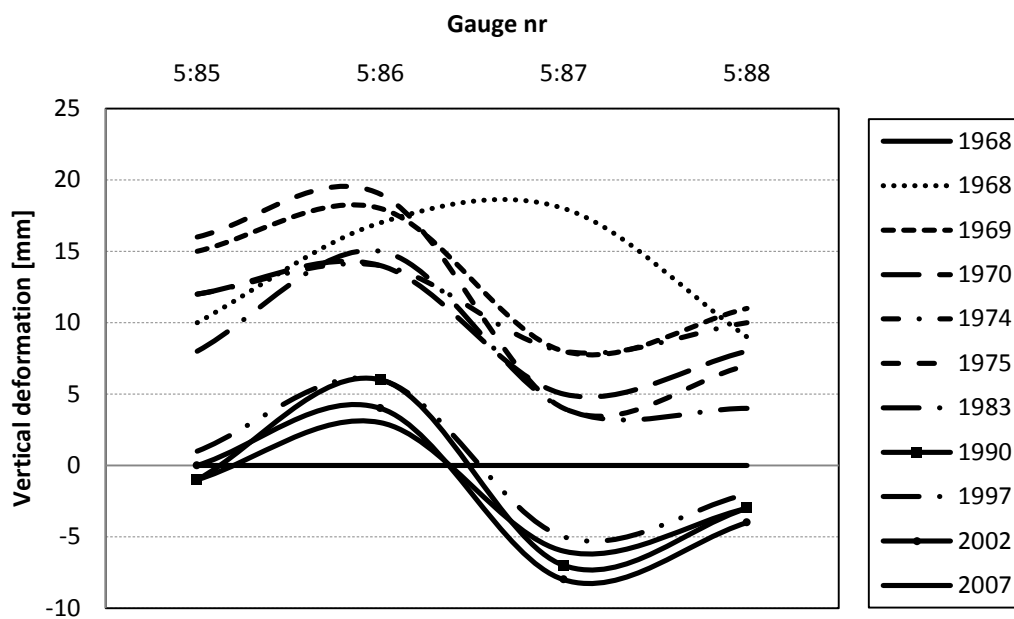


Figure B.8. Differential settlements in Section D for different years.

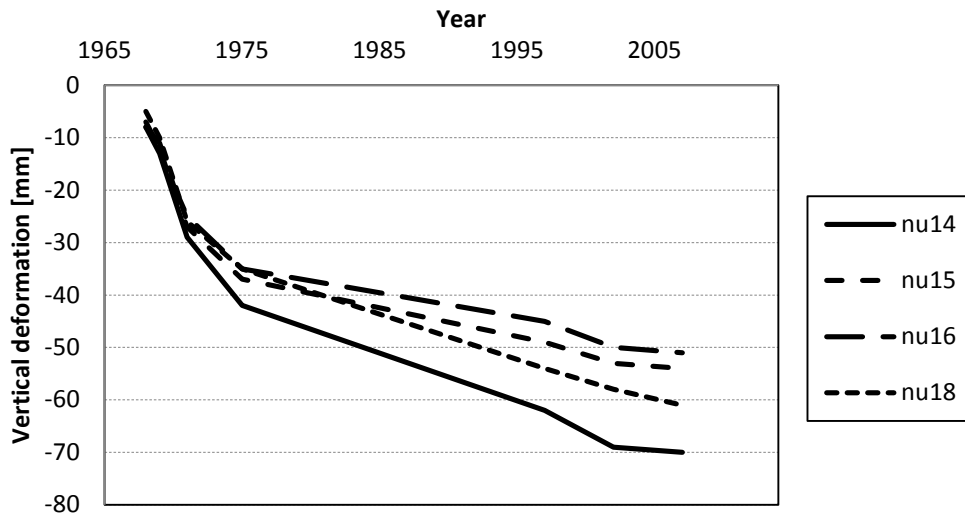


Figure B.9. Measured deformations over time for Section E.

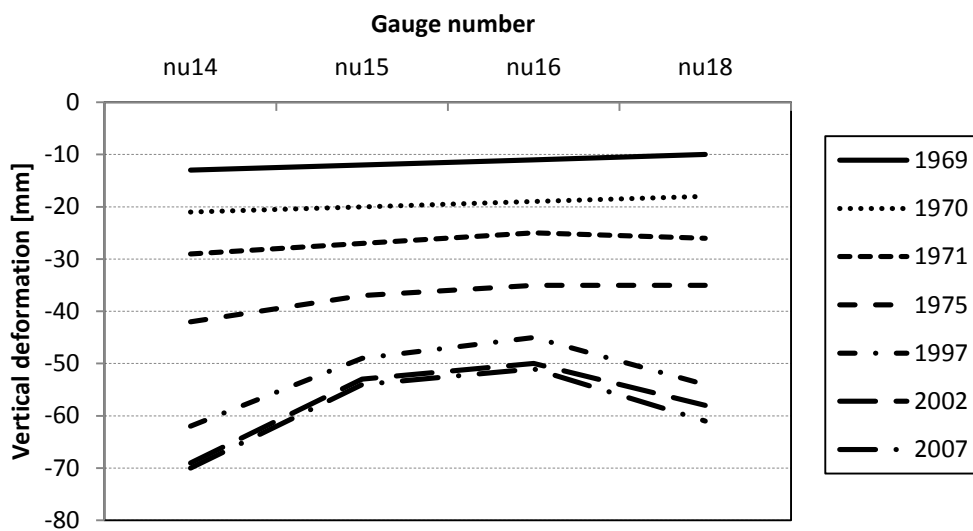


Figure B.10. Differential settlements in Section E for different years.

Appendix C. Soil properties

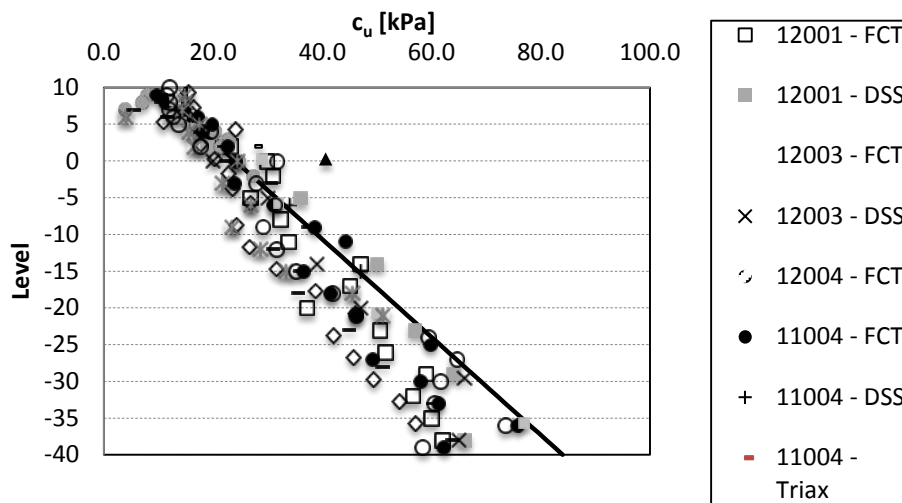


Figure C.2.

Shear strength from boreholes in Marieholm. Evaluated c_{uk} ; $15+1.5z$ with z starting at +5.

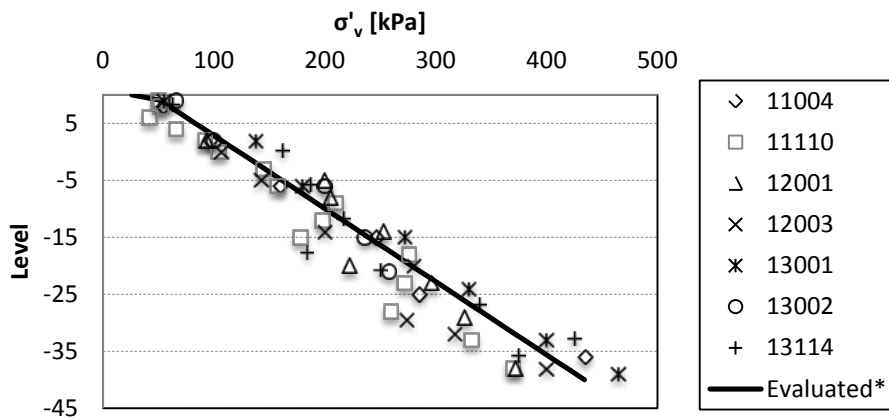


Figure C.3. Preconsolidation pressure from boreholes in Marieholm. Evaluated $OCR=1.3$.

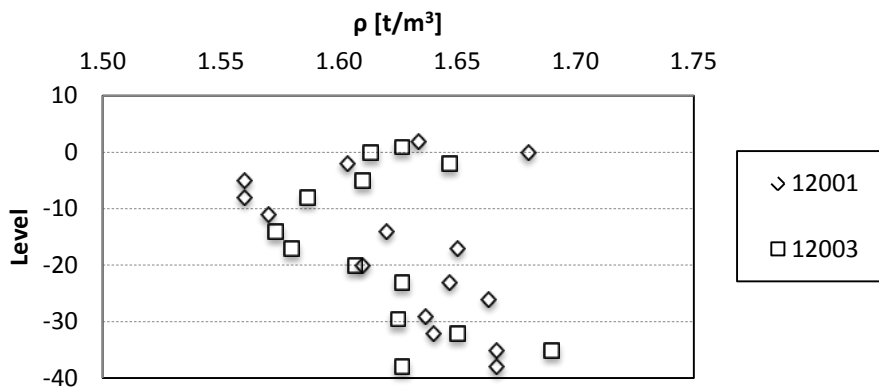


Figure C.4. Density for boreholes in Marieholm.

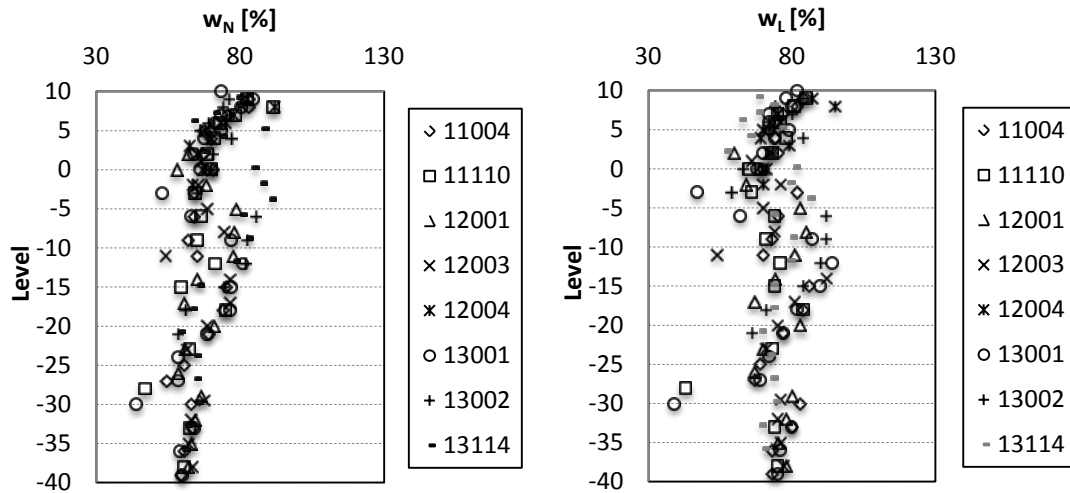


Figure C.5 Natural water content and liquid limit for boreholes in Marieholm.

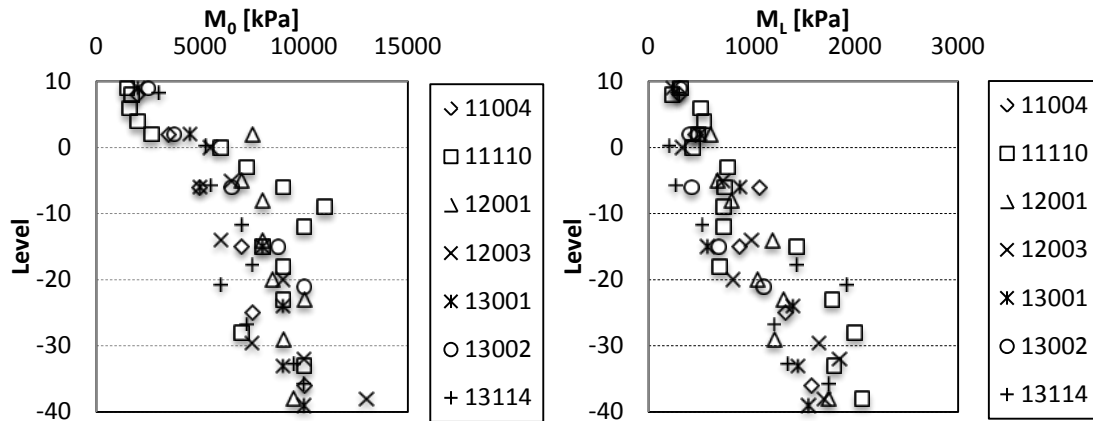


Figure C.6. Oedometer moduli M_0 and M_L for boreholes in Marieholm.

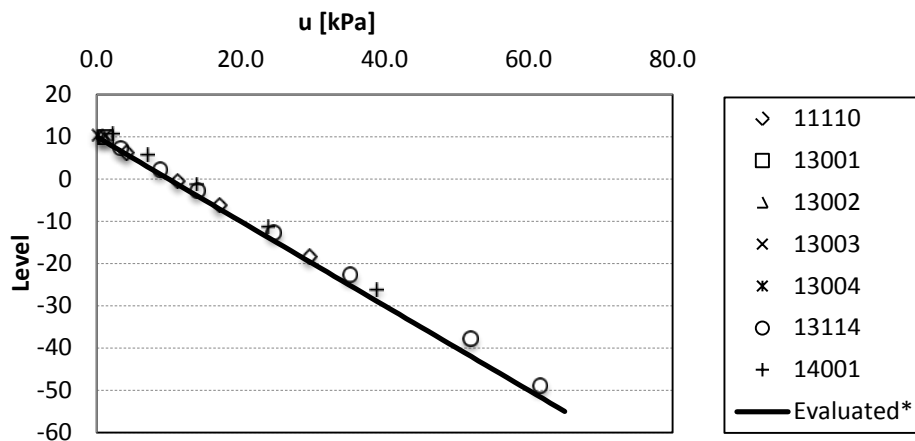


Figure C.7. Pore pressure measurements from boreholes in Marieholm. Evaluated hydrostatic pore pressure from +10 m.

Table C.6. Evaluated range of the permeability from CRS-tests in Marieholm.

Permeability	Average	Standard dev.	Min	Max
k [m/s]	4.7E-5	3.5E-5	1.2E-5	8.2E-5

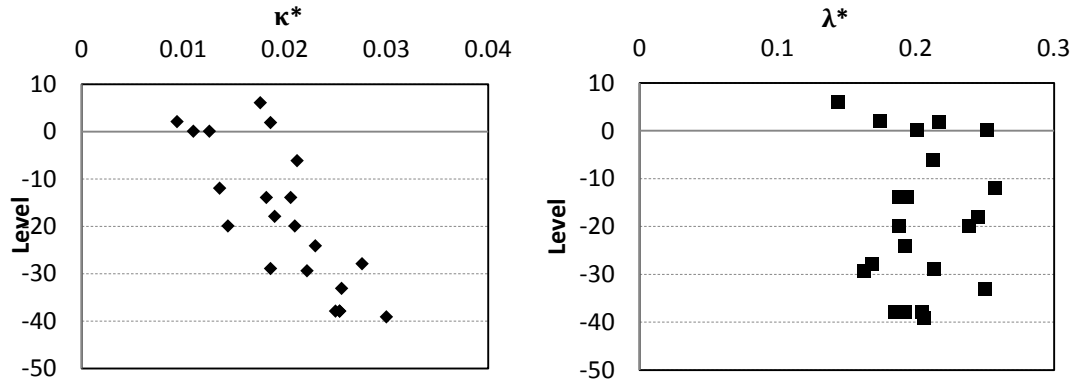


Figure C.8. Distribution of κ^* and λ^* with depth evaluated from boreholes in Marieholm.

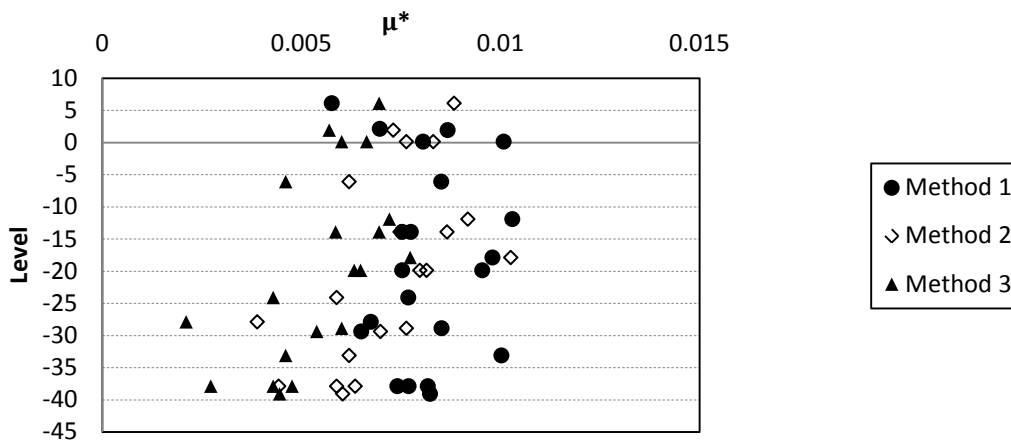


Figure C.9. Evaluation of μ^* with two different methods from boreholes in Marieholm.

Table C.7. Evaluated range of the parameters λ^* , κ^* and μ^* .

Parameter	Average	Standard dev.	Min	Max
λ^*	0.20	0.03	0.17	0.23
κ^*	0.2	0.005	0.015	0.025
μ^* (Method 1)	0.008	0.0012	0.007	0.009
μ^* (Method 2)	0.007	0.0015	0.006	0.009
μ^* (Method 3)	0.005	0.0015	0.004	0.007

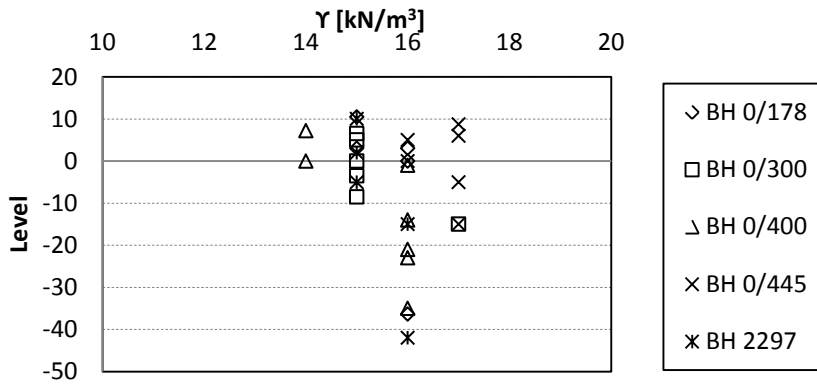


Figure C.10. Soil weight from boreholes at Gullberg junction.

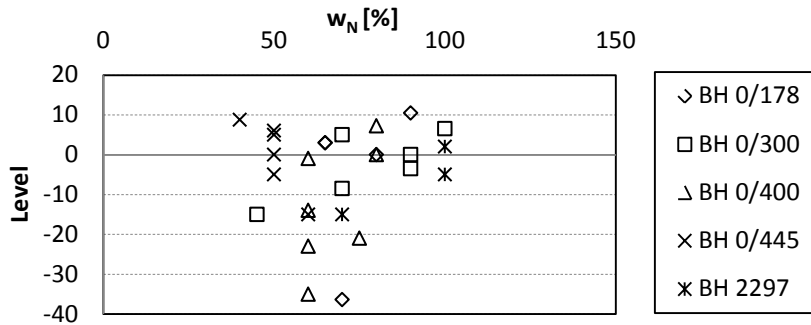


Figure C.11. Natural water content from boreholes at Gullberg junction.

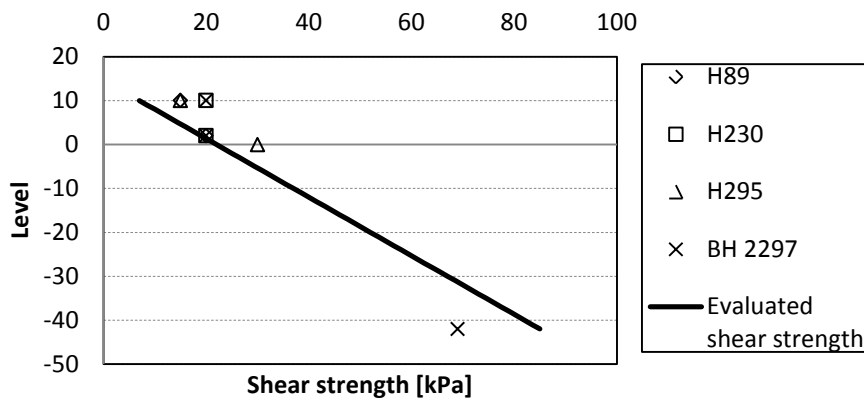


Figure C.12. Shear strength from boreholes at Gullberg junction.

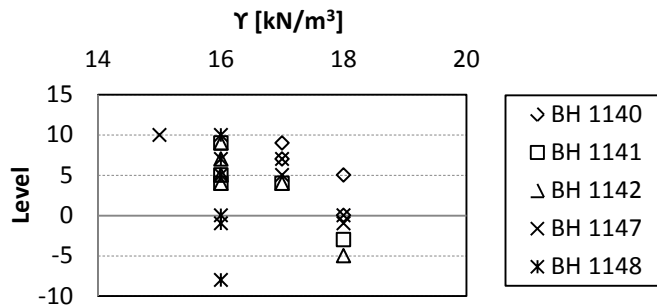


Figure C.13. Soil weight from boreholes at Ringö junction.

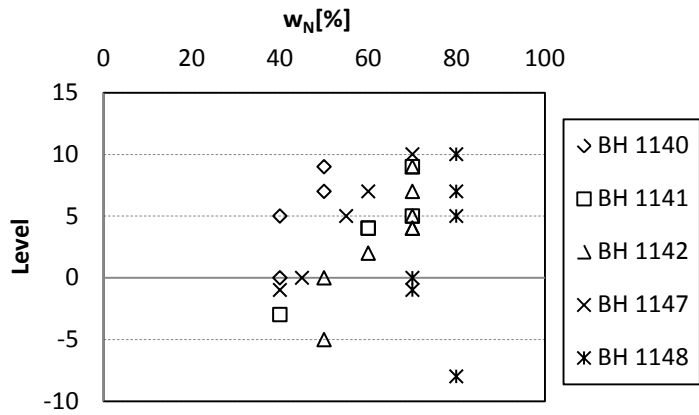


Figure C.14. Natural water content from boreholes at Ringö junction.

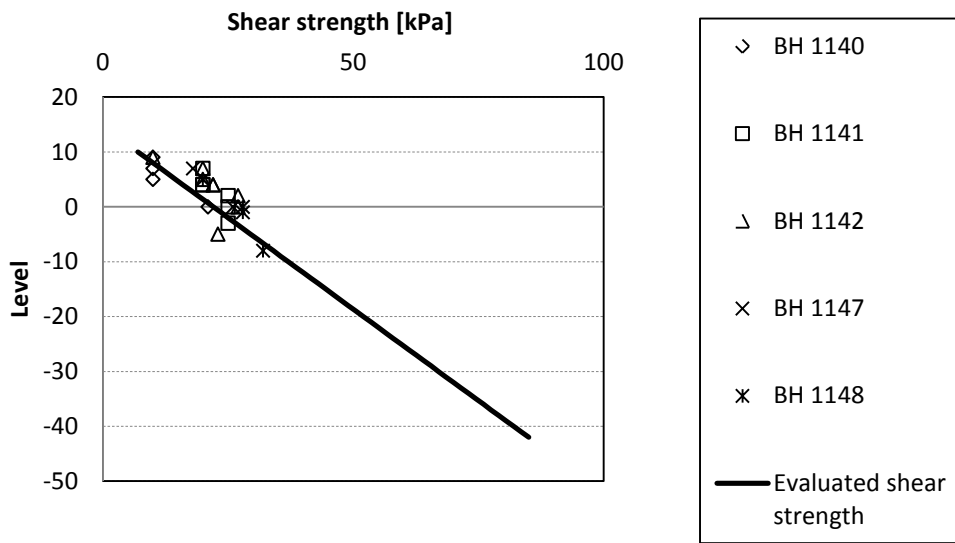


Figure C.15. Shear strength from boreholes at Ringö junction.

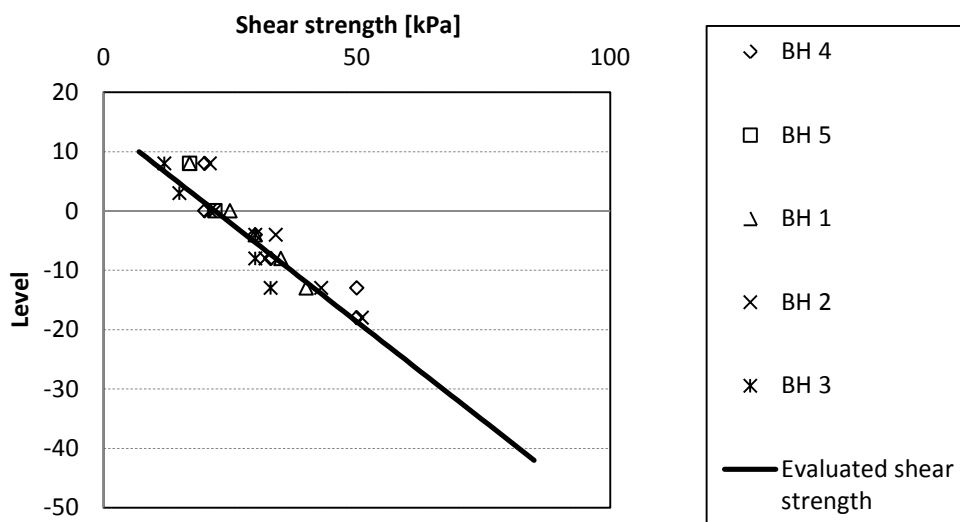


Figure C.16. Shear strength from boreholes at Tingstadsvass.

Appendix D. PLAXIS Input data

Table D.1. Input data for soil materials.

	Clay	Clay	Fill	Let	Gravel	Refill clay	Coke slag
Material model	SSC	HS	LE	LE	LE	LE	LE
Drainage behaviour	Undrained (A)	Undrained (A)	Drained	Undrained (A)	Drained	Undrained (A)	Drained
γ_{unsat}	16	16	21	16	21	16	11
γ_{sat}	16	16	21	16	21	16	11
e_{in}	2	2	-	-	-	-	-
λ^*	0.23	-	-	-	-	-	-
κ^*	0.015	-	-	-	-	-	-
μ^*	0.007	-	-	-	-	-	-
E_{50}^{ref}	-	870	-	-	-	-	-
$E_{\text{oed}}^{\text{ref}}$	-	435	-	-	-	-	-
$E_{\text{ur}}^{\text{ref}}$	-	13300	-	-	-	-	-
m	-	1	-	-	-	-	-
c'_{ref}	3	3	-	-	-	-	-
ϕ'	30	30	-	-	-	-	-
ψ'	0	0	-	-	-	-	-
ν_{ur}'	0.15	0.15	-	-	-	-	-
$k_{x,y}$	5.00E-05	5.00E-05	0.6	5.00E-05	0.6	5.00E-05	0.6
K_0	0.6	0.6	-	-	-	-	-
OCR	1.3	1.3	-	-	-	-	-
E	-	-	2.50E+04	2.50E+04	2.50E+04	2.50E+04	2.50E+04

Table D.2. Input data for piles.

	Tunnel piles	Concrete piles	Bank-piles, long	Bank-piles, short
E	1.20E+07	3.70E+07	1.20E+07	1.20E+07
γ	4.6	25	4.6	4.6
Pile type	Massive circular	Massive square	Massive circular	Massive circular
Diameter/side	0.126	0.25	0.126	0.126
L_{spacing}	1.5	3	2	1.5
T_{top,max}	250	552	365	228
T_{bot,max}	435	975	754	380
F_{max}	3	16	4	3

Table D.3. Input data for the tunnelpart and the ramp

	Material type	EA	EI	w	v
Tunnel/Ramp	<i>LE</i>	5.00E+06	1.00E+06	<i>0</i>	<i>0.2</i>

Table D.4. Changed parameters in stronger SSC Clay for Section A.

c'_{ref}	10
φ'	37
OCR	2

Appendix E. Tunnel load calculation

Cross-sectional area	93 m ²
Weight of concrete	2.5 t/m ³
Tunnel weight/m	233 t/m
Tunnel load/m	2330 kN/m
Tunnel load/m ²	78 kPa \approx 80 kPa

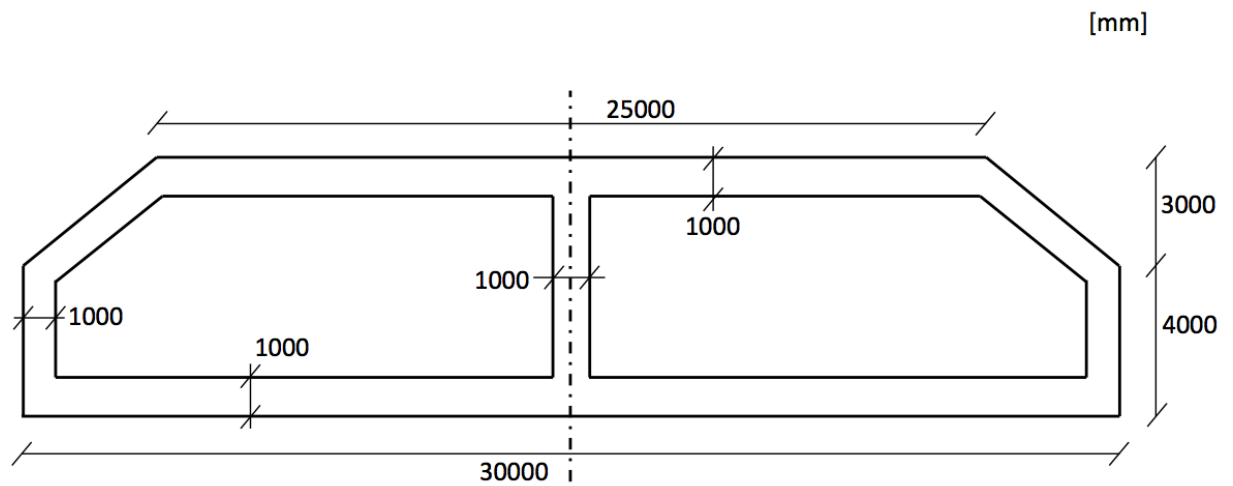


Figure E.1. Cross-section for the tunnel

Appendix F. Pile calculations

Pile equations			
Shaft friction, f_m	$f_m = \alpha c_u$	kN	
Shaft resistance, R_m	$R_m = f_m A_m$	kN	
Toe resistance, R_s	$R_s = N c_u A_s$	kN	
c_u	$24 + 0,8 * h$	kPa	($h_0 = +/- 0$)
Wood pile under tunnel			
Diameter	0.126	m	
L	22	m	
α	1.2		
c_{u_top}	24	kPa	(wood piles starts at +/- 0)
c_{u_bottom}	41.6	kPa	
A_m	8.70	m ²	
R_{m_top}	250	kN	
R_{m_bottom}	435	kN	
N	6		
A_s	0.012	m ²	
R_{s_toe}	3	kN	
Concrete piles under ramp			
Side, a	0.25	m	
L	23	m	
α	1		
c_{u_top}	24	kPa	
c_{u_bottom}	42.4	kPa	
A_m	23	m ²	
R_{m_top}	552	kN	
R_{m_bottom}	975.2	kN	
N	6		
A_s	0.0625	m ²	
R_{s_toe}	15.9	kN	
Bankpiles under fill, long			
Diameter	0.126	m	
L	32	m	
α	1.2		
c_{u_top}	24	kPa	
c_{u_bottom}	49.6	kPa	
A_m	12.6	m ²	
R_{m_top}	365	kN	
R_{m_bottom}	754	kN	
N	6		
A_s	0.012	m ²	
R_{s_toe}	4	kN	
Bankpiles under fill, short			
Diameter	0.126	m	
L	20	m	
α	1.2		
c_{u_top}	24	kPa	
c_{u_bottom}	40	kPa	
A_m	7.9	m ²	
R_{m_top}	228	kN	
R_{m_bottom}	380	kN	
N	6		
R_{s_toe}	3	kN	

Appendix G. Hypothetical calculations

To validate some of the delimitations made for simplification, several hypothetical cases have been investigated in PLAXIS to be able to see the effect of excluding the particular feature or geometry.

G.1. Redirection of S ave an

In conjunction with the construction of the tunnel, the outlet for S ave an was moved further west. This three meter deep excavation caused an unloading scenario on the surrounding area including the investigated cross-sections of the ramp and tunnel, which is located 105 meters from the outlet. Hence a study was made in PLAXIS to determine this influence on these cross-sections. The result, which can be seen in Table G.1 shows that the excess pore pressure at the location of the cross-sections is negligible and can be excluded in further modelling.

Table G.1. Maximum excess pore pressure for different distances from the outlet.

Distance from new outlet [m]	$P_{\text{excess, max}}$ [kPa]
100	2
80	2.5
60	3
40	4.5
20	7

G.2. Bank piling effect

To simplify the geometry in PLAXIS the spacing of the bank piles needed to be reduced. For estimating the effects of the bank piles a simple calculation was made in PLAXIS. In reality the spacing between the piles is two meters. A simple geometry was used where an embankment was added, supported by 32 meter long wood piles. The same soil parameters and pile material as in the actual model was used in the hypothetical case. The aim was to see the difference in deformations with regard to the spacing of the piles in the x-direction. Calculations with a spacing of 2, 4 and 8 meters was performed as well as a calculation with no piles at all. The model was consolidated for 365 days and a comparison was then made of the vertical displacement and the horizontal displacement in one point directly underneath the embankment and one point directly underneath the piles. The result shows in Table G.2.

Table G.2. Vertical and horizontal deformations in two points for different spacing of bank-piles.

Spacing [m]	u_{y1} [cm]	u_{y2} [cm]	u_{x1} [cm]	u_{x2} [cm]
No piles	51	15.6	5.5	12.5
8	31	16.5	1.3	8.6
4	28	18.3	2.3	8.6
2	24	18.7	0.9	7.7

The result shows that the piles have a large effect on the vertical settlement with a 40 percent decrease of deformations with 8 meter spacing piles. The difference in settlement between a spacing of 2 and 8 meters is 22 percent. The difference between 4 and 8 meters is 14 percent. The difference is not negligible but to be able to make calculations more manageable the 8 meter spacing is going to be used with the knowledge that the deformations will be over-estimated.

A comparison of the vertical deformations in the point directly underneath the piles show a small increase in settlement which is reasonable since more load is transferred deeper down into the soil. The horizontal displacements in the point underneath the embankment show a significant decrease with smaller spacing but are still disregarded for the benefit of a simplified geometry.

G.3. Effect of transverse SPWs

In Section A and B the cross-section includes a SPW placed perpendicular to the cross-section in the fill approximately 60 meters away from the tunnel axis. For simplifications these SPWs are removed from the geometry and the effect of this need to be investigated. A simple geometry was created in PLAXIS where a SPW was placed 60 meters away from the axis of symmetry. The deformations with and without the SPW was compared. The result shows in Table G.3.

Table G.3. Vertical and horizontal deformations at two points for calculation with or without a SPW.

	u_{y1} [cm]	u_{y2} [cm]	u_{x1} [cm]	u_{x2} [cm]
SPW	5.7	4.3	0.002	0.005
No SPW	5.7	2.8	0.003	0.01

The result shows that the SPW has little impact on the settlement adjacent to the tunnel.

G.4. Vertical drains

The southern and northern ramps are installed with vertical drains through the concrete slab. These are for geometry simplification not included in the model but the effect must still be investigated. A simple geometry was constructed in PLAXIS with 7 meter long vertical drains under an embankment. The spacing between the drains is 3 meters. Two calculations were performed, one with and one without the drains. The result can be seen in Table G.4 and Figure G.1, where the vertical deformations and the dissipation of excess pore pressure are compared for two different points.

Table G.4. Vertical deformations at two points for calculation with and without vertical drains.

	u_{y1} [cm]	u_{y2} [cm]
Vertical drains	6.7	1.5
No vertical drains	3.1	2.7

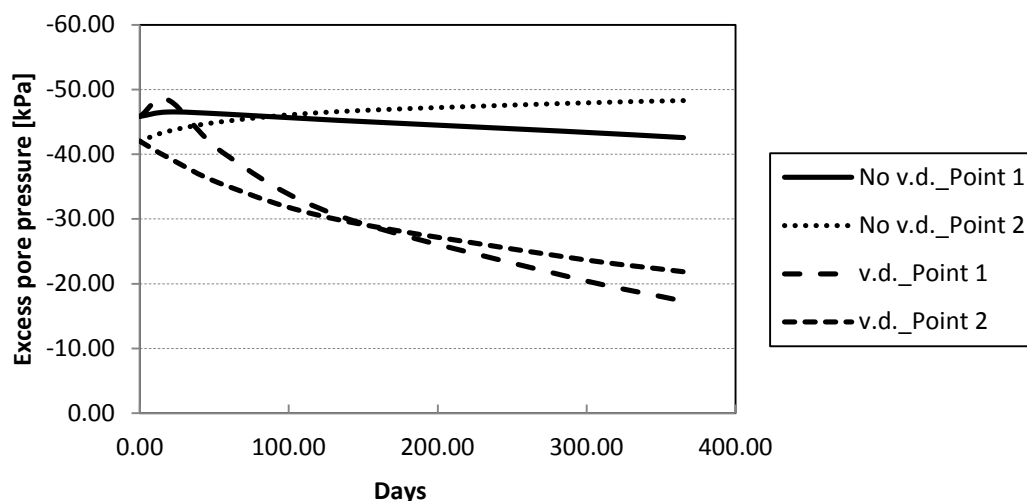


Figure G.1. Dissipation of excess pore pressure over time.

The result show that the vertical drains have a large effect on the dissipation of excess pore pressure and hence the deformations.

G.5. Load effect on Section C from fill

The load from the extensive fill work done on around the southern ramp also affects cross-section C due to load distribution and 3D-effects. To be able to simulate this effect the equivalent load from the fill was calculated according to the procedure described below.

The geometry of the fill was divided into smaller rectangular areas according to Figure G.2 and calculations of the equivalent load effect were calculated for each

area, see Table G.5. This resulted in several different distributed loads on different levels in the cross-section.

q = Load from the fill in each area

L = Length of area

b = Width of area

z = Level for the loading action including bank piling effect

x = Distance from area edge to cross-section C

$z_1=2x$ = Distance from z to level for loading action in cross-section C according to the 2:1-method for load distribution

$$\Delta\sigma_C = \frac{qbl}{(b+z)(l+z)} = \text{Load in cross-section C}$$

$L_C = L+2x$ = Length of load in cross-section C

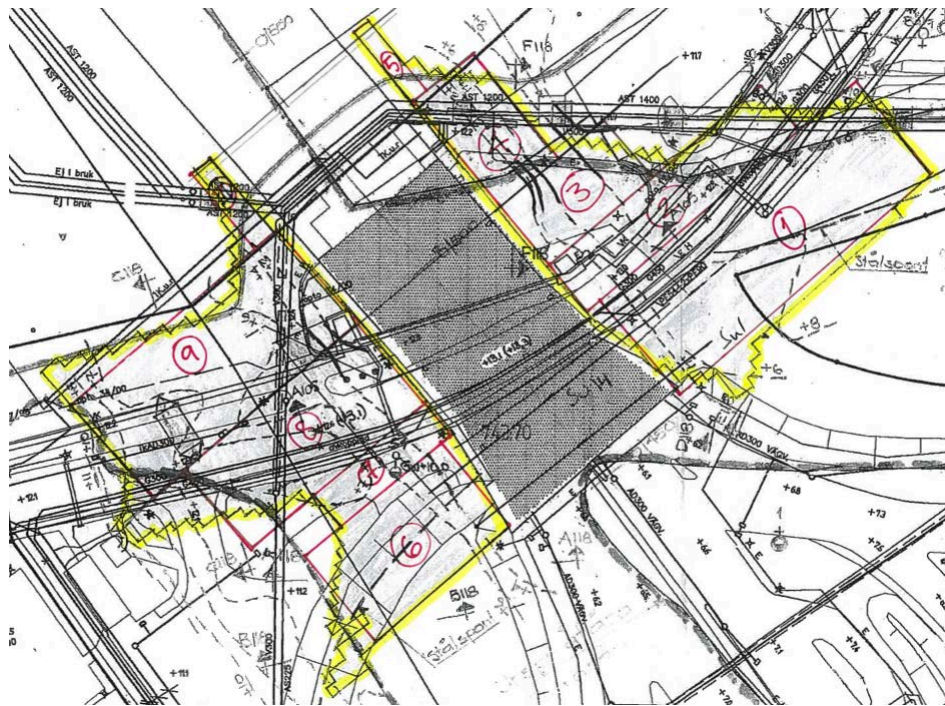


Figure G.2. Division of the refill into smaller areas.

Table G.5. Load calculations of the refill for subareas 1-10. Area 5 and 10 corresponds to the fill used in the model geometry.

Area	q [kPa]	L [m]	b [m]	z	x [m]	z1 [m]	$\Delta\sigma_c$ [kPa]	L _c [m]
1	94	60	22	+15	64	128	4.4	188
2	60	50	10.5	+15	53	106	1.7	156
3	60	25	14	+15	39	78	2.2	103
4	70	14	25	+15	15	30	10.1	44
5*	90	3.5	-	+15	0	0	90	3.5
6	94	32	20	+15	65	130	2.5	162
7	90	26	7	+15	58	116	0.9	142
8	90	42	20	+15	39	78	6.4	120
9	90	49	22	+15	17.5	35	20.3	84
10*	90	5	-	+15	0	0	90	5

The different loads obtained were then used in a hypothetical case in PLAXIS to see the effects on the vertical deformations. The distributed loads were added at the corresponding levels and activated one at a time. The vertical displacements can be seen in Table G.6.

Table G.6. Vertical deformations due to different load combinations.

Load combinations	$u_{y,max}$ [cm]	$\Delta u_{y,max}$ [cm]
1+6	0.09	-
1+6+7	0.16	0.07
1+6+7+2	0.22	0.06
1+6+7+2+3+8	0.39	0.17
1+6+7+2+3+8+4+9	1.4	1.01

As the result shows the settlements due to the fill is quite low with only the last combination showing a settlement above 1 cm. The last addition to the load combination was area 4 and 9 which contributed with 1 cm. These loads were added to the model and the other ones disregarded.